

University of New Hampshire

## University of New Hampshire Scholars' Repository

---

Doctoral Dissertations

Student Scholarship

---

Winter 1992

### Corrosion protection of metals by poly(3-methylthiophene) coatings

Shouxian Ren

*University of New Hampshire, Durham*

Follow this and additional works at: <https://scholars.unh.edu/dissertation>

---

#### Recommended Citation

Ren, Shouxian, "Corrosion protection of metals by poly(3-methylthiophene) coatings" (1992). *Doctoral Dissertations*. 1715.

<https://scholars.unh.edu/dissertation/1715>

This Dissertation is brought to you for free and open access by the Student Scholarship at University of New Hampshire Scholars' Repository. It has been accepted for inclusion in Doctoral Dissertations by an authorized administrator of University of New Hampshire Scholars' Repository. For more information, please contact [Scholarly.Communication@unh.edu](mailto:Scholarly.Communication@unh.edu).

## **INFORMATION TO USERS**

This manuscript has been reproduced from the microfilm master. UMI films the text directly from the original or copy submitted. Thus, some thesis and dissertation copies are in typewriter face, while others may be from any type of computer printer.

**The quality of this reproduction is dependent upon the quality of the copy submitted.** Broken or indistinct print, colored or poor quality illustrations and photographs, print bleedthrough, substandard margins, and improper alignment can adversely affect reproduction.

In the unlikely event that the author did not send UMI a complete manuscript and there are missing pages, these will be noted. Also, if unauthorized copyright material had to be removed, a note will indicate the deletion.

Oversize materials (e.g., maps, drawings, charts) are reproduced by sectioning the original, beginning at the upper left-hand corner and continuing from left to right in equal sections with small overlaps. Each original is also photographed in one exposure and is included in reduced form at the back of the book.

Photographs included in the original manuscript have been reproduced xerographically in this copy. Higher quality 6" x 9" black and white photographic prints are available for any photographs or illustrations appearing in this copy for an additional charge. Contact UMI directly to order.



University Microfilms International  
A Bell & Howell Information Company  
300 North Zeeb Road, Ann Arbor, MI 48106-1346 USA  
313/761-4700 800/521-0600

**Order Number 9307356**

**Corrosion protection of metals by poly(3-methylthiophene)  
coatings**

**Ren, Shouxian, Ph.D.**

**University of New Hampshire, 1992**

**U·M·I**

**300 N. Zeeb Rd.  
Ann Arbor, MI 48106**

CORROSION PROTECTION OF METALS  
BY POLY(3-METHYLTHIOPHENE) COATINGS

BY

Shouxian Ren

BSCHEM, Shanxi University, P.R. China, 1981  
MSCHEM, Academia Sinica, P.R. China, 1984  
MSCHE, University of New Hampshire, 1989

A DISSERTATION

Submitted to the University of New Hampshire  
in Partial Fulfillment of  
the Requirements for the Degree of

Doctor of Philosophy

in

Engineering

December, 1992

This dissertation has been examined and approved.



---

Dissertation Director, Dr. Dale P. Barkey  
Assistant Professor of Chemical Engineering



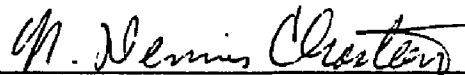
---

Dr. Gael D. Ulrich  
Professor of Chemical Engineering



---

Dr. Palligarnai T. Vasudevan  
Assistant Professor of Chemical Engineering



---

Dr. N. Dennis Chasteen  
Professor of Chemistry



---

Dr. Todd S. Gross  
Associate Professor of Mechanical Engineering

December 3 1992

Date

# Dedication

This dissertation is dedicated to my whole family for their years sacrifices and to the people of my homeland, Shanxi Province, People's Republic of China.

## ACKNOWLEDGEMENT

The author would like to take this opportunity to express his gratitude and thanks to his advisor, Dr. Barkey, for his spirited leadership, sincere assistance, cheerful encouragement and great patience in directing the research in this dissertation.

The author acknowledges Dr. Ulrich, Dr. Vasudevan, Dr. Chasteen and Dr. Gross for serving on the dissertation committee and for their valuable suggestions.

The author would also like to thank Mr. Jonathan E. Newell for his timely help during this work.

Special thanks to Dr. L. W. Dotchin and Ms. Nancy A. Cherim in the UNH instrumentation center for SEM micrographs and EDXS analysis.

This work was supported by the U.S. Army Research Office, Materials Science Division under contract # DAAL03-89-K-0138.

# Table of Contents

Dedication . . . . .	iii
Acknowledgement . . . . .	iv
List of Tables . . . . .	viii
List of Figures . . . . .	ix
Abstract . . . . .	xiv
<b>1 Introduction</b>	<b>1</b>
<b>2 Literature Review</b>	<b>7</b>
2.1 General aspects . . . . .	7
2.2 Electrochemically prepared PT and its derivatives . . . . .	12
2.2.1 Effect of deposition conditions on polymer properties . . . . .	12
2.2.2 Structure, conductivity and charge transport . . . . .	13
2.2.3 Morphology and mechanical properties . . . . .	16
2.2.4 Stability and degradation . . . . .	17
2.3 Conductive polymers in aqueous solution . . . . .	18
2.4 Catalysis in conductive polymers . . . . .	20
2.5 Electrocoating of metals with conductive polymers . . . . .	21
2.6 Metal corrosion control by conductive polymers . . . . .	24
<b>3 Experimental</b>	<b>26</b>
3.1 Technique overview . . . . .	26
3.2 Apparatus and Materials . . . . .	28
3.2.1 Potentiostat/Galvanostat system . . . . .	28



3.2.2	Electrolysis cell for rotating disk electrodes . . . . .	28
3.2.3	Corrosion cell for rotating disk electrodes . . . . .	31
3.2.4	Rotating disk electrodes (RDEs) . . . . .	32
3.2.5	Chemical reagents . . . . .	32
3.3	Procedures . . . . .	32
3.3.1	Preparation of solutions . . . . .	32
3.3.2	Electrode preparation . . . . .	33
3.3.3	Operation of the electrolysis cell . . . . .	35
3.3.4	Operation of the corrosion cell . . . . .	35
3.3.5	Coulometry . . . . .	36
<b>4</b>	<b>Effect of Deposition Conditions on Coating Properties</b>	<b>38</b>
4.1	Coating morphology . . . . .	38
4.2	Exchange current density . . . . .	39
4.3	Redox capacity of P3MT coatings . . . . .	42
4.4	Self-discharge of P3MT coatings . . . . .	46
4.5	Summary . . . . .	54
<b>5</b>	<b>Stabilization of 430SS by P3MT Coatings</b>	<b>55</b>
5.1	Preparation of coatings on Ph430SS . . . . .	55
5.2	Self-discharge in 1 N sulfuric acid solution . . . . .	57
5.3	Galvanic corrosion measurement in 1 N sulfuric acid solution . . . . .	57
5.4	Investigation of the passivation mechanism . . . . .	61
5.5	Reversibility of polymer reduction/oxidation . . . . .	63
5.6	The effect of chloride and hydroxide . . . . .	70
5.7	Durability of coatings in concentrated acid and base solutions . . . . .	74
5.8	Summary . . . . .	76

<b>6</b>	<b>P3MT Coatings on Titanium and Carbon Steel</b>	<b>80</b>
6.1	Preparation of coatings . . . . .	80
6.2	Passivation of titanium by P3MT coatings . . . . .	80
6.3	Electrochemical Impedance of coated titanium electrodes . . . . .	89
6.4	Approaches for protection of carbon steel by P3MT coatings . . . . .	94
6.5	Summary . . . . .	95
<b>7</b>	<b>Conclusions and Recommendations</b>	<b>96</b>
	Nomenclature . . . . .	106
<b>A</b>	<b>Composition and Properties of Metal Samples</b>	<b>108</b>
<b>B</b>	<b>Calculation of Oxygen Concentrations</b>	<b>110</b>
<b>C</b>	<b>A Rough Estimation of Unit Cost for P3MT and PP Coatings</b>	<b>112</b>

# List of Tables

2.1	Band-gap energies, $E_g$ , and equilibrium potential, $E^0$ , of various metal oxide electrodes (after Cheung et al. [82]). . . . .	22
3.1	Classification of tests for P3MT-coated RDEs in aqueous solutions. . . . .	34
4.1	$i_0$ of P3MT coatings in aqueous solutions ( $\mu\text{A}$ ). Deposition condition: $i_d=159\text{ mA/cm}^2$ , $\Omega=2.62\text{ rad/s}$ . . . . .	41
5.1	Loss of materials in galvanic corrosion tests (time period: 33 min) in 1 N sulfuric acid solution . . . . .	59
5.2	Material loss and Tafel plot results of P3MT-coated Ph430SS after discharge in aqueous solutions for 1.5 h. P3MT deposition condition: $300\text{ mA/cm}^2$ and $2.62\text{ rad/s}$ for 5 s. . . . .	73
5.3	Material loss and Tafel plot results of P3MT-coated Ph430SS after discharge in NaCl solutions for 1.5 h. . . . .	75
A.1	Physical Properties of Metals . . . . .	108
A.2	Composition of Metal Samples (%) . . . . .	109
C.1	1978 Typical Material Costs for Paint and Protective Coatings . . . . .	115
C.2	1978 Coating Cost data for Structural Steel on the Ground . . . . .	116

# List of Figures

1.1	Potential-pH diagram for iron in sulphate solutions. (1) Unprotected specimen; (2) Cathodically protected specimen; (3) Anodically protected specimen (after Wranglen [11]). . . . .	2
1.2	Polarization diagram of 430SS in 1 N air-saturated sulfuric acid solution. . . . .	4
1.3	An illustration of anodic protection of an exposed steel sample by a galvanically coupled conductive polymer coating. . . . .	5
1.4	An illustration of the protection system of a metal. . . . .	6
2.1	Molecular orbital and band for motion (after Balcius [2]) . . . . .	8
2.2	Creation of mobile carriers by doping (after Balcius [2]). . . . .	9
2.3	Approximate conductivities of selected polymers and inorganic materials (after Kuan [5]). . . . .	10
2.4	Cross-section view of a sandwich Al/Al <sub>2</sub> O <sub>3</sub> /Polypyrrole (after Hulser et al. [14]). . . . .	23
3.1	Introductory Tafel plot (after Uhlig [12]). . . . .	27
3.2	Corrosion research apparatus in this laboratory. w: working electrode, c: counter electrode, r: reference electrode . . . . .	29
3.3	RDE electrolysis cell system. . . . .	30
3.4	A typical corrosion cell. . . . .	31
4.1	SEM micrographs of P3MT coatings on C1010. Film deposition conditions: <i>Top</i> : 200 mA/cm <sup>2</sup> , 1.57 rad/s. <i>Bottom</i> : 200 mA/cm <sup>2</sup> , 105 rad/s. . . . .	40

4.2	Effect of purge gas on open circuit potentials of P3MT coating and scratched P3MT coating on Pt RDE as well as Pt RDE itself in 1 N air-saturated sulfuric acid solution. . . . .	42
4.3	Exchange current density, $i_0$ , of P3MT-coated Pt RDE. <i>Top</i> : versus $\Omega^{-1/2}$ at $i_d=8.0$ mA/cm <sup>2</sup> , <i>Bottom</i> : versus $i_d$ at $\Omega=10.5$ rad/s. . . . .	43
4.4	Effect of the deposition time during 3MT polymerization on $i_0$ . $i_d=80$ mA/cm <sup>2</sup> and $\Omega=10.5$ rad/s on Pt RDE. . . . .	44
4.5	Redox capacity of P3MT coatings on Pt RDE in propylene carbonate. <i>Top</i> : versus $\Omega^{-1/2}$ at $i_d=8.0$ ; 80 and 480 mA/cm <sup>2</sup> , <i>Bottom</i> : versus $i_d$ at $\Omega=10.5$ rad/s. . . . .	45
4.6	Redox capacity of P3MT coatings on Pt RDEs varied with deposition time during 3MT polymerization. $i_d=80$ mA/cm <sup>2</sup> , $\Omega=10.5$ rad/s. . . . .	46
4.7	Self-discharge curves of P3MT coatings on Pt RDEs in 1 N air-saturated sulfuric acid solution. . . . .	47
4.8	Charge capacity of P3MT coatings on Pt RDEs versus potential. <i>Top</i> : as a function of $\Omega^{-1/2}$ at $i_d=8.0$ mA/cm <sup>2</sup> , <i>Bottom</i> : as a function of $i_d$ at $\Omega=2.62$ rad/s. . . . .	49
4.9	Inverse of the charge capacity of P3MT coatings versus time. <i>Top</i> : as a function of $\Omega^{-1/2}$ at $i_d=8.0$ mA/cm <sup>2</sup> , <i>Bottom</i> : as a function of $i_d$ at $\Omega=2.62$ rad/s. . . . .	50
4.10	Initial and final charge decay coefficients for a second-order decay mechanism. <i>Top</i> : versus $\Omega^{-1/2}$ at $i_d=8.0$ mA/cm <sup>2</sup> , <i>Bottom</i> : versus $i_d$ at $\Omega=2.62$ rad/s. . . . .	51
4.11	Inverse of the charge capacity of a P3MT coating versus number of potential cycles in 1 N air-saturated sulfuric acid solution. Deposition condition: $i_d=80$ mA/cm <sup>2</sup> , $\Omega=2.62$ rad/s. . . . .	52
4.12	$E_{oc}(st)$ of P3MT coating on Ph430SS. <i>Top</i> : versus $\Omega^{-1/2}$ at $i_d=105$ mA/cm <sup>2</sup> , <i>Bottom</i> : versus $i_d$ at $\Omega=2.62$ rad/s in 1 N air-saturated sulfuric acid solution. . . . .	53
5.1	SEM micrographs. <i>Top</i> : the porous surface of a Ph430SS. <i>Bottom</i> : A P3MT coating on Ph430SS. Coating deposition condition: 60 mA/cm <sup>2</sup> , 10.5 rad/s. . . . .	56

5.2	Self-discharge curves for 430SS, Ph430SS and P3MT-coated Ph430SS in 1 N sulfuric acid solution. . . . .	58
5.3	Galvanic corrosion test (1): open-circuit potential of 430SS, coupled with a P3MT-coated Ph430SS, in 1 N air-saturated sulfuric acid solution for 8 h. . .	60
5.4	Galvanic corrosion test (2): open-circuit potential of working electrodes (430SS) versus time at different area ratios of $A_p/A_s$ in 1 N air-saturated sulfuric acid solution. . . . .	61
5.5	Galvanic corrosion test (3): open-circuit potential of 430SS RDE versus time, while disconnecting from and reconnecting to the P3MT-coated Ph430SS RDE in 1 N sulfuric acid solution with air or $N_2$ purge. D: Disconnected from the P3MT coating. R: Reconnected to the P3MT coating. . . . .	62
5.6	Open-circuit response of P3MT-coated Ph430SS in sulfuric acid solutions. <i>Top</i> : effect of concentration, <i>Bottom</i> : effect of purge gas in 1 N sulfuric acid solution. . . . .	64
5.7	Open-circuit response of P3MT-coated Ph430SS in 1 N air-saturated sulfuric acid solution. <i>Top</i> : at -0.4 V and -0.5 V, <i>Bottom</i> : at -0.3 V. . . . .	66
5.8	Cyclic voltammograms of P3MT-coated Ph430SS and Ph430SS in 1 N air-saturated sulfuric acid solution. . . . .	67
5.9	$E_{oc}$ versus time curves of a 430SS RDE coupled with a P3MT-coated Ph430SS in 1 N air-saturated sulfuric acid solution after being held at negative potentials. . .	68
5.10	Open-circuit response of P3MT-coated Ph430SS in 1 N nitric acid solution. . .	69
5.11	Self-discharge curves of P3MT-coated Ph430SS in dilute acid solutions. . .	71
5.12	Self-discharge curves of P3MT-coated Pt in dilute acid solutions. The electrodes were first held at 0.8 V for 2 min, then opened the circuit. . . . .	72
5.13	Self-discharge curves of P3MT-coated Ph430SS in sodium chloride solutions. . .	74
5.14	Self-discharge curves of the pretreated P3MT-coated Ph430SS in 1 N sodium chloride solution. . . . .	76

5.15	Self-discharge curves of a P3MT-coated Ph430SS in 2 N potassium hydroxide solution. . . . .	77
5.16	Cyclic voltammograms of P3MT-coated Ph430SS in dilute acid and base solutions. Initial potential: 0.8 V, Vertex potential: -0.6 V, Final potential: 0.8 V. Scan rate: 20 mV/s. . . . .	78
5.17	Self-discharge curves of pretreated galvanic samples ( $A_p/A_s=1.0$ ) in 1 N air-saturated sulfuric acid solution. <i>Top</i> : pretreated in severe acid solutions, <i>Bottom</i> : pretreated in severe base solutions. . . . .	79
6.1	SEM micrographs showing pits on a TiGr2 surface. Anodic deposition condition: 10 mA/cm <sup>2</sup> and 0.52 rad/s for 20 s in 0.5 M 3MT/0.1 M TBATFB/0.1 (g/ml) ZnCl <sub>2</sub> propylene carbonate solution. . . . .	81
6.2	SEM micrographs. <i>Top</i> : a P3MT thin film. The same deposition condition as in Fig. 6.1 except for 40 s. <i>bottom</i> : a P3MT full coating. 200 mA/cm <sup>2</sup> and 1.57 rad/s for 7.5 s in 1.0 M 3MT solution. . . . .	82
6.3	SEM micrographs showing pits on a C1010 surface. Anodic deposition condition: 500 mA/cm <sup>2</sup> and 0.52 rad/s for 20 s in 0.1 M 3MT/0.1 M TBATFB/0.1 (g/ml) ZnCl <sub>2</sub> propylene carbonate solution. . . . .	83
6.4	Self-discharge curves of TiGr2, P3MT-precoated TiGr2 and P3MT-coated TiGr2 at room temperature. <i>Top</i> : in 4 N sulfuric acid solution. <i>Bottom</i> : in 4 N hydrochloric acid solution. . . . .	85
6.5	Self-discharge curves of TiGr2 and P3MT-coated TiGr2 at 50°C. <i>Top</i> : in 4 N sulfuric acid solution. <i>Bottom</i> : in 4 N hydrochloric acid solution. . . . .	86
6.6	Self-discharge curves of TiGr2 and P3MT-coated TiGr2 at 70°C. <i>Top</i> : in 4 N sulfuric acid solution. <i>Bottom</i> : in 4 N hydrochloric acid solution. . . . .	87
6.7	Galvanic current versus time curve of galvanic couples in 4 N sulfuric acid solution at 45°C. Working electrode: treated TiGr2; Reference working electrode: P3MT-coated TiGr2. . . . .	88

6.8	Galvanic current versus time curves of TiGr2 coupled with the P3MT-coated TiGr2 in 4 N sulfuric acid solution at 70°C. The test was interrupted by temporarily opening the circuit for 2 s. . . . .	89
6.9	Possible equivalent circuits for organic coatings (after [90]). . . . .	90
6.10	Bode plots for a P3MT-coated TiGr2 in 1 N sulfuric acid solution. P3MT deposition condition: 200 mA and 1.57 rad/s and 7.5 s. (A). after 1 hour, (..). after 1 day, (B). after 2 days. . . . .	91
6.11	Bode plots for a P3MT-coated TiGr2 in 1 N sulfuric acid solution. P3MT deposition condition: 200 mA, 52.4 rad/s and 7.5 s. (..). initial test, (-). after exposed in ambient air for 40 days. . . . .	93
6.12	Tafel plots of C1010 and the prepassivated C1010 in 1 N air-saturated sulfuric acid solution. The prepassivation of C1010 was conducted by holding C1010 at 0.6 V in 70% nitric acid solution (10.5 rad/s) for 1.5 h. . . . .	94



## ABSTRACT

### CORROSION PROTECTION OF METALS BY POLY(3-METHYLTHIOPHENE) COATINGS

by

Shouxian Ren

University of New Hampshire, December, 1992

Electrochemically prepared poly(3-methylthiophene) (P3MT) films were used as conductive polymer coatings to poise a substrate metal in the passive potential range in corrosive media. To firmly adhere P3MT coatings onto substrate metals, different methods were developed for each metal; stainless steel (430SS), titanium (TiGr2) and carbon steel (C1010). The samples were either pretreated by anodization in phosphate solution to form a uniform porous surface or pitted by chloride ions simultaneously with the formation of an adhesive thin film. Coatings were characterized for various galvanostatic electropolymerization conditions on both platinum and phosphated 430SS (Ph430SS) rotating disk electrodes (RDEs). Both applied current density and rotation rate affected subsequent redox capacity, polarization and self-discharge behavior of the coatings in 1 N sulfuric acid solution.

With Ph430SS as substrate, the stability of P3MT coatings was investigated in various corrosive media. It was observed that the reversibility of the coatings above -0.3 V in several aqueous acid solutions contributed to their stability. In the presence of chloride ions, the coatings failed to protect Ph430SS because of penetration of  $\text{Cl}^-$  ions through the coating and resulting pit formation on the substrate.

Galvanic corrosion experiments were conducted to evaluate the effectiveness of the coatings in stabilizing Ph430SS and titanium in the passive state. In these experiments, a coated electrode was coupled to a bare electrode, and both electrodes were immersed. The coatings stabilized the exposed substrate in certain corrosive media at room temperature

under either air or nitrogen purge.

Coatings on titanium were tested in 4 N sulfuric and hydrochloric acid solutions at various temperatures. The coatings stabilized the substrate at temperatures below 50°C. Electrochemical Impedance Spectroscopy (EIS) was used to evaluate the short-term stability of P3MT coatings on titanium both in solution and in ambient air.

Although C1010 carbon steel can be passivated by anodic pretreatment, P3MT coatings did not sustain the passive state after immersion in corrosive media.

# Chapter 1

## Introduction

Conductive polymers, such as polyacetylene, polyaniline, polypyrrole and polythiophenes have been intensively studied in the last decade [1,2,4,5,6,7] with attention to synthesis methods, structure and morphology characterizations, electrical, optical and mechanical properties as well as stability and degradation. At the present time, the most successful application is in rechargeable batteries. The application of conductive polymers in anodic metal protection is still in an early stage [8,9,10]. In this study, we aimed to apply electrochemically prepared P3MT coatings to protection of passivating metals, such as 430 stainless steel (430SS) and grade-2 titanium (TiGr2) in aqueous media.

There are many approaches for metal corrosion protection, such as formulation of the composition or structure of a metal, addition of inhibitors to the corrosive medium, and application of metallic, inorganic or organic coatings. Since the corrosion of metals in aqueous or moist environments is of an electrochemical nature, one approach to reduction of corrosion is by electrochemical protection [11]. According to whether the protected metal potential is displaced in the negative or positive direction, the electrochemical protection can be divided into two categories, cathodic protection and anodic protection. To illustrate these two categories, a potential-pH diagram of iron is shown in Fig. 1.1. According to the diagram, there are two ways to protect iron from corrosion through control of the potential. By displacing the potential in the negative direction, the iron is brought to a thermodynamically stable state. This is called cathodic protection. On the other hand, if the potential is displaced in the positive direction into the passive region, the corrosion

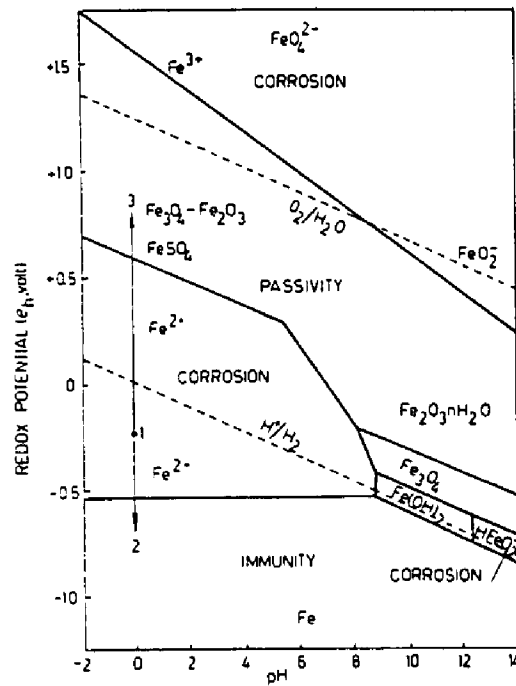


Figure 1.1: Potential-pH diagram for iron in sulphate solutions. (1) Unprotected specimen; (2) Cathodically protected specimen; (3) Anodically protected specimen (after Wranglen [11]).

rate is substantially reduced. In this condition, the metal is thermodynamically unstable, but dissolves very slowly due to the presence of a passive film of oxygen or of corrosion products. This is the principle of anodic protection. Cathodic or anodic protection can be achieved by either galvanic or electrolytic methods, defined as follows [11]:

- *Galvanic method:* In cathodic protection, the protected metal is taken as the cathode of a galvanic cell. The anode of the cell is a sacrificed metal (Mg, Zn, Al) which corrodes spontaneously. In anodic protection, a noble metal (Pt, Pd, Ag, Cu) or a conductive polymer coating is coupled to the protected metal, which becomes an anode of the galvanic cell and stays in its passive potential range.

- *Electrolytic method:* A direct cathodic or anodic current from an outside source is

supplied and the potential of the protected metal is regulated by galvanostatic polarization.

For anodic protection to be possible, the protected metal must be passive in some potential range. Metals qualified to be protected anodically include chromium, stainless steel, titanium and certain types of carbon steel. Passivation of the metal is caused by a film formed on its surface. There are two common theories regarding the nature of passive films [12]. The first theory considers the passive film as a diffusion-barrier layer of corrosion products, such as metal oxide, which slows down the dissolution process. The second view is that the passive metal is covered by a chemisorbed film, for example, a stable adsorbed film formed by dissolved positively charged metal ions combining with the adsorbed layers of negatively charged oxygen ions and molecules. The second theory applies to the case of very thin passive films. Chloride ions break down or prevent the formation of passive films on most metals with the exception of titanium.

A potentiostatic polarization diagram of 430SS in 1 N air-saturated sulfuric acid solution measured in this laboratory is shown in Fig. 1.2. The behavior of the metal changes through three different potential ranges: active, passive and transpassive. Transpassive corrosion occurs at potentials sufficiently positive to drive current through the passive film.

Conductive polymers can be used to poise a passive metal in its passive potential range according to the principle of anodic protection (Fig. 1.3). In Fig. 1.3, a steel sample is galvanically coupled with a polymer-coated steel. Both samples are immersed in a dilute sulfuric acid or nitric acid solution. Because the open-circuit potential ( $E_{oc}$ ) of the charged polymer coating is within the passive potential range of the steel, the exposed steel (anode) is passivated by the coupled polymer coating (cathode) and has a very low dissolution rate. As electrons pass from anode to cathode, the polymer is reduced. However, the conductive polymer coating contains a reversible couple which can be sustained by an oxidant, normally oxygen, in the environment. The reduced polymer coating can therefore be reoxidized by an oxidant. The net reaction on the cathode is the reduction of the oxidant. The key point here is that the coupled polymer coating would be fully discharged without reduction of an

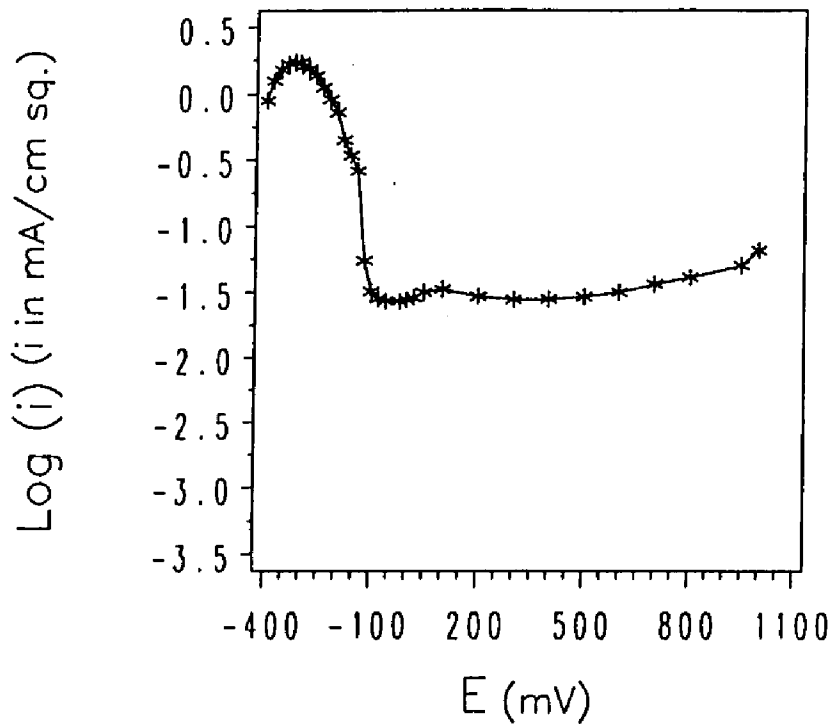


Figure 1.2: Polarization diagram of 430SS in 1 N air-saturated sulfuric acid solution.

oxidant. The addition of an oxygen-reduction catalyst to conductive polymer coatings can therefore assist in stabilization of the coating and substrate [8]. In contrast with organic and inorganic paints which perform only as physical barriers, a scratch on a conductive polymer coating does not affect its ability to protect the substrate metal from corrosion, since the exposed surface remains passive as long as it is in galvanic contact with the coating.

To be able to anodically protect a passive metal, there are three fundamental requirements for conductive polymer coatings.

- The open-circuit potential of a given polymer coating has to be within the passive potential range of a protected metal.
- Reduction of an oxidant has to take place at the polymer/electrolyte interface to keep the polymer coating from being discharged.
- The polymer coating has to be chemically stable in a given corrosive medium.

Poly(3-methylthiophene) (P3MT) coatings have open-circuit potentials ( $E_{oc}$ ) within

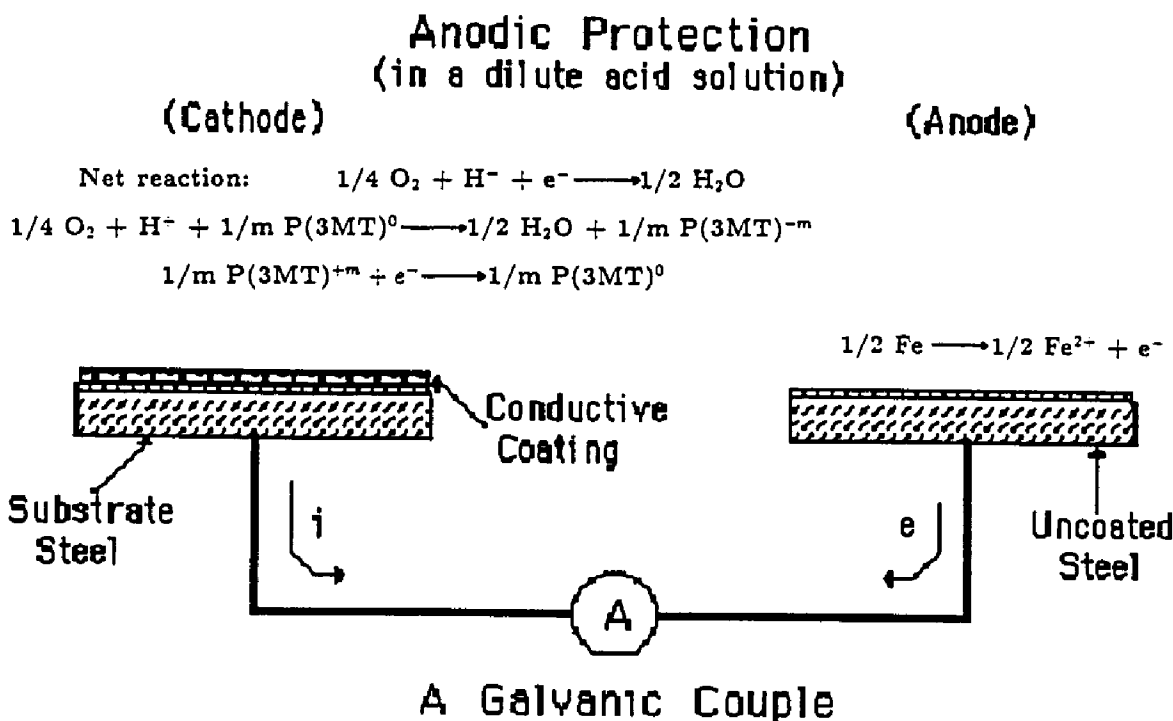


Figure 1.3: An illustration of anodic protection of an exposed steel sample by a galvanically coupled conductive polymer coating.

passive potential ranges of both 430SS and TiGr2. In addition, P3MT coatings are more stable than other conductive polymers [62,63,65]. Therefore, P3MT coatings were chosen to protect the metals from corrosion in this study. The protection system of a metal is illustrated in Fig. 1.4. A passive metal, initially with or without a passive film, is coated with a porous P3MT coating. The composite electrode is then immersed in a corrosive medium to evaluate the stability of the coating and its efficiency for protecting the substrate or the exposed metal from corrosion.

A conductive polymer coating can be formed by both chemical and electrochemical means [1]. I am not aware of any previous study in which a passive metal was protected by chemically synthesized conductive polymer coatings. With electrochemical polymerization,

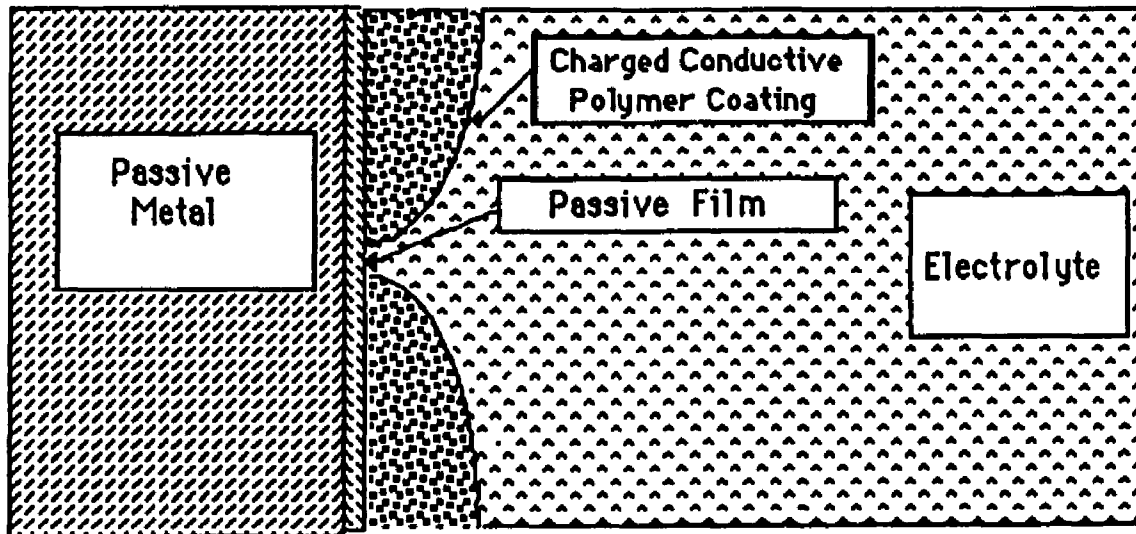


Figure 1.4: An illustration of the protection system of a metal.

the thickness and oxidation state of the coatings is easily controlled [1]. Electrochemical polymerization of 3-methylthiophene (3MT) onto the substrate was therefore used in this study. Both cyclic voltammetry [8,9] and galvanostatic [13,14] techniques have previously been applied in electrochemical polymerization. The galvanostatic technique, in which a constant current density is applied during the polymerization, was chosen for this study. Applied current density ( $i_d$ ), rotation rate of the RDE ( $\Omega$ ) and deposition (polymerization) time ( $t_d$ ) are the process variables for this technique.



# Chapter 2

## Literature Review

### 2.1 General aspects

In the history of polymer technology, one of the most valuable properties of synthetic polymers has been their high electric resistance at both high voltages and high frequencies. Nevertheless, in 1977 MacDiarmid et al. discovered that when polyacetylene is treated by Lewis acids or bases, its conductivity increases by 13 orders of magnitude [21]. The treatment, called 'doping', results in removal or addition of electrons from or to the polymers. Since 1977, much attention has been given to development of a range of conjugated polymers with the property of electric conductivity. A significant achievement was made by BASF scientists, Dr. Naarmann and his coworkers [7], who treated polyacetylene with iodine. The doped polymer possesses a room-temperature conductivity about a third that of copper on a volume basis. On a weight basis, the polymer's conductivity is twice that of copper. This amazing result accelerated the search for 'organic metals'. Lockheed scientists, led by Kuan have been developing stable, conductive, processible and inexpensive conducting polymers to build up a new generation of combat aircraft with various advantages [5]. Other applications of conductive polymers in rechargeable (secondary) batteries, semiconducting devices, catalysis, sensors and so on, have been proposed [1,4].

The conductivity of conductive polymers can be reasonably described by the molecular orbital theory. In a given electronic system, such as a conjugated polymer, there are energy levels corresponding to the highest filled molecular orbit (HFMO) and the lowest empty molecular orbit (LEMO). By analogy with the theory of metal (or semiconductor)

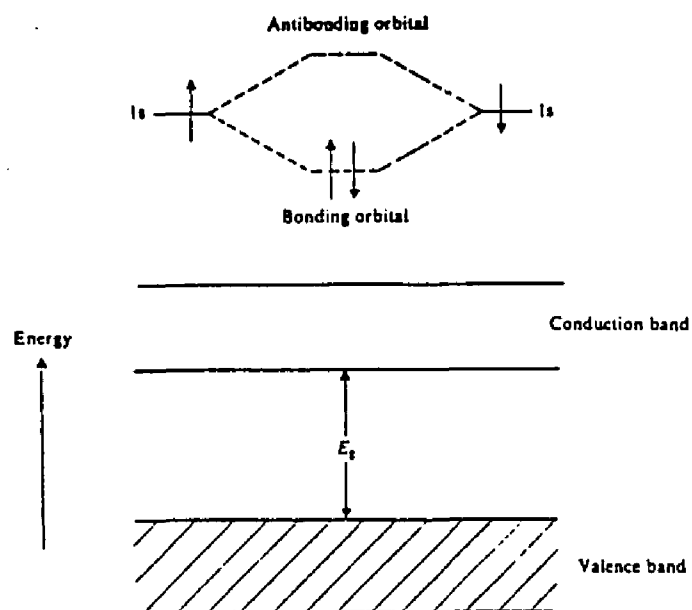


Figure 2.1: Molecular orbital and band for motion (after Balcius [2])

conduction, the HFMO and LEMO refers to the conduction band and the valence band respectively (see Fig. 2.1).

Electric conduction takes place when either positive vacancies (holes) are introduced in the valence band, or electrons are pumped up to the empty conduction band through energy promotion. The lattice structure of polymers can be described by two parameters, i.e., band width and band gap [2]. The band width represents the degree of conjugation for a given polymer; a broad band is indicative of a higher degree of delocalized orbital overlap. The band gap is a measure of the energy required to promote the electrons in the valence band to the conduction band. A polymer with a broad valence band and a narrow band gap should possess the capability of being made conductive. However, even the most ordered and conjugated polymers tend to resist electric conduction owing to the large energy for electron promotion [2]. A doping process, in which electron donating or accepting molecules (or ions) are incorporated into a polymer matrix, can increase the conductivity of the polymers by as much as 18 orders of magnitude [3]. Therefore, the electronic properties of the polymers

can be controlled by doping in the range from insulator to metal.

Electron donating species (n-type dopant) such as Na, K and Li, can form an energy state just below the conduction band and facilitate population of the conduction band. On the other hand, Lewis acids or bases act as electron acceptors (p-type dopant) to create an energy level just above the valence band and capture electrons from it resulting in a generation of holes (positive vacancies) [2]. Fig. 2.2 presents an illustration of this principle. A comparison of electric conductivities among selected polymers, corresponding

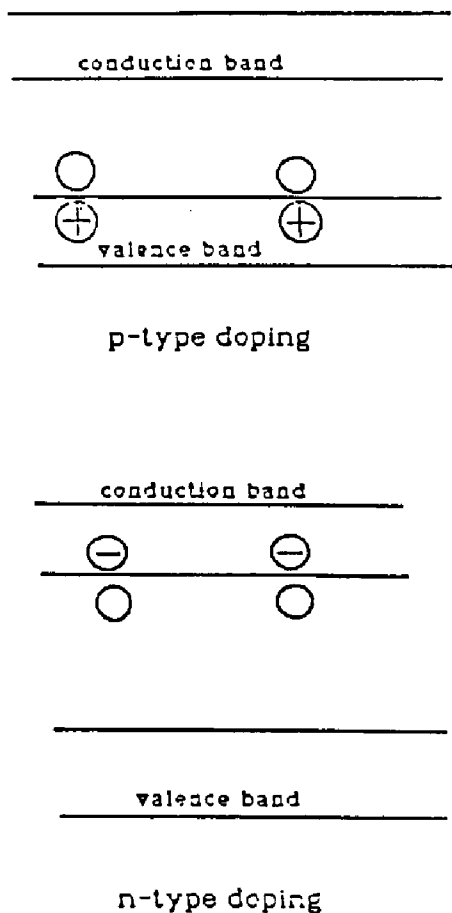


Figure 2.2: Creation of mobile carriers by doping (after Balcius [2]).

doped-polymers and inorganic materials is shown in Fig. 2.3. Baughman et al. discussed a

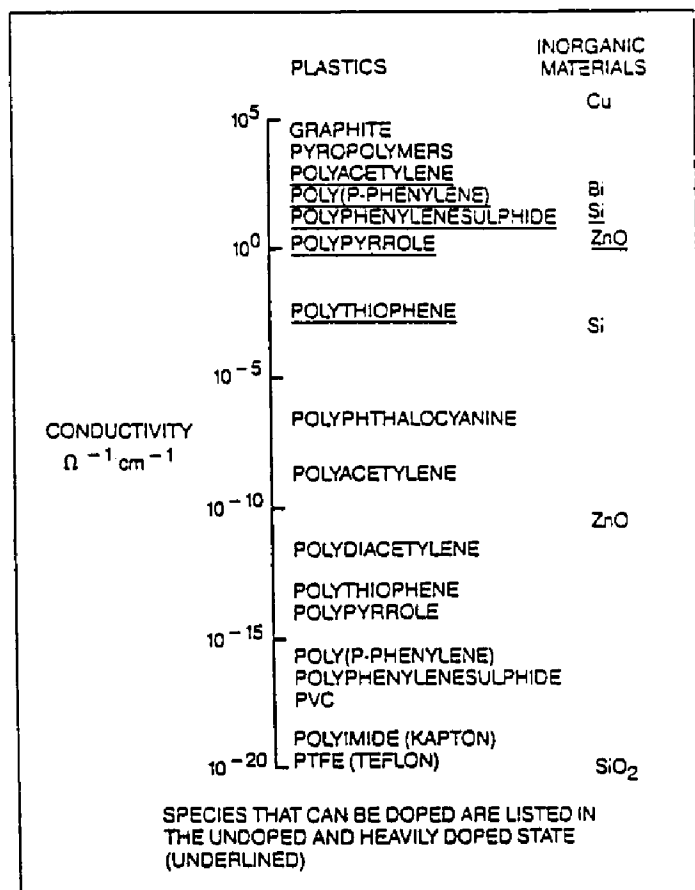


Figure 2.3: Approximate conductivities of selected polymers and inorganic materials (after Kuan [5]).

second class of conductive polymers which undergo irreversible chemical modification during doping. In this case, the dopant can form a covalent bond with the doped polymer and give the polymer more conjugated character [3].

Conductive polymers can be synthesized by chemical methods from monomer solutions. Billingham and Calvert have given a detailed review [1]. The major advantage of chemical synthesis is its flexibility for introducing certain active chemical groups onto the polymer backbones. These groups can make the polymers soluble in non-aqueous or aqueous solutions depending on their properties and in turn create more processible conductive

polymers [22,23,24]. The introduced group also can work as a bridge between the polymer backbone and other chemical branches to improve properties [25]. Recently, a method for plasma polymerization of thiophene and 3-methylthiophene has also been reported [26].

Electrochemical polymerization can also be used to generate electrically conductive polymers. An advantage of this method is improved control of the initiating species concentration and the reaction rate [1]. Electrosynthesis has primarily been used to generate thin films on substrate metals. Waltman and coworkers investigated the mechanism of electrochemical polymerization. They found that when a monomer (R) is electrooxidized to its radical cation ( $R^{\cdot+}$ ) at the electrode surface, the transfer of electron is much faster than the diffusion of R from the bulk solution to the electrode surface. This ensures the formation of a cluster of  $R^{\cdot+}$  on the electrode surface at the applied voltage. The cluster can be continuously maintained by diffusion of R from the bulk solution. The radical cations in the cluster undergo a series of follow-up reactions to form a polymer film on the electrode [4].

More recently, electrochemical copolymerization has received extensive interest owing to its potential for modifying the physical properties of conductive polymers. The copolymerization of thiophene or 3-methylthiophene with other monomers has been described in recent publications [27,28,29,30,31].

Most electrochemical polymerizations take place in non-aqueous media which are expensive in general. To reduce the cost of conductive polymers, polypyrrole (PP) has been successfully generated in aqueous solutions [84,33]. Dong et al. developed a method to electrochemically polymerize 3-methylthiophene in aqueous phosphoric acid solution. However, the poly(3-methylthiophene) (P3MT) films had poorer conductivity than films produced in organic media [34].

Because of the great number of papers on conductive polymers, this review mainly considers electrochemically prepared polythiophene (PT) and its derivatives.

## 2.2 Electrochemically prepared PT and its derivatives

### 2.2.1 Effect of deposition conditions on polymer properties

Electrochemical polymerization of thiophene is an excellent method for generating stable and flexible PT films with high conductivity [35]. Tourillon and Garnier found oxidation potential of thiophene to be about 1.6 V/SCE at platinum electrodes [35]. Reynolds et al. found that the oxidation potential of 3-methylthiophene varied from 1.55 to 1.65 V/SCE with the type of electrolyte [36]. The use of a saturated calomel reference electrode is questionable. Since it is an aqueous electrode, it is not clear that it reaches a well-defined potential with respect to the working electrode in an organic solvent.

Roncali et al. studied the effect of initial monomer concentration on the properties of poly(3-methylthiophene) (P3MT) films formed by cyclic voltammetry (CV). It was evident that high monomer concentrations (greater than 0.5 M) led to powdery P3MT films on Pt anodes with poor cohesion. The D.C. conductivity of their films was in the range of 1 to 10  $\text{ohm}^{-1}\text{cm}^{-1}$ . Decreasing the monomer concentration improved the cohesion of the films and markedly increased the conductivity of the P3MT films (up to 450  $\text{ohm}^{-1}\text{cm}^{-1}$  for [3MT]=0.1 M) [37]. In contrast to Roncali's conclusion, Otero et al. observed an increase of conductivity with increased monomer concentration. The key to control of conductivity of PT films was the thickness of the polymer layer. The growth of the PT film initially resulted in an increase in its conductivity. However, as film thickness increased beyond a certain extent, the film's conductivity began to drop due to a decrease of ionic conductivity and chemical activity of the PT film [38].

In a study of galvanostatic (constant current) polymerization, Ito et al. found that a change of current density changed the direction of fiber alignment of PT films. As applied current density was increased from 0.7 to 5.0  $\text{mA}/\text{cm}^2$ , the conductivity of the film (along the film surface) first increased and then decreased with a maximum value (40.2  $\text{ohm}^{-1}\text{cm}^{-1}$ ) at 3.0  $\text{mA}/\text{cm}^2$  [39].

Zotti et al. investigated PT film formation by CV and developed relationships between

net irreversible charge density and the number of cycles as well as scan rate. They found that PMT deposition was mass transfer limited at their polymerization condition [40].

By employing thiophene and 3-methylthiophene oligomers with different unit sizes as the 'monomers', Laguren-Davidson et al. showed that the degree of polymer porosity increased, and the physical stability decreased with increase of the 'monomer' size [42].

Kaneto et al. reported the effect of electrolyte composition on the properties of PT films. By comparing electric conductivity and open-circuit potential of the films formed in several electrolytes, the  $\text{LiBF}_4\text{-C}_6\text{H}_5\text{CN}$  combination was singled out as the best choice of nitrile-based electrolytes [43].

Polymerization temperature also affects the properties of conductive polymer films. Hotta et al. prepared P3MT film containing  $\text{ClO}_4^-$  groups on an indium-tin oxide surface galvanostatically. At a lower temperature ( $5^\circ\text{C}$ ), denser and tougher films were obtained, while films prepared at  $25^\circ\text{C}$  were bulky and brittle [41]. Otero et al. studied PT films generated between  $-12$  and  $60^\circ\text{C}$  by the CV method. It was observed that both the polymerization current efficiency and the charge-storage efficiency increased when the temperature was decreased. This could be attributed to the increase of mobility of the monomer ion radicals in the diffusion layer. A faster polymerization process could be achieved with the temperature increase from  $0$  to  $20^\circ\text{C}$ . However, At  $40^\circ\text{C}$ , the film was not conducting [44,45].

### **2.2.2 Structure, conductivity and charge transport**

Baughman et al. compared the electric conductivity of various kinds of conductive polymers. It was found that when two carbon atoms share the substituent (e.g., N for pyrrole and S for thiophene) which bridges the polyene backbone of the polymer, higher conducting complexes appear. Polyacetylene is the only exception. It possesses higher conductivity without a bridged polyene structure [3].

Scanning Tunneling Microscopy (STM) images of electrochemically deposited PT and P3MT films were investigated by Caple et al. The STM images of P3MT were quite

different from those of PT. A highly structured zigzag pattern was observed for P3MT with approximately a  $90^\circ$  kink every 100-110 Å (about every 30 thiophene units) [46].

Yang et al. reported SEM results for PT films. It was shown that microislands were formed during the initial growth. The microislands were composed of many discernible polymer strands, appeared semicrystalline, and were often interconnected by multiple polymer strands. The polymer strands were helices with 10-11 individual thiophene molecules per coil. The counter ion affected the structure of the helices due to its insertion into the coil. The structure of the conductive polymers gradually changed from an ordered crystalline array at the surface to an amorphous materials in the bulk depending on polymerization conditions [47].

Gostafsson and his coworkers studied the structure of poly(3-octylthiophene) (P3OT) which was stretched at  $100^\circ\text{C}$ . From X-ray diffraction, the degree of crystallinity was evaluated as 0.23. A layered structure was also seen. The main chains were stacked on top of each other forming parallel planes separated by alkyl side-chains. The layer spacing depended on the length of the alkyl groups [48].

Using Fourier Transform Infrared Spectroscopy (FTIS), Neugebauer et al. observed that electrochemically prepared P3MT (undoped) had a structure corresponding to an  $\alpha-\alpha'$  coupling of the thiophene units. The infrared spectrum also demonstrated the difference between undoped (neutral state) and doped (oxidized state) P3MT films [49].

Tourillon et al. [50] and Waltman et al. [51] separately studied the effect of  $\beta$  substituted groups on properties of polythiophenes. They conclude that when bulky groups were substituted on the  $\beta$  carbon atoms in the thiophene unit, steric hinderance increased quickly as the size of substituted group increased. This made polymeric oxidation more difficult due to the loss of planary conjugation of polymer chains. With  $\beta$  substitution of a  $-\text{CH}_3$  group, the polymer became more easily oxidized, and the  $-\text{CH}_3$  substituent seemed to assist chain conjugation. The characteristic of long conjugated polymeric chains of PT and P3MT was confirmed by visible spectroscopic data.



While evaluating materials for rechargeable batteries, Panero et al. found that among PT, P3MT and polydithiophene, P3MT was the most suitable material to be used as cathode in the batteries owing to its higher capacity and better rechargeability [52].

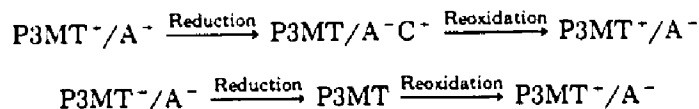
Nagatomo et al. reported the conductivity of P3MT film, synthesized by electrochemical polymerization at 25°C, reached about 100  $\text{ohm}^{-1}\text{cm}^{-1}$  with  $\text{LiBF}_4$  and about 200  $\text{ohm}^{-1}\text{cm}^{-1}$  with  $\text{LiAsF}_6$  in propylene carbonate (PC) [53]. The conductivity of P3MT thin films was also studied by Yassar et al.. It was found that an increase of morphological disorder steeply decreased the film conductivity. When the polymer growth was limited to a few nanometers thickness, the film conductivity was as high as  $2 \times 10^3 \text{ ohm}^{-1}\text{cm}^{-1}$  [54].

Sato et al. studied the electrical and thermal properties of drawn PT films. For drawn and  $\text{I}_2$ -doped films, the electric conductivity parallel and perpendicular to the draw direction were 150  $\text{ohm}^{-1}\text{cm}^{-1}$  and 45  $\text{ohm}^{-1}\text{cm}^{-1}$  respectively. This anisotropy was also observed in thermal diffusivity. These anisotropies may be attributed to the oriented structure of drawn PT films [55].

Tourillon et al. studied the effect of dopants on the properties of PT and its derivatives. It was claimed that the conductivity of the polymers could be improved by doping with various dopants in  $\text{CH}_3\text{CN}$ . The conductivity was slightly affected by the type of dopant. However, the type of dopant applied had greater effect on the conductivity of P3MT films.  $\text{CF}_3\text{SO}_3^-$  had the best performance, increasing P3MT's conductivity to 100  $\text{ohm}^{-1}\text{cm}^{-1}$ . A weak interaction between the anion and the S atoms occurred when the P3MT film was progressively doped during an oxidation process. The doping led to a reduction of the  $\pi - \pi^*$  band gap producing an increase in the conductivity of the polymers. Poor interchain contacts limited the conductivity of the polymers [56,57].

Reynolds et al. [36] systematically studied properties of electrochemically prepared P3MT films. The oxidation potential of the films ranged from 0.35 to 0.55 V/SCE depending on both electrolyte and deposition methods (potentiostatic or galvanostatic). Charge transport in P3MT films followed the model of a porous metallic electrode in which current

in the voltammogram is treated as double layer charging. With cations and anions present in the neutral polymer film, the mechanism of reduction and oxidation of P3MT film may be explained as follows



This mechanism is in contrast to the older concept that intermolecular charge transport in conductive polymers involves a faradaic current [36].

Bredas et al. reported the charge distributions in a repeat unit of PT. In the undoped state, the S atom showed a positive charge (0.2711 e) as compared with negative charges in the carbon atoms [58]. Foot et al. [59] and Kaneto et al. [64] measured the dopant diffusion coefficients in PT films and found that the diffusion coefficients were in the range of  $10^{-12} - 10^{-10} \text{ cm}^2/\text{s}$ .

### 2.2.3 Morphology and mechanical properties

Control of the morphology of a conductive polymer is important from both fundamental and practical viewpoints, and has been studied extensively. Tourillon et al. analyzed the morphologies of PT and P3MT films doped with various anions by scanning and transmission electron microscopy. They found that the surface of the thin film (about  $10^3$  to  $2 \times 10^3$  Å thick) was very homogeneous for both polymers, no matter what anion was used in the electrolyte. As the film thickness increased, its surface became more and more rough, eventually powdery at thickness of about a few micrometers. Undoped P3MT films showed fibrils 25 nm in diameter. With perchlorate counter-ions, fibrils were swelled to 80 nm in diameter [60].

For growth of P3MT films on platinum electrodes, Reynolds et al. defined five generally distinguishable morphological features in the film surfaces; thin films, nuclei, blisters,

blankets and nodular deposits. The type of dopant affected film morphology. In particular, it was shown that the P3MT-TBABF<sub>4</sub> system generated a more consistent film surface with a fast electrochemical response. Lower current density processes yielded smoother films than higher current density processes. The smooth films behaved better than rough films in general [36]. Nagatomo et al. observed similar phenomenon in the variation of P3MT film morphology with applied current density [53].

With regard to morphology of poly(3-alkylthiophene), Gustafsson et al. pointed out that a folded-chain model, which described the crystalline state of these polymers, may not be plausible. The large 3-substituted group makes this model unlikely. More suitable would be the fringed micelle model in which the polymer consists of a continuous amorphous region with dispersed crystallites. The crystallites may undergo orientation imposed by a stress field [48].

Ito et al. investigated the effect of polymerization conditions on mechanical properties of PT films. It was evident that the modulus, strength and deformability of the films decreased with increase of applied current density [61]. Nevertheless, Satoh et al. found that the increase of applied potential increased the elongation (%) of drawn PT films to a maximum of 65% at about 13 V, following a decrease of the film elongation as the potential increased further [55].

#### **2.2.4 Stability and degradation**

Tourillon and Garnier studied the stability of conducting PT and derivatives. It was observed that this group of polymers were much more stable than most other conductive polymers, such as polyacetylene, polypyrrole (PP) and so on. After 8 months storage time in air, both doped and undoped P3MT films gave the same infrared spectra, indicating that the films remained undegraded. In addition, P3MT films also exhibited good electrochemical stability. While polypyrrole derivatives degrade after about  $10^3 - 10^4$  cycles, P3MT remained 80% activity after  $1.2 \times 10^5$  cycles in CH<sub>3</sub>CN + LiClO<sub>4</sub> [62,63].

When applying PT films to color switching cells, Kaneto et al. found that a stable cycle life of more than  $5 \times 10^5$  times could be achieved in  $\text{CH}_3\text{CN} + \text{Pb}(\text{ClO}_4)_2$  in a potential scan ranged from -2 V to 2 V. A higher applied voltage (greater than 2 V) caused degradation of the PT film [64].

Spectrochemical studies of P3MT films were conducted by Hoier et al.. The presence of isopotential points in cyclic voltammtry (CV) indicated a fixed region for doping (oxidation) and undoping (reduction) P3MT films with a fixed stoichiometry. The isosbestic point in absorbance spectra supported this indication. These phenomena also demonstrated the high reversibility and stability of the films [65].

Wang et al. investigated P3MT-coated glassy carbon electrodes in solutions containing phenolic compounds that exhibited rapid surface fouling at conventional electrodes. The CV results showed that the P3MT modified glassy carbon electrodes were much more stable than unmodified glassy carbon electrodes, because the microporous structure of the film resulted in steric hindrance to the dimerization of the phenoxy radicals. The P3MT film was recommended to address electrode fouling problems [66].

## 2.3 Conductive polymers in aqueous solution

Three categories in the study of conductive polymers in aqueous solution are reviewed here. The first is the effect of dopants on the electric conductivity of the polymers [50,67,68,69]; the second 'ion gate' and 'ion sieving' effects of the polymer thin films [71,72,73] and the third self-doped conductive polymers [74,75].

Tourillon et al. studied electrochemical doping of PT and P3MT films in aqueous solutions with the supporting salts:  $\text{LiClO}_4$ ,  $\text{KAu}(\text{CN})_2$ ,  $\text{K}_2\text{PtCl}_6$ ,  $\text{K}_2\text{IrCl}_6$ ,  $\text{K}_2\text{RuCl}_6$  and  $\text{K}_2\text{Pt}(\text{CN})_4$ . It was evident that the polymers can be electrochemically doped to a conductive state ( $5 \cdot 10 \text{ ohm}^{-1}\text{cm}^{-1}$ ) as easily as in organic media. During long doping-undoping periods, the polymers retained their physico-chemical and electrical properties [67]. Increase of side groups on the backbone reduced the dopant-polymer interaction owing to

steric effects [50].

Sunde et al. observed that P3MT films were very sensitive to dopant anions in aqueous solutions. Voltammograms of the P3MT film consisted of two anodic peaks, whose positions depended on the type of anion. The behavior of the first peak corresponded to doping of the polymer, while the second peak corresponded to polymer degradation. Both doping and degradation took place simultaneously. Oxidation of a P3MT film by anions, such as  $\text{NO}_3^-$  and  $\text{ClO}_4^-$ , was suggested as the doping mechanism [68].

Czerwinski et al. investigated the conductivity of poly(3-substituted Thiophene-2,5-diyls) in aqueous solutions with dopants. It was shown that water played an important role in the conductivity of the  $\text{Cu}^{+2}$ -doped polymer. The conductivity of the polymer changed from  $10^{-7}$  to  $10^{-1} \text{ ohm}^{-1}\text{cm}^{-1}$  when a dry polymer film was exposed to water [69].

Burgmayer et al. discovered that polypyrrole (PP) films can work as 'ion gate' membranes to control the flux of chloride ions moving from a high concentration to a low concentration electrolyte by electrochemically manipulating the oxidized or reduced state of the polymer film. The oxidized film had a  $\text{Cl}^-$  permeability 100 times greater than that of the reduced film [71]. Shinohara et al. found that the PP film was permeable to  $\text{Cl}^-$  and anions with comparable diameter but prevented larger anions from penetrating the matrix [72]. Zhang et al. observed a similar 'ion sieving' effect from P3MT films in aqueous solutions. Only anions with a radius less than 0.4 nm were able to pass through the P3MT film [73].

Patil et al. developed self-doped conductive polymers, such as sodium salts and acids of poly-3-(2-ethanesulfonate)thiophene, where the counterions are covalently bounded to the polymer backbone. Because the proton is the smallest and most mobile ion, the acid of the substituted polythiophene led to relatively rapid doping kinetics [74,75].

## 2.4 Catalysis in conductive polymers

Metal particles dispersed in conducting polymer films can function as catalysts for various electrode reactions [76,77,78].

Tourillon et al. reported the inclusion of Pt and Ag aggregates into PT and P3MT conductive films by electrodeposition. It was demonstrated that the Ag aggregates were mainly located along the polymer fibers and enhanced the conductivity of the polymer films even in their neutral undoped state. The Pt aggregates, which were dispersed uniformly on the polymer surface, showed very high catalytic activity for electrochemical reduction of protons. However, Pt aggregates didn't enhance polymer conductivity [76].

While investigating chemically responsive microelectrochemical devices made by platinized P3MT films, Thacheray et al. showed that Pt particles, deposited on P3MT films, depolarized the  $O_2/H_2O$  and  $H_2O/H_2$  redox couples. The Pt particles did not change the potential dependence of the film conductivity. Pt also had no effect on the conductivity of the P3MT film. However, the conductivity of the P3MT/Pt device could be varied up to 5 orders of magnitude in acid solution by changing the gas purge from hydrogen to oxygen [77].

Recently, Leone et al. studied the electrochemical behavior of polyaniline (PA) and polypyrrole (PP) films containing dispersed Pd particles. They found that both the number density of Pd particles and their total surface area depended on the Pd deposition overpotential. Bulk hydrogen evolution took place on Pd-modified PA films in the reduced (electrochemically insulating) state. Nevertheless, bulk hydrogen oxidation was only observed after oxidation of the film to its conductive state. For oxygen reduction, the higher rate was due to the smaller sizes and higher surface area of Pd particles [78].

It was observed that electrodes modified by heteropolyacids (HPA), such as  $H_3PW_{12}O_{40}$  and  $H_3PMo_{12}O_{40}$ , catalyze oxygen reduction [79,80]. Keita et al. studied the electrochemical immobilization of HPA in polypyrrole and poly(3-methylthiophene) conductive polymers and showed that HPA can yield soluble complexes in acetonitrile solutions

of pyrrole and 3-methylthiophene [81,83]. Oxidation of the complexes produces conductive polymers doped by HPA anions. The polymerization was possible even in the presence of a large amount of water (from the hydrated HPA powders) owing to the formation of complexes between HPA and monomers.  $\text{PW}_{12}\text{O}_{40}^-$  and  $\text{SW}_{12}\text{O}_{40}^-$  doped P3MT films gave very similar electrochemical behavior in acetonitrile with 0.2 M  $\text{LiClO}_4$  and 0.5 M  $\text{HClO}_4$ . Two or three oxygen reduction states were observed in the range -1 to 0 V by cyclic voltammetry (CV). Three monoelectronic reduction-oxidation steps of a  $\text{PMo}_{12}\text{O}_{40}^-$  doped P3MT film appeared in the potential range of 0.2 to 1 V [83]. It will be seen that for the purpose of metal corrosion control,  $\text{H}_3\text{PMo}_{12}\text{O}_{40}$  is the only suitable HPA which catalyzes oxygen reduction.

Most recently, Swathirajan et al. electrochemically dispersed Pt-Sn catalysts on P3MT coatings to make a corrosion-resistant electrode for methanol oxidation in a methanol-air cell. Pt-Sn catalysts deposited in the hydrogen adsorption potential region (-0.2 V/SCE) demonstrated higher surface area and methanol oxidation activity. The Pt-Sn catalysts were dispersed on the internal surface of the polymer coating at Pt loadings below  $60 \mu\text{g}/\text{cm}^2$ . Above this loading limit, the particles began to grow on the external surface of the polymer as well [85].

## 2.5 Electrocoating of metals with conductive polymers

In the studies reviewed above, the polymer films were usually electrochemically coated on an inert anode such as platinum, gold or glassy carbon. The coatings were coherent and adhesive in general. There were few papers which dealt with electrocoating of common metals [82,84,14].

Cheung et al. investigated the possibility of electrochemical coating of different electrodes with polypyrrole films containing the toluenesulphonate counter-ion. During CV experiments, black continuous films were formed on Pt, Brass, Fe and Ti electrodes respectively. The current densities obtained on Ti and Fe were lower than those obtained on Pt.

Table 2.1: Band-gap energies,  $E_g$ , and equilibrium potential,  $E^0$ , of various metal oxide electrodes (after Cheung et al. [82]).

Metal	Film	$E_g$ (eV)	$E^0$ * (V)
Al	$Al_2O_3$	9.5	Al/ $Al_2O_3$ -1.35
Ti	$TiO_2$	3.6	$Ti_2O_3/TiO_2$ -0.556
Fe	$Fe_3O_4/Fe_2O_3$	1.6 2.2	$Fe_3O_4/Fe_2O_3$ 0.221
Pt	PtO	1.3	Pt/PtO 0.98
Brass	CuO	-	CuO/Cu -0.439
	ZnO		ZnO/Zn -0.262

\* Equilibrium potential of the corresponding metal oxide electrode (versus hydrogen electrode)

Films could not be formed on Al electrodes. This result suggests that an insulating layer was formed on the Al surface before or during the electropolymerization. Somewhat thinner insulating layers may also have formed on Ti and Fe although they didn't markedly affect the formation of PP films. The insulating layers were thought to be metal oxide films, since the polymerization potential is more positive than the equilibrium potentials of the metal oxide electrodes (See Table 2.1). The presence of an oxide film on a metal surface could reduce the rate of electron transfer by eight or nine orders of magnitude as compared with the unoxidized metal. Brass was unusual in this case; the presence of a thin oxide film seemed to be necessary for the formation of a PP coating [82].

Galvanostatic electropolymerization of PP films from various nonaqueous and aqueous electrolytes containing different anions on substrates including Pt, Au, Cu, Ti, stainless steel/V2A and Fe was studied by Schirmeisen et al.. Electrodeposition proceeded smoothly in many aqueous electrolytes when metals such as Pt, Au, V2A or Ti were used as electrodes. However when nonpassive metals, such as copper or iron, were employed as substrates in electrolytes with pH value below 7, the metals dissolved at the anodic potential required for polymerization. As a result, no coating was obtained. The only exception was a PP



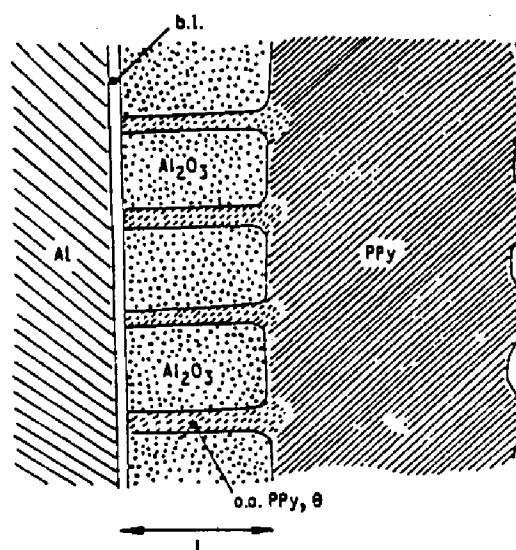


Figure 2.4: Cross-section view of a sandwich Al/Al<sub>2</sub>O<sub>3</sub>/Polypyrrole (after Hulser et al. [14]).

coating formed on Fe from an aqueous bath containing KNO<sub>3</sub> and pyrrole [84].

Hulser et al. [14] studied electropolymerization of pyrrole on aluminium in twenty aqueous electrolytes. To obtain homogeneous PP films, pretreatment of the metal by polishing with diamond spray at a rotating textile disk followed by galvanostatic activation in 0.1 M HNO<sub>3</sub>/0.1 M pyrrole was necessary. The purpose of anodic activation was to form uniform pitted pores (30 μm in diameter) on the oxide film (Al<sub>2</sub>O<sub>3</sub>) which were then partially filled with polymer. Bulk polymerization onto the pretreated substrate took place in aqueous electrolytes containing 0.1 to 0.8 M oxalic acid and 0.1 to 1 M pyrrole. A cross-section of an Al/Al<sub>2</sub>O<sub>3</sub>/PP sample is shown in Fig. 2.4.

Deng et al. found that P3MT films did not grow on the oxide layer (TiO<sub>2</sub>) of Ti. The conductive polymer had to be directly contacted with the bulk of the metal to make an adhesive coating [15].

McGee et al. deposited platinum-modified polypyrrole film on polished stainless steel (18/8 Cr/Ni) and used the composite electrode to decompose CCl<sub>4</sub>. 0.1 M pyrrole with 0.1 M

KCl aqueous solution was employed to anodically form the conductive polymer coatings [16].

## 2.6 Metal corrosion control by conductive polymers

Even though much work has been done on electrically conductive polymers, there has been little attention to metal corrosion control by these new materials. This may be attributed to the difficulty of forming adhesive polymer coatings on the surface of common metals and the relatively high expense of this type of coatings.

DeBerry first addressed corrosion protection of stainless steels with electrochemically polymerized polyaniline (PA) coatings. Type 410 and 430 stainless steels (410SS and 430SS) were used as substrate metals. The electroactive PA coatings were obtained in a 1.0 M aniline, pH 1.0 perchloric acid solution by cyclic voltammetry. The first few scans generated a passive metal oxide film on the substrate surface. Additional scans gradually built up a PA coating on top of the passive film. Electron transfer between the stainless steel metal phase and the PA coatings was assumed to be mediated by the passive film. Adhesion of the PA coatings on the employed metals was not discussed in the paper. The effect of PA coatings on metal corrosion behavior was first examined in chloride-free solutions. It was found that post-treatment of PA-coated metal affected the protectiveness of the coatings. Unless the PA-coated metal was first cycled in dilute sulfuric acid solution, the coating broke down after about 1 hour in deaerated 0.2 M  $\text{H}_2\text{SO}_4$ . With cycling, the life of the PA coating was extended to 17 hours. A post-treated PA coating was stable in 1.0 M sulfuric acid solution for 50 days. Uncoated samples became active and corroded within a few minutes. The corrosion current appeared to be balanced by oxygen reduction at the PA coating. Scratching the coating had little effect as should be expected for electrochemical as opposed to physical protection. In 0.2 M  $\text{H}_2\text{SO}_4$  + 0.2 M NaCl (PH=8), oscillations in the open-circuit potential around 0.1 V were observed. Apparently, the passive film was periodically undergoing localized breakdown in acid chloride solution and was then being healed with the aid of the coated PA coating. With a decrease in NaCl concentration, the

oscillation was reduced or stopped [9].

The application of P3MT films to stabilize the Ti/TiO<sub>2</sub> interface was proposed by Deng et al.. It was proposed that the role of electrically conductive polymers is to poise the potential of the oxide-covered metal within its passive range. To do so, the passive dissolution current of the metal must be compensated to stabilize the system. Coupling or coating the conductive polymer film to the passive film will result in an irreversible galvanic current and in turn discharge the polymer itself. Polymer discharge must therefore be balanced by reduction of oxygen. Based on this principle, platinum particles were deposited on the P3MT-coated glassy carbon electrode. The oxygen reduction rate in aqueous solution containing 0.1 M LiClO<sub>4</sub> was dramatically increased by the catalytic action of the Pt particles. The rate of oxygen reduction on the Pt-modified coating was sufficient to balance the passivation current and prevent the substrate from corroding [8].

# Chapter 3

## Experimental

### 3.1 Technique overview

Several techniques were used to evaluate the properties of P3MT coatings and their effectiveness for passivating metals:

- *Self-discharge and reversibility test*: The dependence of open-circuit potential ( $E_{oc}$ ) on time for P3MT-coated metals or bare metals in a given corrosive medium was recorded.  $E_{oc}$  is a measure of the charge-state of the polymer. Its stability or rate of discharge is a measure of the effectiveness of the coating in controlling the substrate potential.

- *Cyclic voltammetry (CV)*: In this technique, the potential of a RDE was scanned from an initial potential to a final potential and then back to the initial potential. The oxidation-current and reduction-current were plotted against potential (or time) to determine the charge capacity of P3MT coatings as well as to identify and evaluate the half cell reactions of the coated electrode.

- *Polarization diagrams*: Galvanostatic polarization diagrams or Tafel plots, are graphs of potential versus log current density. An illustration of the Tafel plot is shown in Fig. 3.1. Both the corrosion potential,  $\phi_{corr}$  (a mixed potential for the cathodic and anodic reactions in a corrosion process), and the corrosion current,  $i_{corr}$ , can be evaluated from the diagram. Tafel plots can also be used to measure the transpassive current. Potentiostatic polarization diagrams (current density changes with potential) can be used to investigate the passivation behavior of metals (see Fig. 3.1).

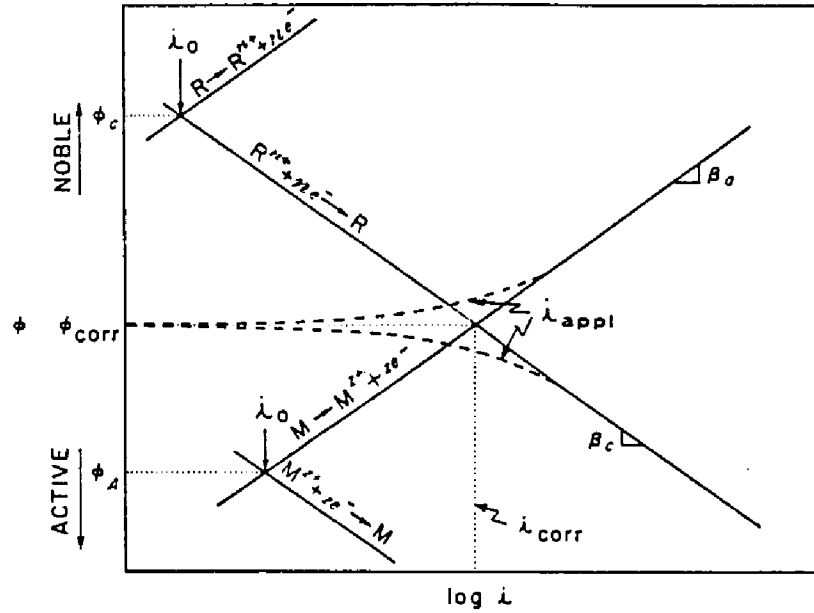


Figure 3.1: Introductory Tafel plot (after Uhlig [12]).

- *Galvanic corrosion tests:* A bare metal RDE (working electrode) is coupled with a P3MT-coated RDE (reference working electrode) in aqueous solution. The galvanic current between these two electrodes is recorded, indicating an interaction of the P3MT coating with the exposed metal surface. The self-discharge and self-recharge curves of the galvanic couple can also be plotted.

- *Gravimetric measurement:* Metal samples are weighed before and after corrosion testing to determine the amount of material lost.

- *Electrochemical Impedance Spectroscopy (EIS):* EIS has found a number of applications in the field of corrosion and protection [17]. EIS techniques use very small signals which do not disturb the electrode properties during measurement [18,19,20]. In EIS an electronic model can be used to represent an electrochemical cell. The electrode/electrolyte interface which undergoes an electrochemical reaction is modeled as an electronic circuit consisting of a combination of resistors and capacitors whose magnitudes can be related to specific electrochemical processes such as discharge and double-layer charging. The total

impedance ( $Z$ ) and the phase shift ( $\theta$ ) for each applied frequency can be obtained from the potential and current data. The dependence of those variables on frequency is used to obtain electrochemical information. In this study, Bode plots have been used to evaluate the stability of P3MT coatings on titanium in acid solutions.

## **3.2 Apparatus and Materials**

### **3.2.1 Potentiostat/Galvanostat system**

A model 273 Potentiostat/Galvanostat controlled by a computer (IBM System 2 Model 30) with Model 342 Corrosion Measurement Software and Head Start Electrochemistry Software installed was used for galvanostatic polymerization; polarization; cyclic voltammetry; potentiostat and galvanic corrosion measurements. Unless otherwise mentioned, all equipment was obtained from EG&G Princeton Applied Research Co. (EG&G PARC) (see Fig. 3.2).

For some experiments, a model 362 Scanning Potentiostat was used with a Model RE 0092 X-Y Recorder and a Model VD41 Strip Chart Recorder (Kipp & Zonen). The X-Y Recorder was only used for redox capacity measurements. The Strip Chart Recorder was employed for plotting self-discharge and reversibility test curves of a rotating disk electrode (RDE).

A Model 5210 Lock-in Amplifier, combined with the Model 273 Potentiostat, was used for AC impedance measurements. The experiment was controlled and analyzed by computer with a PARC Model 378 Electrochemical Impedance Software.

### **3.2.2 Electrolysis cell for rotating disk electrodes**

An electrolysis cell (Fig. 3.3), consisting of a Model 616 RDE cell (50 ml), a RDE, a reference electrode, a counter electrode and a gas-purge tube, was assembled for this study. The rotation rate of the RDE can be controlled up to 670 rad/s (6400 rpm). For galvanostatic polymerization of 3-methylthiophene (3MT) on RDEs, both reference and counter electrodes

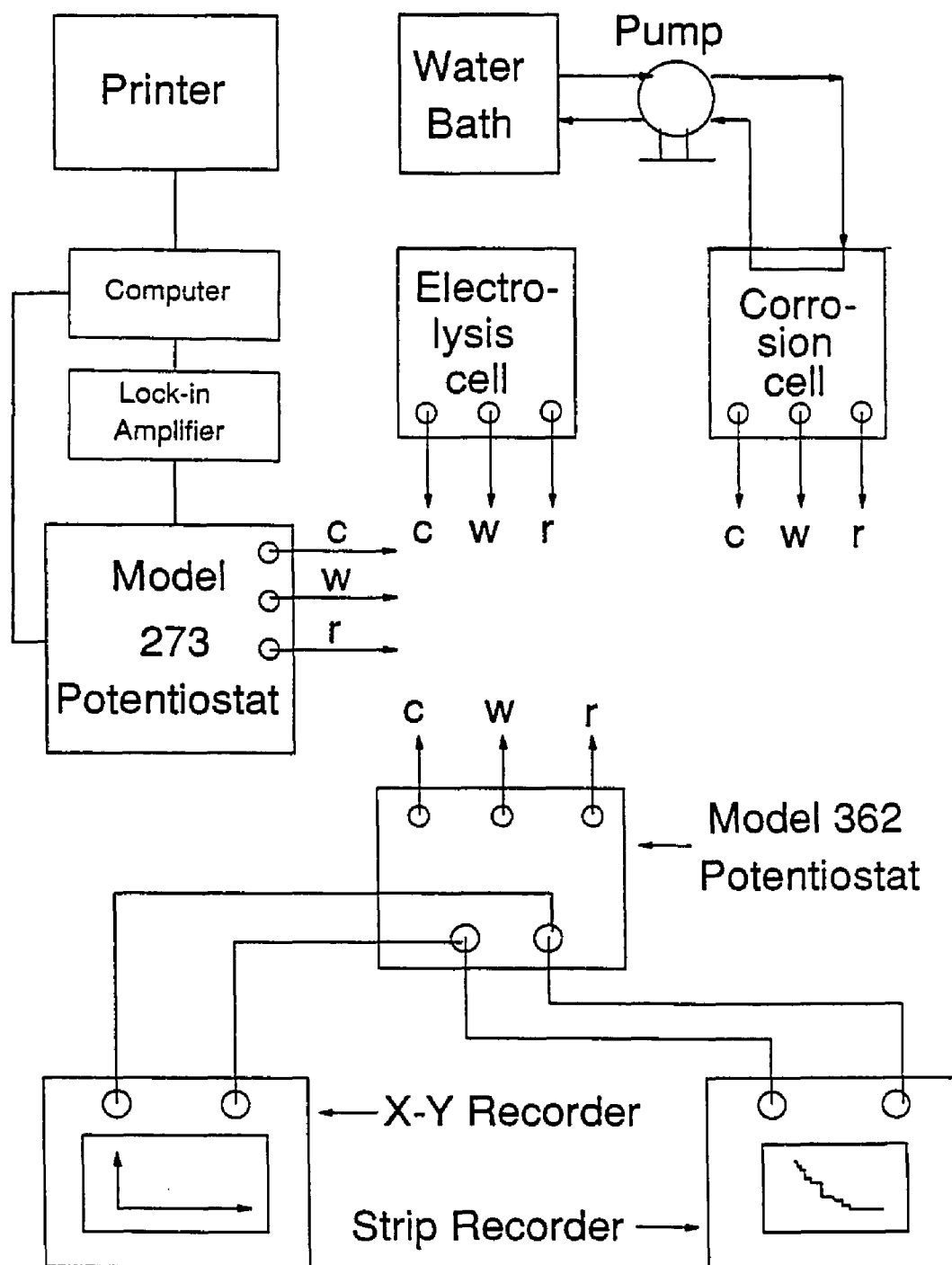


Figure 3.2: Corrosion research apparatus in this laboratory. w: working electrode, c: counter electrode, r: reference electrode

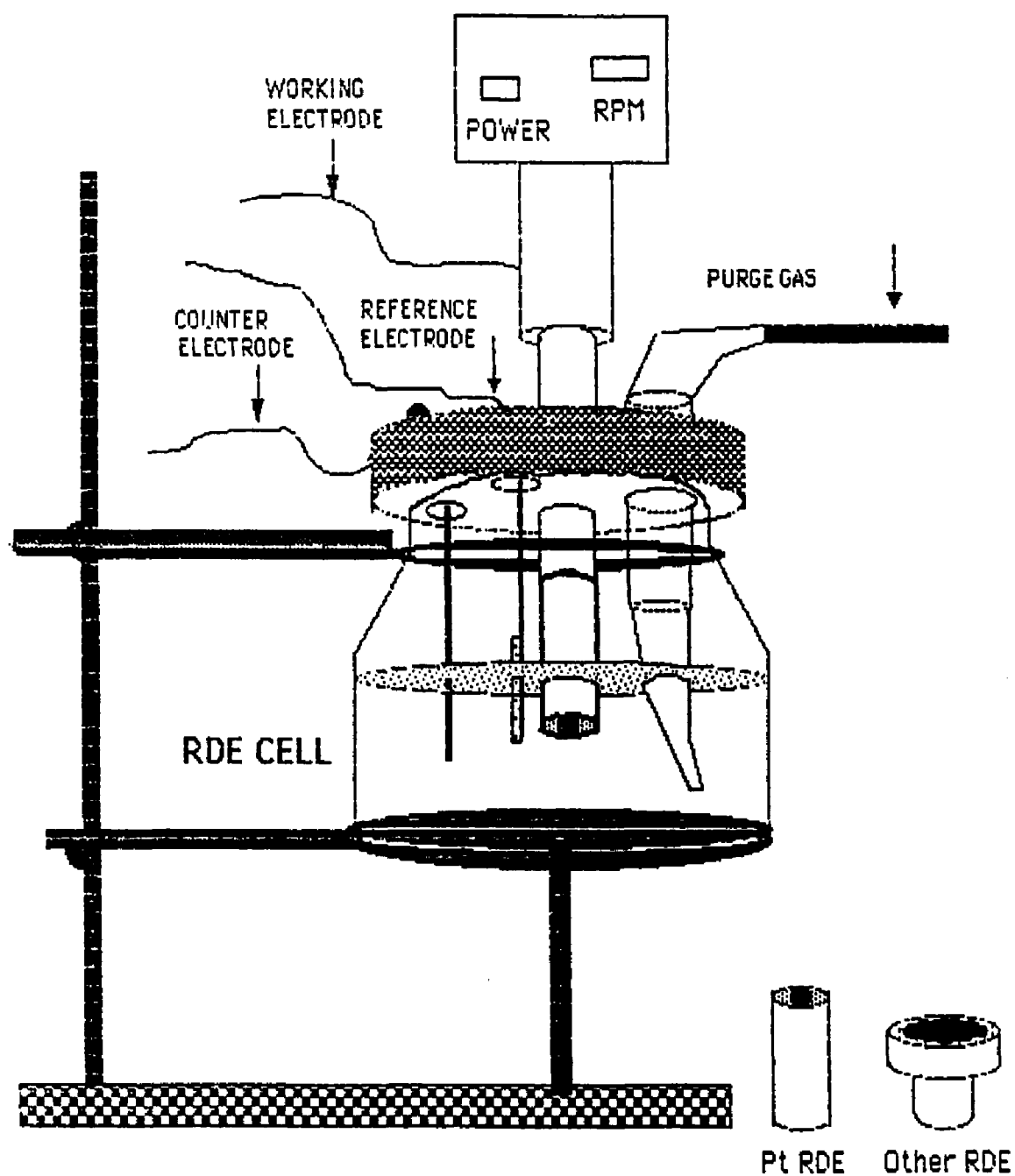


Figure 3.3: RDE electrolysis cell system.



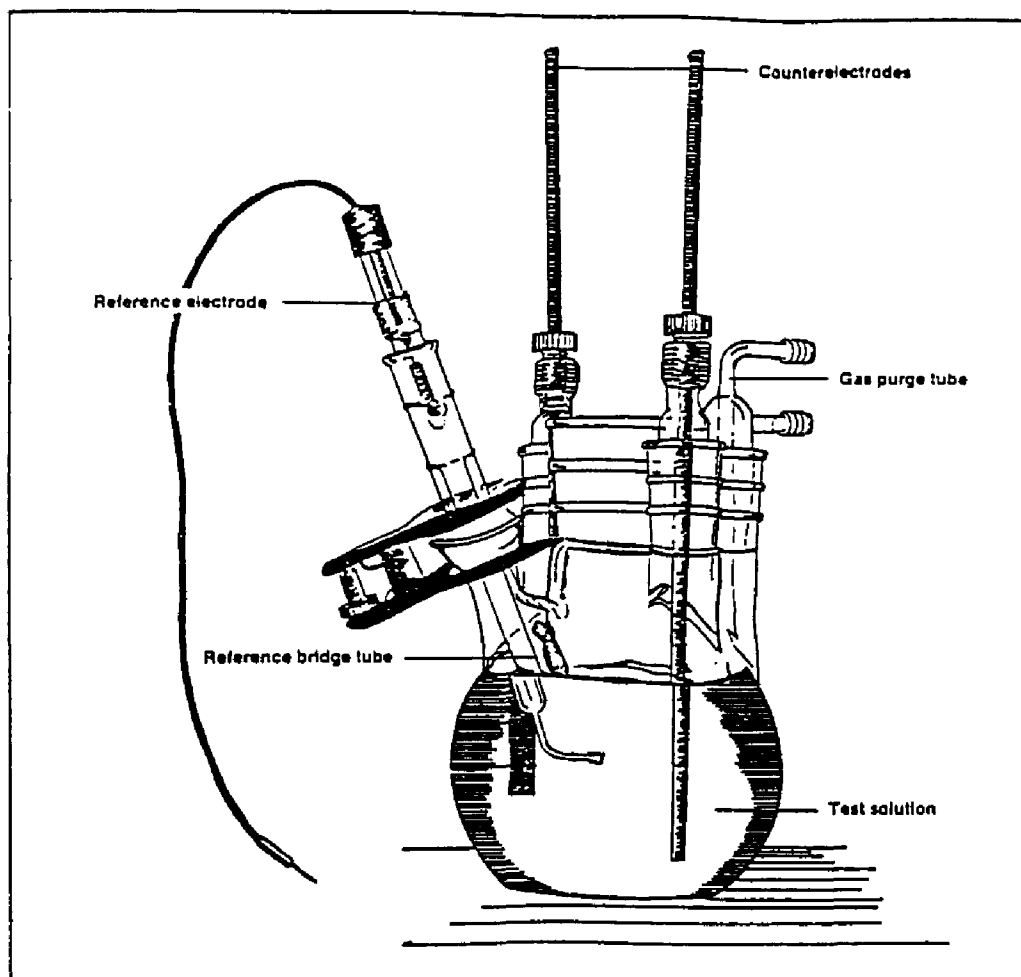


Figure 3.4: A typical corrosion cell.

were copper wires (1 mm in diameter). Nitrogen was purged into the monomer solution to remove dissolved oxygen.

### 3.2.3 Corrosion cell for rotating disk electrodes

A Model K47 Corrosion Cell System (1 L) is shown in Fig. 3.4. An Ag/AgCl reference electrode and two glassy carbon counter electrodes were used in this system. A gas-purge tube supplied air, nitrogen or oxygen. The Model 616 RDE controller was employed to hold

a RDE in the solution and control its rotation rate. A system for corrosion tests at elevated temperature is shown in Fig. 3.2 and will be described in detail in Chapter 7.

#### **3.2.4 Rotating disk electrodes (RDEs)**

The Pt RDE was made by EG&G PARC. The RDE is imbedded in a teflon sleeve and attached by a ceramic screw-cap holder (Fig. 3.3). The diameter of the RDE is 0.40 cm and the active area is 0.126 cm<sup>2</sup>.

Stainless Steel (430SS), Grade-2 Titanium (TiGr2) and Carbon Steel (C1010) RDEs were made by Metal Samples Co.. These replable RDEs were imbedded into a teflon sleeve (EG&G RDE001). An adaptor (EG&G RDE001) is employed to mount the sleeve and RDE onto the Model 616 RDE controller. The diameter of the metal RDEs is 1.128 cm and the active area is 1.0 cm<sup>2</sup>. The chemical and physical properties of the RDEs are listed in Appendix I.

#### **3.2.5 Chemical reagents**

The chemicals used in this study were 3-methylthiophene (3MT) (99+%, Aldrich); Tetra-butylammonium tetrafluoroborate (TBATFB) (99%, Aldrich); Propylene carbonate (99+%, Aldrich); Sulfuric acid (95.6%, Baker); Standard sulfuric acid solution (1 N, Baker); Nitric acid (71.09%, Fisher); o-Phosphoric acid (85%, Fisher); Hydrochloric acid (36.5% - 38.1%, Fisher); Potassium hydroxide (86.8%, Baker) and Sodium chloride (99.96%, VWR).

### **3.3 Procedures**

#### **3.3.1 Preparation of solutions**

A solution of 1.0 M 3MT in propylene carbonate was prepared for polymerization of P3MT coatings on pretreated RDEs. 0.1 M TBATFB was added to the solution as supporting electrolyte.

The test of P3MT-coated RDEs were conducted in various aqueous solutions summarized in Table 3.1. 1 N standard sulfuric acid solution was used as received. The nitric, hydrochloric and other sulfuric acid solutions were prepared from the received concentrated solutions. The KOH and NaCl solutions were prepared from reagent grade powder. Distilled water was used to prepare all aqueous solutions.

### 3.3.2 Electrode preparation

Electrode pretreatment played an important role in the performance of P3MT coatings. On platinum, it was found that if the electrode was not well cleaned, the P3MT coatings would have poor adhesion. The Pt RDEs were cleaned by scanning the potential from -1.0 V to 1.0 V at a rate of 50 mV/s in 1 N KOH aqueous solution for one hour. The disks were then rinsed for fifteen minutes in distilled water and for fifteen minutes in propylene carbonate before electropolymerization.

It was evident that P3MT coatings did not adhere to clean, mechanically polished 430SS, TiGr2 and C1010 RDEs. To firmly bond P3MT onto these metals, the substrate had to be pretreated in certain ways. To my knowledge, a successful method for pretreating these metals has not been reported before. In this study, a few methods have been developed to make these metals acceptable for P3MT coatings.

Fresh 430SS RDEs were first cleaned in a hot concentrated KOH solution and then rinsed with distilled water. The RDEs were then anodized at a potential of 2.0 V vs. Ag/AgCl for 33 min in 10% phosphoric acid solution. The phosphated 430SS (Ph430SS) RDE had a uniform microporous surface.

TiGr2 RDEs were first polished with 400 grit sandpaper and then degreased in boiling hexane for two minutes. They were then galvanostatically anodized at 10 mA/cm<sup>2</sup> and 0.52 rad/s (5 rpm) for 40 s in 0.5 M 3MT/0.1 M TBATFB containing 0.1 g/ml of zinc chloride (ZnCl<sub>2</sub>). The purpose of adding ZnCl<sub>2</sub> was to form pits in the titanium surface during electropolymerization of a thin P3MT strike layer. The pits provided a grip for the

Table 3.1: Classification of tests for P3MT-coated RDEs in aqueous solutions.

Aqueous Solutions	Coated Platinum	Coated Ph430SS	Coated TiGr2	Coated C1010
1 N H <sub>2</sub> SO <sub>4</sub>	Yes	Yes	Yes	Yes
4 N H <sub>2</sub> SO <sub>4</sub>			Yes	
Conc. H <sub>2</sub> SO <sub>4</sub>	Yes	Yes		
1 N HCl	Yes	Yes		
4 N HCl	Yes		Yes	
1 N HNO <sub>3</sub>	Yes	Yes		Yes
70% HNO <sub>3</sub>	Yes	Yes		
10% H <sub>3</sub> PO <sub>4</sub>	Yes			
2 N KOH	Yes	Yes		
Satur. KOH	Yes	Yes		
0.01 N NaCl		Yes		
0.10 N NaCl		Yes		
0.25 N NaCl		Yes		
1.00 N NaCl		Yes		Yes
1 N H <sub>2</sub> SO <sub>4</sub> + 1 N NaCl	Yes	Yes		
10% H <sub>3</sub> PO <sub>4</sub> + 1 N NaCl	Yes	Yes		

P3MT strike.

C1010 RDEs were first polished and degreased in the same manner as TiGr2 RDEs. To deposit an adhesive P3MT thin film on the surface of a C1010 RDE, 0.1 M 3MT/0.1 M TBATFB propylene carbonate solution containing 0.1 g/ml  $\text{ZnCl}_2$  was used. The polymerization condition was 500 mA/cm<sup>2</sup> and 0.52 rad/s (5 rpm) for 20 s.

To investigate the interaction between  $\text{TiO}_2$  oxide film and P3MT coatings through galvanic coupling, a  $\text{TiO}_2$  thick film was formed on the surface of the TiGr2 RDE. To do this, the electrode was immersed in 1 N sulfuric acid solution and scanned from 0.0 V to 3.0 V at a rate of 1 mV/s [8]. This treatment produced a bright and smooth surface.

### 3.3.3 Operation of the electrolysis cell

P3MT coatings were formed by galvanostatic polymerization in 1.0 M 3MT/0.1 M TBATFB propylene carbonate solution under a nitrogen purge on the pretreated electrodes. Applied deposition current densities ( $i_d$ ) ranged from 8.0 to 10<sup>3</sup> mA/cm<sup>2</sup>. The rotation rate,  $\Omega$ , of the RDEs was varied between 2.6 and 670 rad/s (25 to 6400 rpm).

P3MT films were deposited to various thickness on the Pt RDE. Deposit charge density varied between 0.1 and 2.4 C/cm<sup>2</sup>. 3MT electropolymerization on Ph430SS, TiGr2 and C1010 was carried out to a constant charge density of 1.5 C/cm<sup>2</sup>.

The P3MT-coated electrodes were rinsed in propylene carbonate for 15-30 min (depending on the coating thickness) to remove residual monomer, then rinsed in distilled water for another 15-30 min to remove the propylene carbonate. The cleaned composite RDEs were then transferred to an aqueous solution in a corrosion cell to test their performance.

### 3.3.4 Operation of the corrosion cell

Unless otherwise mentioned, all electrodes were rotated at a rate of 105 rad/s (1000 rpm) in the test solutions at room temperature (about 22°C). Tafel plots (or polarization curves) were obtained at a scan rate of 0.2 mV/s in various aqueous solutions with or without gas

purge. Cyclic voltammetry (CV) was conducted in a given potential range at a scan rate of 20 mV/s in aqueous solutions.

To record a self-discharge (or reversibility test) curve, a sample was first held at an initial potential for a period of time before the circuit was opened.

In the galvanic corrosion test, a metal RDE (working electrode) and a P3MT-coated RDE (reference working electrode) were placed in electrical contact through an insulated copper wire attached to the external leads. The working electrode was rotating at 105 rad/s while the reference working electrode was kept stationary. Both self-discharge and reversibility test curves of the working electrode were recorded. Galvanic current between the coupled electrodes was measured sometimes.

To evaluate the degree of P3MT coating degradation in strong acid and base solutions, a coated Ph430SS electrode was immersed in a corrosive medium for 2 hours at a rotation rate of 10.5 rad/s. Then 50% of the P3MT coating was cut off from the substrate (Ph430SS) to partially expose the metal and make a galvanic sample. The self-discharge curve of the sample was plotted in 1 N air-saturated sulfuric acid solution.

Electrochemical Impedance Spectroscopy (EIS) was used to evaluate the stability of P3MT coatings on TiGr2 in 1 N sulfuric acid solution. Bode plots were obtained over a frequency range between  $10^{-3}$  to  $10^5$  Hz.

### 3.3.5 Coulometry

For the quantitative measurement of the film redox capacity,  $C_p$ , of P3MT coatings, the films were first polymerized on the Pt RDE at different deposition conditions. The coating was then immersed in 0.1 M TBATFB propylene carbonate solution without monomer. A cyclic voltammogram at a scan rate of 100 mV/s was recorded. A compensating Polar Planimeter (Keuffel & Esser Co.) was used to integrate the cathodic peak of the voltammogram. The current charge due to double-layer charging was neglected at this low scan rate. The Polar Planimeter has a fixed tracer arm and it reads directly in square centimeters to tenths,

that is 1 vernier unit = 0.1 cm<sup>2</sup>. Every current peak was measured three times, an average vernier number (AVN) as well as an average peak area were obtained by the measurement. The charge passed due to reduction of a P3MT coating can be calculated by,

$$C_p = \frac{A_c * C_t}{A_w} \quad (3.3.1)$$

where  $A_c$  is the measured cathodic peak area,  $A_w$  the whole graph area and  $C_t$  the charge corresponding to the whole graph area, which can be calculated based on the values of scan rate and current range.

For the kinetic study of coating discharge, the charge capacity,  $C_a$ , of P3MT coatings was measured against potential in 1 N air-saturated sulfuric acid solution at a scan rate of 5 mV/s. The Polar Planimeter was also used for this purpose.

## Chapter 4

# Effect of Deposition Conditions on Coating Properties

A stable and adherant P3MT coating is a primary criterion for corrosion protection of the substrate metal. Based on previous investigations [36,37,38,39,40,43,41], polymerization conditions have a substantial effect on the properties of conductive polymers. However, we are not aware of any studies of electrochemically deposited coatings in which deposition rate and transport conditions were varied independently.

In this study, electropolymerization and deposition were conducted galvanostatically. The effects of various parameters, such as deposition current density ( $i_d$ ), rotation rate ( $\Omega$ ) of the RDE and deposition time ( $t_d$ ), on coating properties were studied systematically. Platinum (Pt) RDEs were primarily used for this purpose owing to their inert nature. The deposit charge density ( $i_d * t_d$ ) was fixed at 0.48 C/cm<sup>2</sup> for coatings on Pt and 1.50 C/cm<sup>2</sup> for coatings on other RDEs when the effect of either  $i_d$  or  $\Omega$  was investigated.

### 4.1 Coating morphology

P3MT coatings prepared electrochemically on Pt were apparently smooth and uniform and were deep blue or black for all conditions tested.

On Ph430SS, the uniformity of the dull black coatings depended on deposition conditions. At a fixed deposit charge density, increase of rotation rate ( $\Omega$ ) increased the uniformity of the coatings in the case of low  $i_d$  (10.5 mA/cm<sup>2</sup>). However, at a high  $i_d$



(210 mA/cm<sup>2</sup>), higher rotation rates produced non-uniform coatings, with a spiral-pattern of striations and incomplete coverage. When the rotation rate was further increased beyond 105 rad/s (1000 rpm), the coating became uniform again. The reason for this phenomenon is unknown. At constant rotation rate and deposition charge, higher deposition current density ( $i_d$ ) produced a thicker coating. A similar effect of deposition conditions on coating morphology was observed for P3MT coatings on TiGr2 and C1010. Effect of rotation rate on coating morphology is illustrated in Fig. 4.1. A low rotation rate gives a high concentration of radical cations (e.g.,  $R_+^{\cdot}$ ) on the electrode surface. This results in more complete occupation of nucleation sites and finally generates a thick coating with small hemispheres. On the other hand, a high rotation rate convects radical cations away from the metal surface and generates a thin coating with bigger hemispheres.

## 4.2 Exchange current density

The effect of deposition conditions on the exchange current density,  $i_0$ , of P3MT-coated Pt RDEs was examined. The exchange current density is defined on the basis of the superficial area of the electrode (0.13 cm<sup>2</sup>). The exchange current represents steady reduction of some species in solution, probably O<sub>2</sub>, excluding any transient processes, such as intercalation or film reduction.  $i_0$  values for P3MT coatings in different aqueous media were measured by Tafel plots. The results are shown in Table 4.1. It was evident that the exchange current density in sulfuric acid solutions depends strongly on the concentration of O<sub>2</sub> in solution. It is likely that oxygen reduction is the principal reduction process under these conditions. Low  $i_0$  values in NaOH solutions are attributed to deactivation of the polymer at high pH (refer to Chapter 6).

To test the reversibility of oxygen reduction by P3MT coatings, a P3MT-coated Pt RDE, a scratched P3MT-coated Pt RDE and a clean Pt RDE were each immersed in 1 N sulfuric acid solution at a rotation rate of 105 rad/s. The solution was purged alternately with nitrogen and oxygen. The open-circuit potentials ( $E_{oc}$ ) vs. time are plotted in Fig 4.2.

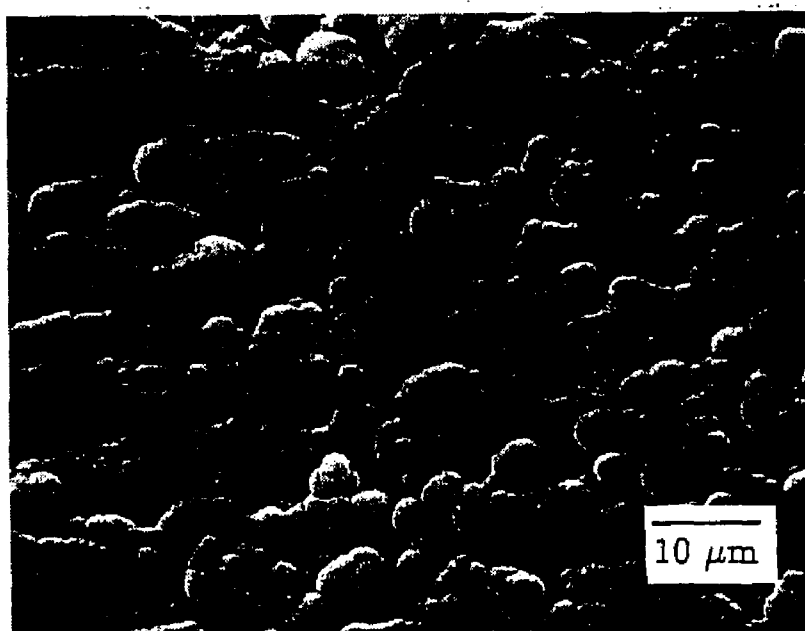
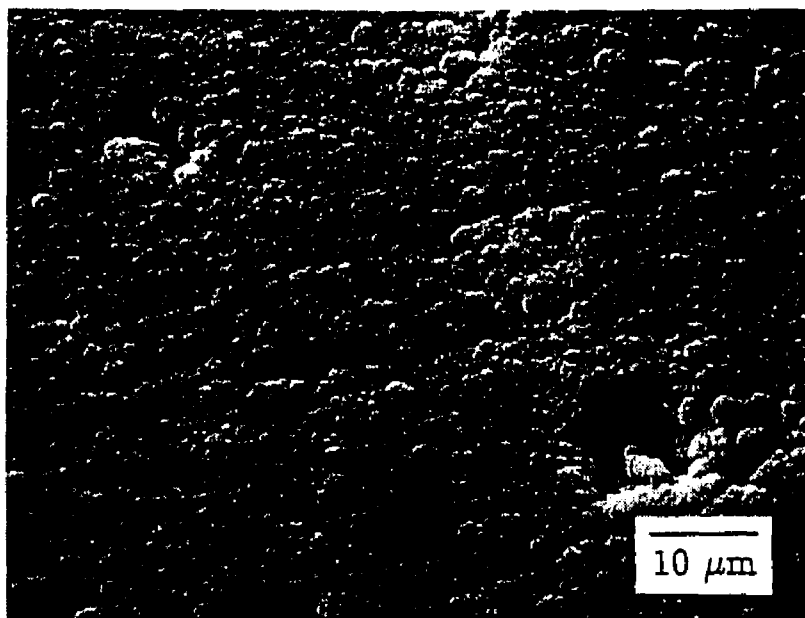


Figure 4.1: SEM micrographs of P3MT coatings on C1010. Film deposition conditions:  
*Top:* 200 mA/cm<sup>2</sup>, 1.57 rad/s. *Bottom:* 200 mA/cm<sup>2</sup>, 105 rad/s.

Table 4.1:  $i_0$  of P3MT coatings in aqueous solutions ( $\mu\text{A}$ ). Deposition condition:  $i_d=159 \text{ mA/cm}^2$ ,  $\Omega=2.62 \text{ rad/s}$ .

Solution	O <sub>2</sub>	Air	N <sub>2</sub>
1 N H <sub>2</sub> SO <sub>4</sub>	8.60	5.73	0.12
4 N H <sub>2</sub> SO <sub>4</sub>	9.4		0.24
0.1 N NaOH	0.955		0.637
1 N NaOH	1.67		1.27

The P3MT-coated Pt showed no response to oxygen, while the electrodes with exposed platinum did. The larger the exposed Pt area, the greater the response was to oxygen. The P3MT coatings were not reversible oxygen electrodes. However, the data in Table 4.1 suggest that the oxygen reduction is the principal steady-state reaction when the potential is shifted negative of  $E_{oc}$ .

Consecutive measurements of  $i_0$  were conducted on a P3MT-coated Pt RDE with a rotation rate of 105 rad/s in 1 N air-saturated sulfuric acid solution within thirty hours. The  $i_0$  value decreased about  $0.7 \mu\text{A/cm}^2$  after two hours and then remained almost constant for the rest of the time period. This indicates that the coating was stable and did not become deactivated in thirty hours.

For P3MT-coated Pt RDEs, the exchange current in 1 N air-saturated sulfuric acid solution varied with coating deposition conditions. At the given deposit charge density, the effect of deposition conditions on  $i_0$  is shown in Fig. 4.3.  $i_0$  increased with decreasing  $\Omega$  and increased up to a limiting value with increasing  $i_d$ . Both results are consistent with the view that coating thickness increases with increasing current density and decreases with increasing rotation rate.

A plot of  $i_0$  vs. deposition time ( $t_d$ ) at constant  $i_d$  and  $\Omega$  is shown in Fig. 4.4. The exchange current approached a limiting value with increasing  $t_d$  and then decreased with

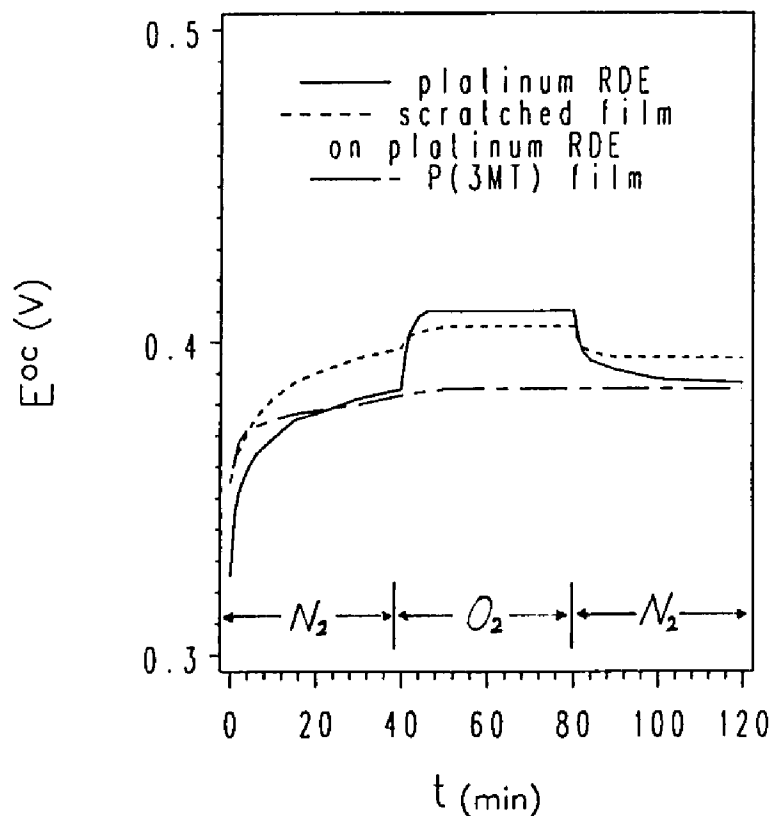


Figure 4.2: Effect of purge gas on open circuit potentials of P3MT coating and scratched P3MT coating on Pt RDE as well as Pt RDE itself in 1 N sulfuric acid solution.

further increase of deposition time. It is possible that the diffusion of gas molecules inside the thicker P3MT coatings may restrict the exchange current of the composite RDEs.

### 4.3 Redox capacity of P3MT coatings

The redox capacity,  $C_p$ , in propylene carbonate is a measure of the coating thickness and reversibility [54]. It was measured by integration of the cathodic charging current [54] in cyclic voltammetry (CV) from -1.0 V to +1.75 V. The cathodic peak charging current,  $i_p$ , was a linear function of scan rate up to 100 mV/s. A scan rate of 100 mV/s was used based on the assumption that the charging process is not limited by mass transport at scan rates

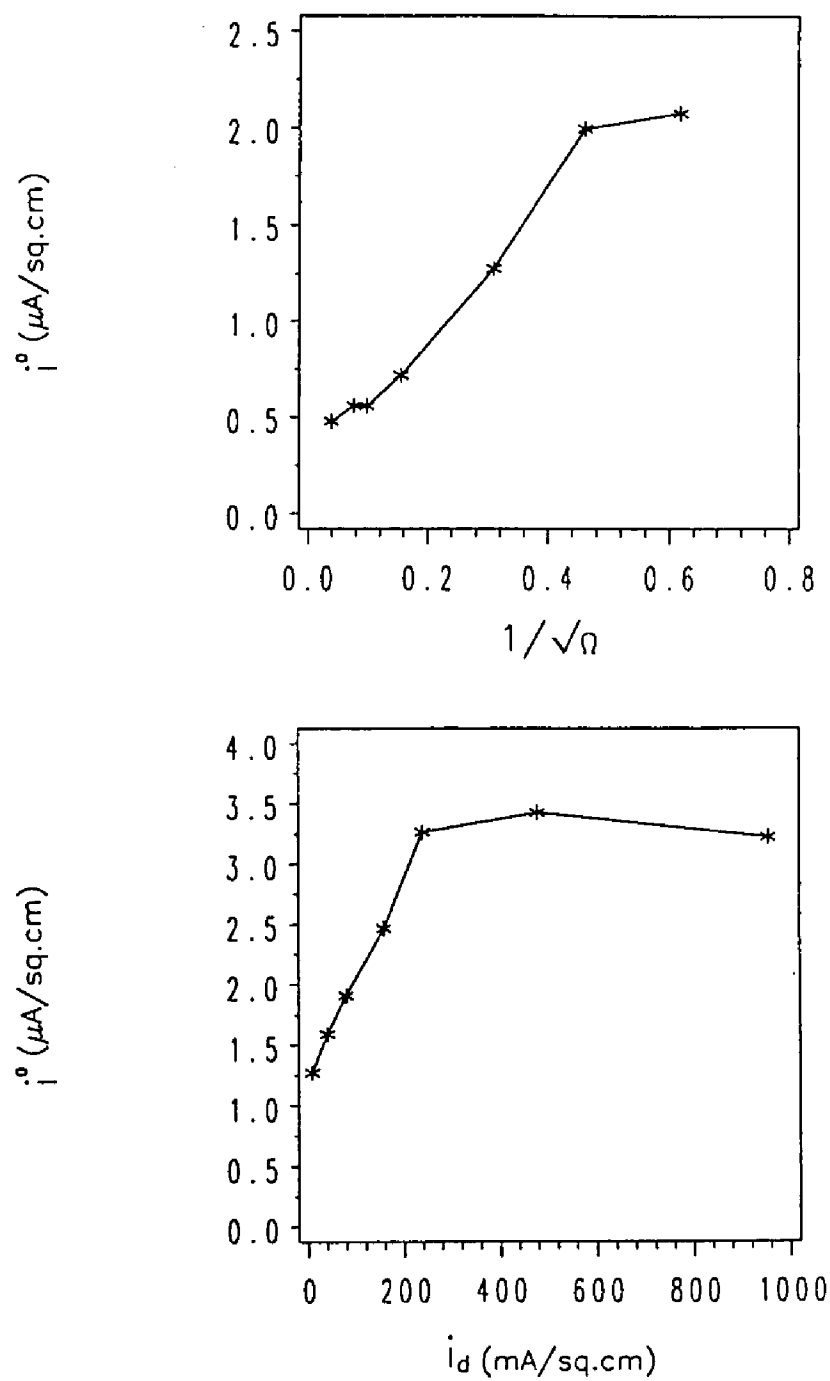


Figure 4.3: Exchange current density,  $i_0$ , of P3MT-coated Pt RDE. *Top:* versus  $\Omega^{-1/2}$  at  $i_d=8.0$  mA/cm<sup>2</sup>, *Bottom:* versus  $i_d$  at  $\Omega=10.5$  rad/s.

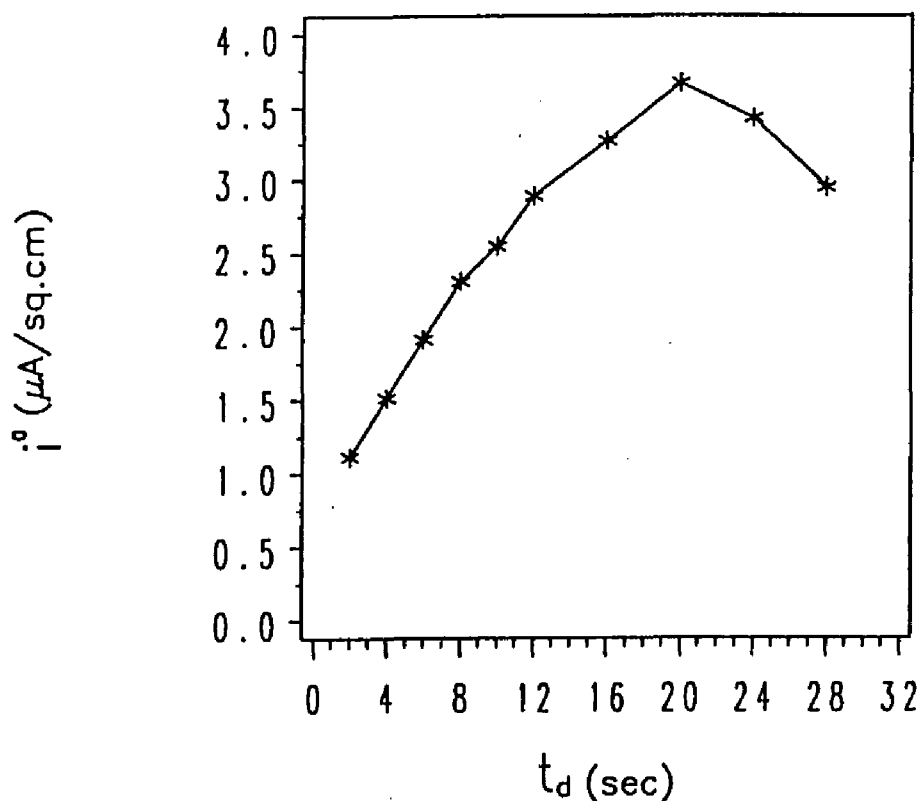


Figure 4.4: Effect of the deposition time during 3MT polymerization on  $i_0$ .  $i_d=80 \text{ mA}/\text{cm}^2$  and  $\Omega=10.5 \text{ rad/s}$  on Pt RDE.

below  $100 \text{ mV/s}$  (the linear range).

The effect of deposition conditions on the redox capacity (or the thickness) is illustrated in Fig. 4.5. It is evident that an increase of rotation rate,  $\Omega$ , or decrease of  $\Omega^{-1/2}$ , decreases the  $C_p$ . As deposition current density,  $i_d$ , was increased, the effect of the rotation rate ( $\Omega$ ) on  $C_p$  became weaker.  $C_p$  increased up to a maximum value with increasing  $i_d$ . A decrease of  $C_p$  was observed with increasing  $i_d$  beyond  $500 \text{ mA}/\text{cm}^2$ . It could be that at very high interfacial concentrations some step other than mass-transfer limited the rate of deposition. At fixed  $i_d$  and  $\Omega$ ,  $C_p$  is proportional to deposition time (see Fig. 4.6).

Based on the correlation between charge capacity and film thickness [8], P3MT coating thickness varies from one to ten micrometers in our case. Thicker coatings with higher

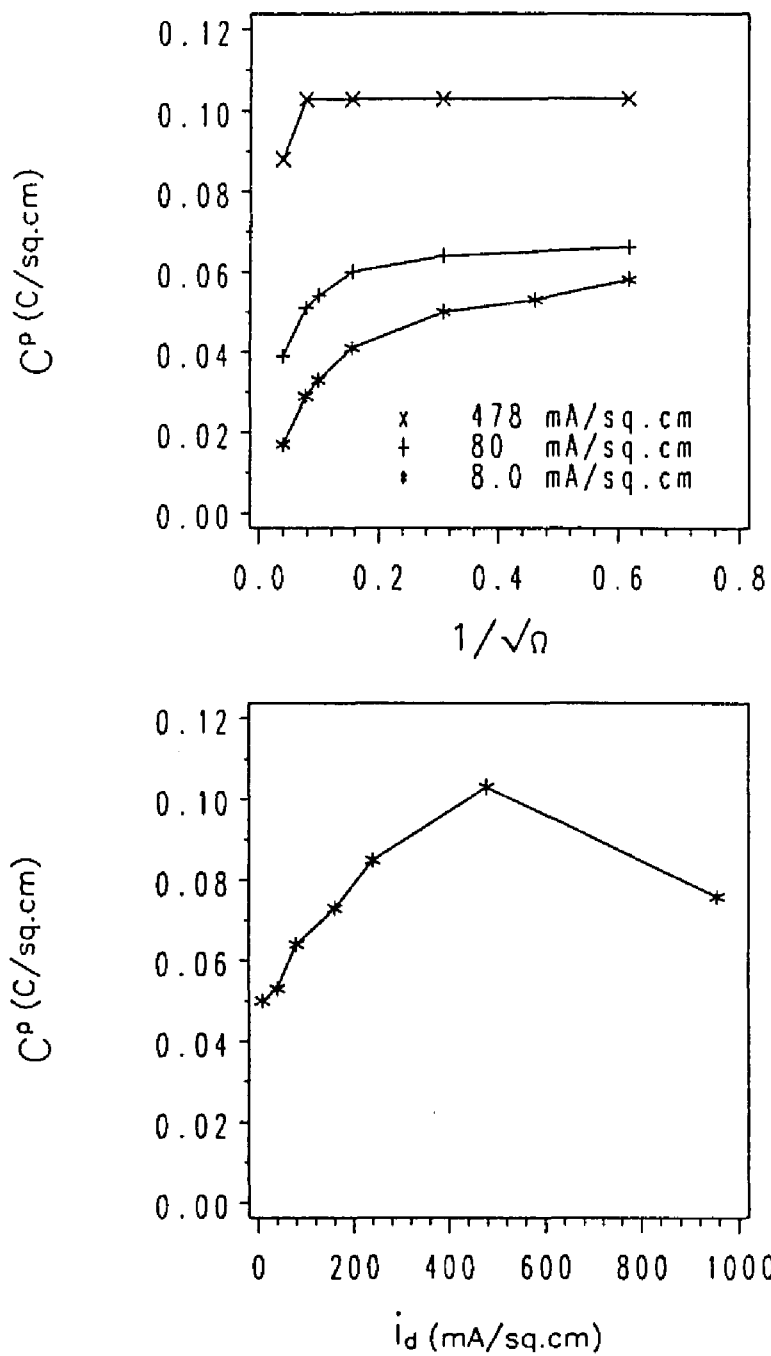


Figure 4.5: Redox capacity of P3MT coatings on Pt RDE in propylene carbonate. *Top:* versus  $\Omega^{-1/2}$  at  $i_d=8.0$ ; 80 and 480 mA/cm<sup>2</sup>, *Bottom:* versus  $i_d$  at  $\Omega=10.5$  rad/s.

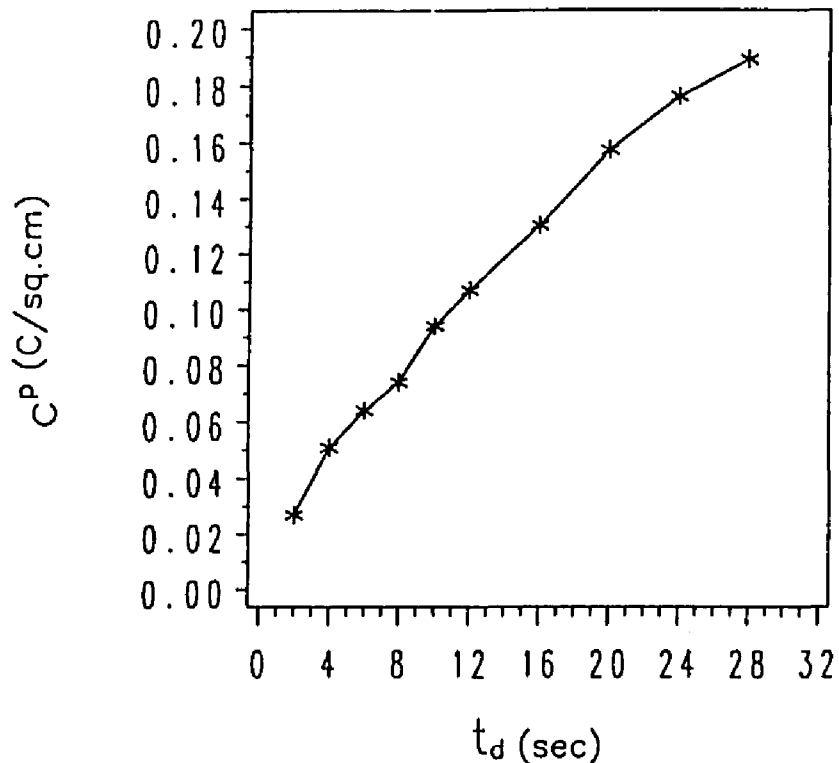


Figure 4.6: Redox capacity of P3MT coatings on Pt RDEs varied with deposition time during 3MT polymerization.  $i_d=80 \text{ mA/cm}^2$ ,  $\Omega=10.5 \text{ rad/s}$ .

redox capacity were produced at higher deposition current density and lower rotation rate. This dependence is probably due to the resulting higher concentration of free radicals at the electrode-solution interface during deposition. Under these conditions, more oxidized monomers are deposited and less are convected away from the substrate.

#### 4.4 Self-discharge of P3MT coatings

Drift of the open circuit potential,  $E_{oc}$  of an oxidized electroactive polymer coating toward a negative value in aqueous solution indicates discharge of the coating by a chemical process [8]. The self-discharge curve (i.e., an open circuit potential,  $E_{oc}$ , vs. time curve of an



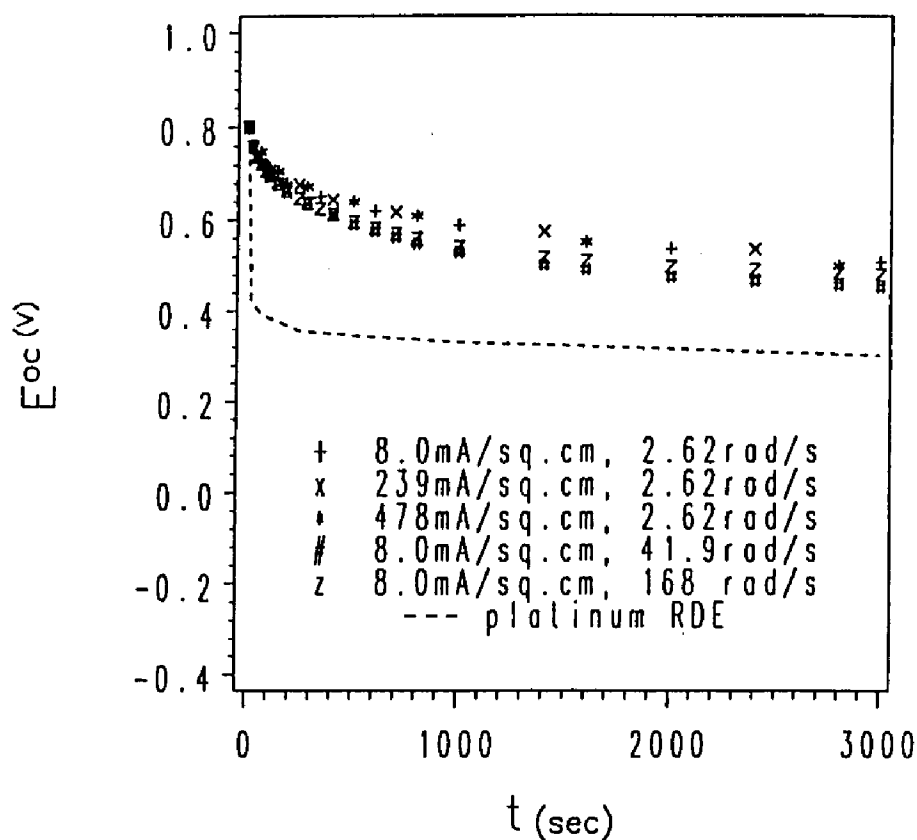


Figure 4.7: Self-discharge curves of P3MT coatings on Pt RDEs in 1 N air-saturated sulfuric acid solution.

oxidized coating) is a measure of the kinetics of this charge capacity decay. In this study, self-discharge behaviors of oxidized P3MT coatings on both Pt and Ph430SS RDEs were investigated in 1 N sulfuric acid solution as they depend on coating preparation conditions. All of the self-discharge data were obtained at a constant rotation of 105 rad/s.

To examine the self-discharge behavior, P3MT coatings were first deposited onto Pt RDEs (deposit charge:  $0.48 \text{ C/cm}^2$ ) and then immersed in 1 N air-saturated sulfuric acid solution. The RDEs were then held at a positive potential (0.8 V). After two minutes, the circuit was opened and the self-discharge curves were recorded for 50 min. The self-discharge curves of P3MT coatings prepared at different deposition conditions on Pt RDEs are shown in Fig. 4.7. Coating deposition conditions had little effect when Pt substrates

were used.

Charge capacity ( $C_a$ ) vs. potential curves of the coatings were obtained in 1 N air-saturated sulfuric acid solution in a potential range between 0.0 V and 0.8 V. A P3MT-coated Pt RDE was first immersed in the solution. Cyclic voltammograms were then recorded between 0.0 V and a vertex potential (less than or equal to 0.8 V) at a scan rate of 5 mV/s. The charging peaks in the voltammograms were then integrated to obtain the charge capacities corresponding to the different vertex potentials. The vertex potential of the voltametric sweep is the potential indicated in the capacity-potential curves.

The charge capacity ( $C_a$ ) vs. potential (E) curves of P3MT coatings prepared at several deposition conditions are shown in Fig. 4.8. Increase of  $\Omega$  decreases the charge capacity ( $C_a$ ) of the coating, with the exception of the points at 168 rad/s.  $C_a$  increases with increasing  $i_d$ .

The data from the self-discharge curves can be displayed in plots of  $1/C_a$  vs. time (see Fig. 4.9). If the assumption of a second-order decay process is made [8], each curve of  $1/C_a$  vs. time shows a dynamic transition from a higher decay coefficient,  $k_1$ , to a lower decay coefficient,  $k_2$ . Both  $k_1$  and  $k_2$  are plotted against  $\Omega$  and  $i_d$  in Fig. 4.10. It can be seen that with increasing  $i_d$ ,  $k_1$  decreases.  $k_2$  is small in all cases. A higher current density ( $i_d$ ) produces a coating with a lower initial charge-capacity decay rate. One expects that  $k_1$  should also decrease with decreasing  $\Omega$  (or increasing  $\Omega^{-1/2}$ ), although the data do not permit a definite conclusion (see Fig. 4.10). Both conditions correspond to a thicker coating.

To test the charge capacity decay of a P3MT coating with potential cycles in solution, a P3MT-coated Pt RDE was immersed in the acid solution and repeatedly scanned between 0.0 V and 0.8 V at a scan rate of 100 mV/s. The corresponding charge capacities were measured every few cycles. A plot of  $1/C_a$  vs. number of cycles is given in Fig. 4.11. A linear correlation between  $1/C_a$  and number of cycles was obtained within 27 CV cycles. The capacity decay coefficient,  $k(c)$ , derived from this measurement is shown in the figure.

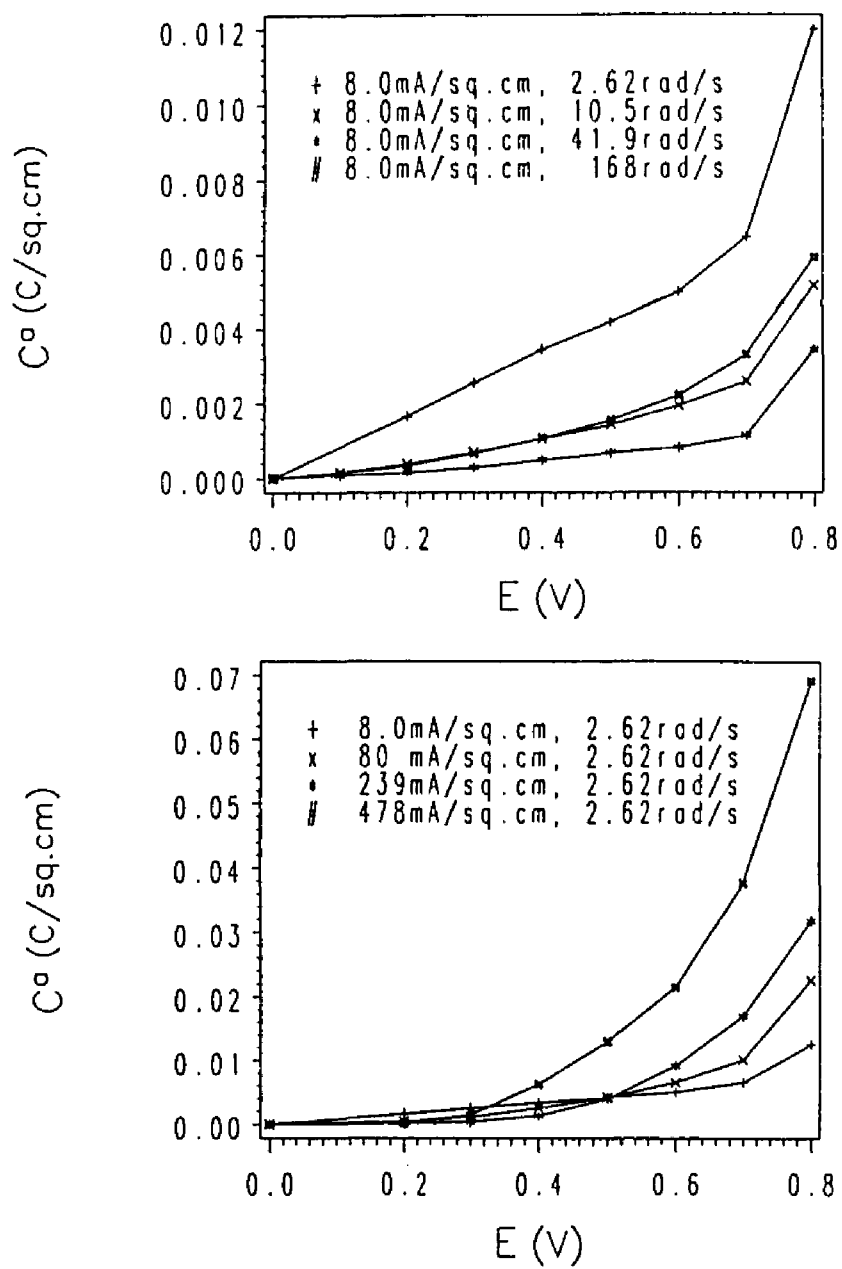


Figure 4.8: Charge capacity of P3MT coatings on Pt RDEs versus potential. *Top*: as a function of  $\Omega^{-1/2}$  at  $i_d = 8.0 \text{ mA/cm}^2$ , *Bottom*: as a function of  $i_d$  at  $\Omega = 2.62 \text{ rad/s}$ .

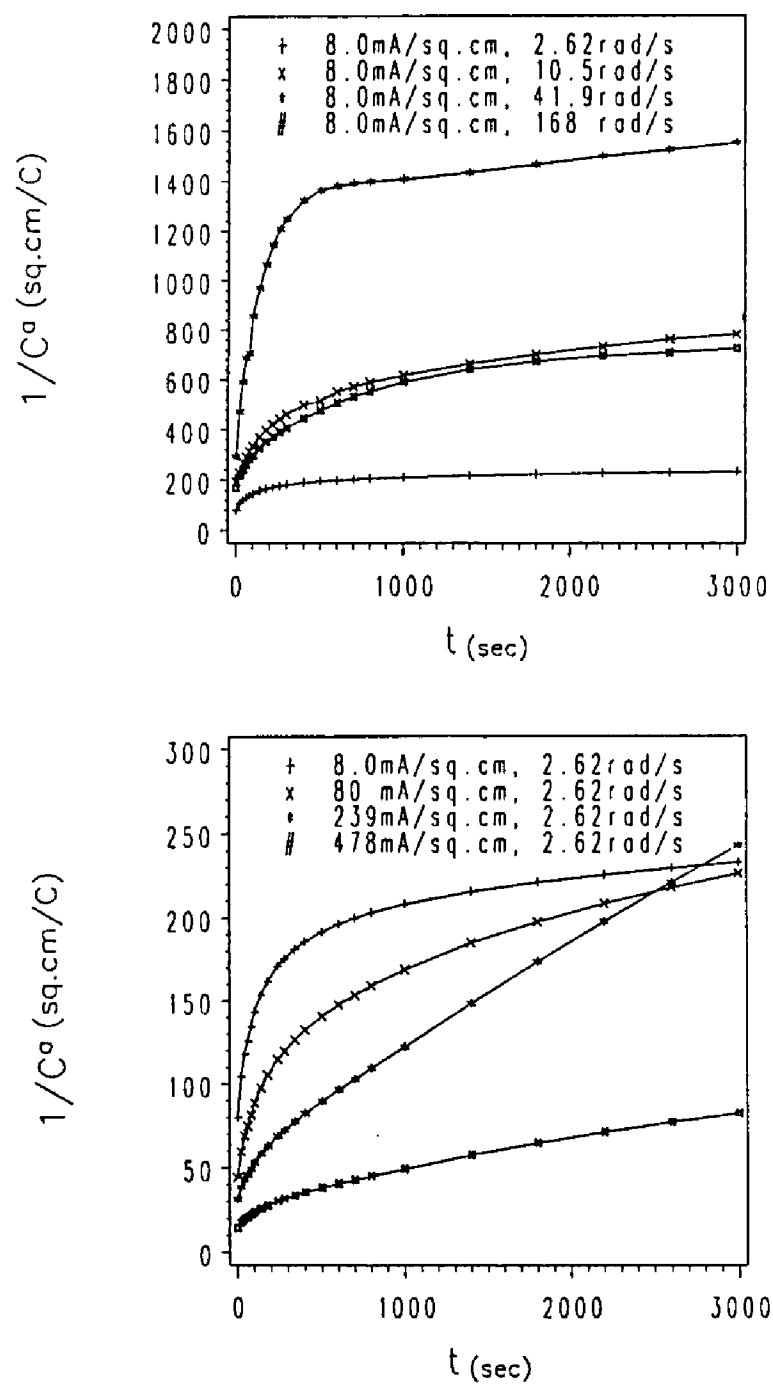


Figure 4.9: Inverse of the charge capacity of P3MT coatings versus time. *Top*: as a function of  $\Omega^{-1/2}$  at  $i_d = 8.0 \text{ mA/cm}^2$ , *Bottom*: as a function of  $i_d$  at  $\Omega = 2.62 \text{ rad/s}$ .

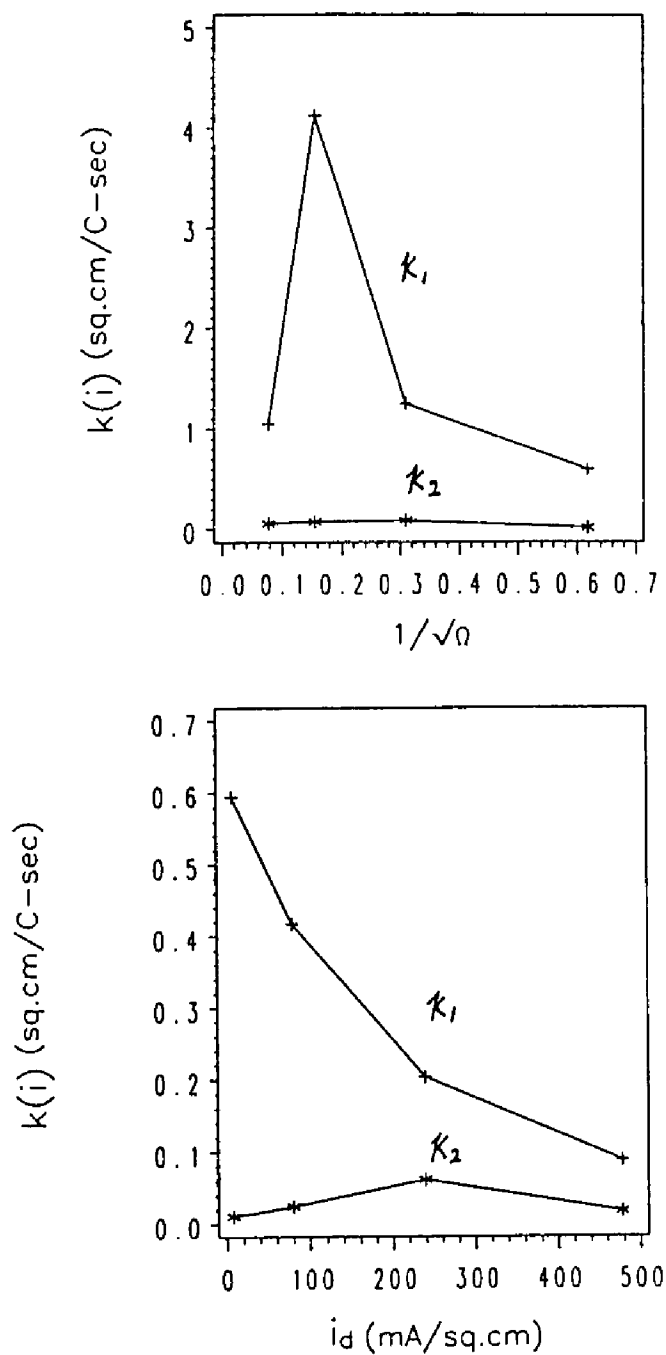


Figure 4.10: Initial and final charge decay coefficients for a second-order decay mechanism.  
*Top:* versus  $\Omega^{-1/2}$  at  $i_d = 8.0 \text{ mA/cm}^2$ , *Bottom:* versus  $i_d$  at  $\Omega = 2.62 \text{ rad/s}$ .

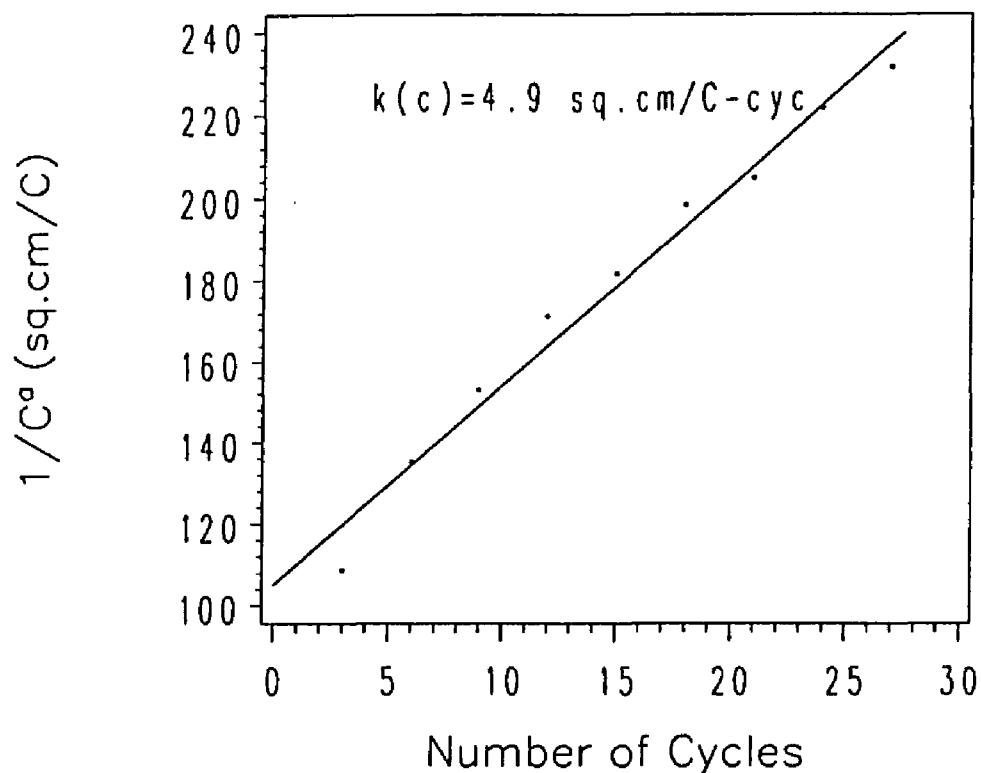


Figure 4.11: Inverse of the charge capacity of a P3MT coating versus number of potential cycles in 1 N air-saturated sulfuric acid solution. Deposition condition:  $i_d=80 \text{ mA/cm}^2$ ,  $\Omega=2.62 \text{ rad/s}$ .

The steady open-circuit potential of a P3MT-coated Ph430SS RDE (deposit charge:  $1.58 \text{ C/cm}^2$ ) in 1 N air-saturated sulfuric acid solution was obtained by holding the sample in the solution for 5 h until the open-circuit potential approached a steady value  $E_{oc}(st)$ . The dependence of  $E_{oc}(st)$  on coating preparation conditions is shown in Fig. 4.12. At constant  $i_d$ ,  $\Omega$  has little effect on  $E_{oc}(st)$ . Increase of  $\Omega$ , or decrease of  $\Omega^{-1/2}$ , slightly decreases  $E_{oc}(st)$ . On the other hand,  $i_d$  has a substantial effect on subsequent open-circuit behavior. With increasing  $i_d$ ,  $E_{oc}(st)$  first decreased and then became constant around a value of  $+0.35 \text{ mV}$ . In every case, it is within the passive potential range of our steel samples (from  $0.3 \text{ V}$  to  $0.8 \text{ V}$  in 1 N air-saturated sulfuric acid solution).

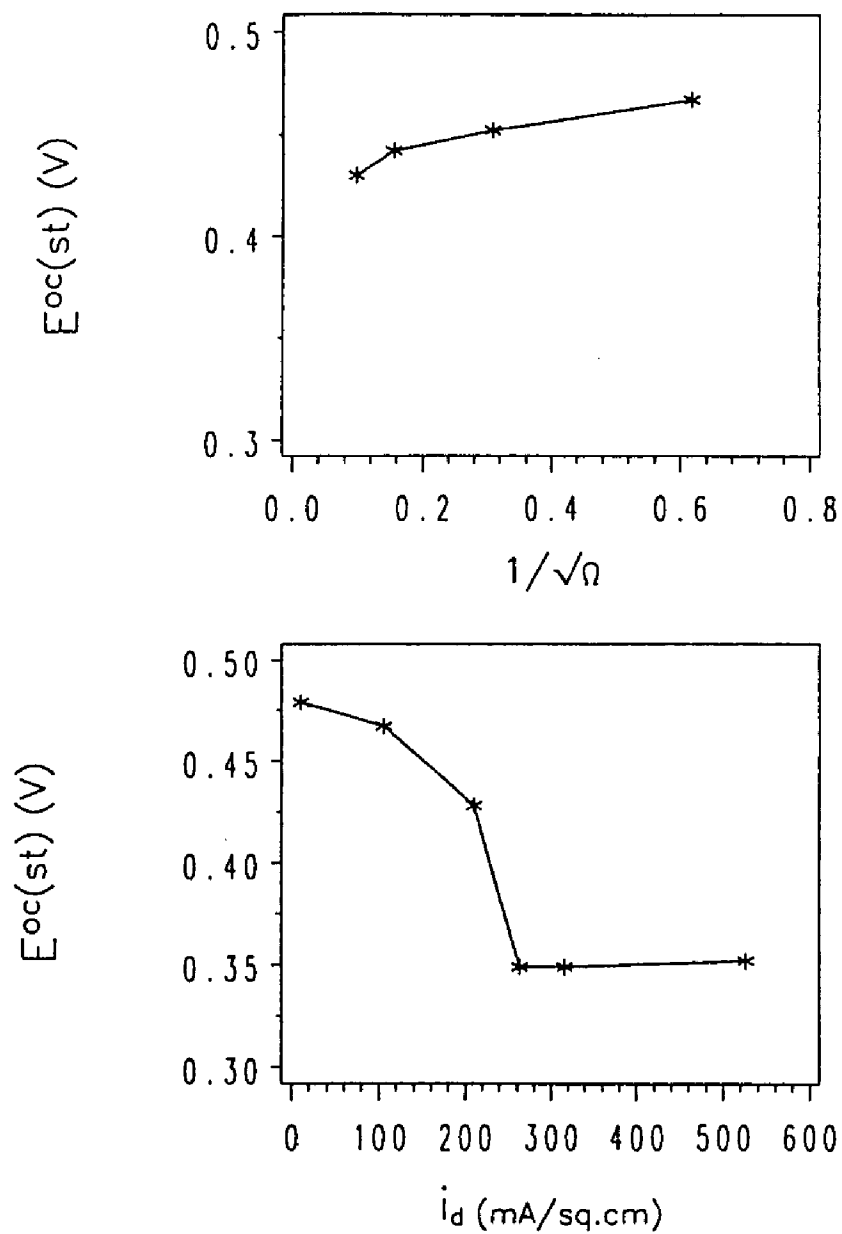


Figure 4.12:  $E_{oc(st)}$  of P3MT coating on Ph430SS. *Top:* versus  $\Omega^{-1/2}$  at  $i_d=105$  mA/cm<sup>2</sup>, *Bottom:* versus  $i_d$  at  $\Omega=2.62$  rad/s in 1 N air-saturated sulfuric acid solution.

## 4.5 Summary

With a fixed deposit charge density ( $0.48 \text{ C/cm}^2$ ) on Pt RDEs, increase in deposition current density ( $i_d$ ) or decrease in rotation rate of the electrode ( $\Omega$ ) resulted in:

- increase in the apparent exchange current density ( $i_0$ ) for oxygen reduction on the coating.
- increase in the redox capacity density ( $C_p$ ), or thickness, of the coating.
- decrease in the initial charge decay rate of the coating in 1 N sulfuric acid solution.

Either  $i_0$  and  $C_p$  are desirable for corrosion protection. They measure, respectively, the corrosion current that can be sustained by the polymer, and the total charge capacity of the polymer.

The deposition conditions also affected the steady state open-circuit potential ( $E_{oc}$ ) of the coating on Ph430SS. Nevertheless, all the  $E_{oc}$  values are within the passive potential range of the substrate metal.



## Chapter 5

# Stabilization of 430SS by P3MT

## Coatings

The properties of P3MT films have been studied intensively by a number of investigators [36,37,46,51,54,53,60,62,63,77]. The effect of dopants on P3MT films in aqueous salt solutions has also been reported [50,67,68,73]. However, the performance of P3MT coatings in corrosive acid and base solutions has drawn little attention [9,8]. Previous investigations of metal corrosion protection were mainly conducted in lithium perchloride or dilute sulfuric and perchloric acid solutions [8,9,10]. Only Deberry has reported studies in chloride containing solutions [9]. This study is an investigation of the capability of P3MT coatings to protect 430SS RDEs in various corrosive media including concentrated acid and base solutions as well as solutions containing chloride. Since 430SS is passive in the positive potential region adopted by P3MT in many aqueous solutions, it is therefore a candidate for anodic protection by P3MT coatings.

### 5.1 Preparation of coatings on Ph430SS

Samples were first phosphated according to the procedure given in Chapter 3. A SEM micrograph of a Ph430SS with a phosphated surface is shown in Fig. 5.1. The porous surface provides an adherent base for the P3MT coating. Deposition conditions, especially the deposition current density ( $i_d$ ), affect the steady open-circuit potential ( $E_{oc(st)}$ ) of coated electrodes as discussed in the previous chapter. The coatings used for the passivation

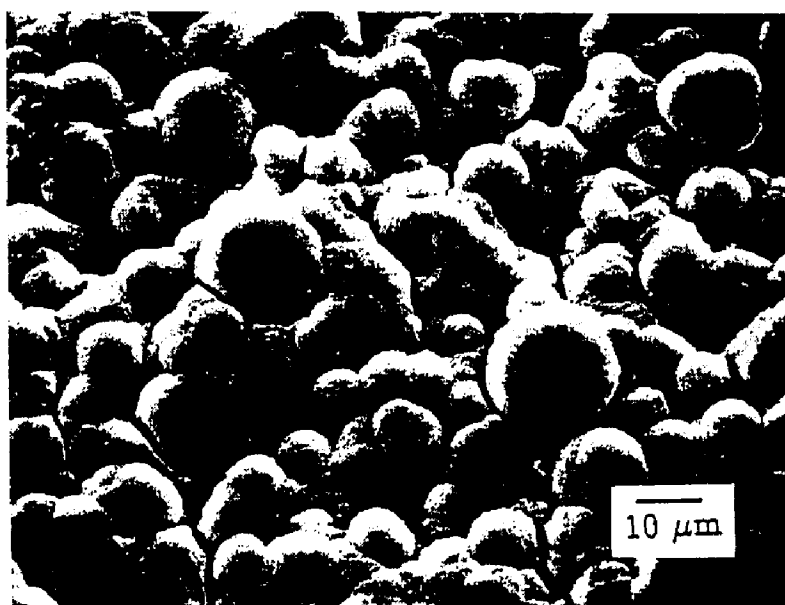
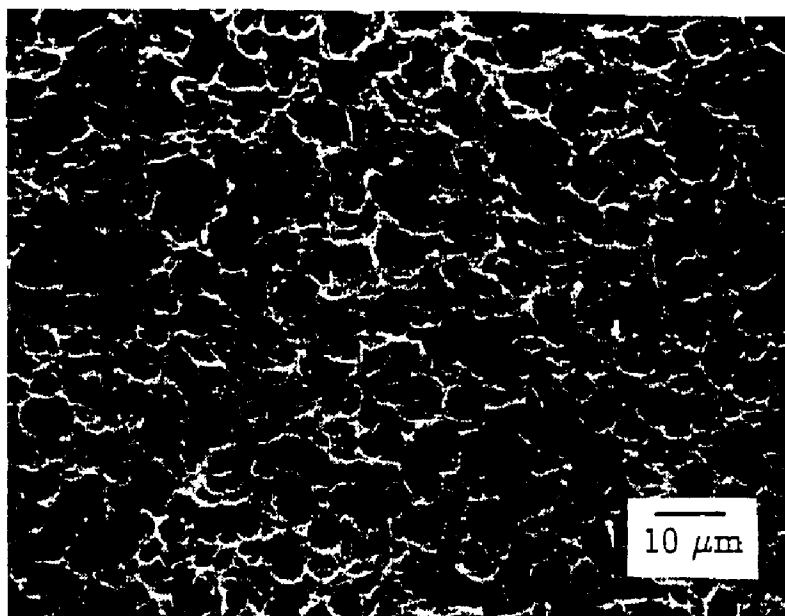


Figure 5.1: SEM micrographs. *Top*: the porous surface of a Ph430SS. *Bottom*: A P3MT coating on Ph430SS. Coating deposition condition:  $60 \text{ mA/cm}^2$ ,  $10.5 \text{ rad/s}$ .

and stability tests in this chapter were deposited at 300 mA/cm<sup>2</sup> and 2.62 rad/s for five seconds. The microtexture of the coatings on Ph430SS RDEs was made up of overlapping hemispheres 5 to 20  $\mu$ m in diameter (see Fig. 5.1). The coatings were rougher than those generated on TiGr2 and C1010.

## 5.2 Self-discharge in 1 N sulfuric acid solution

A self-discharge curve is a time record of the open-circuit potential of a sample. It provides a measure of the rate of approach to equilibrium after a change in the environment. Self-discharge curves of bare 430SS, Ph430SS and P3MT-coated Ph430SS in 1 N sulfuric acid solution are shown in Fig. 5.2. It can be seen that the bare 430SS or Ph430SS moved to an active corrosion potential (around -0.5 V) after a short time in the solution. The phosphating step did not substantially change the properties of 430SS. On the other hand, Ph430SS coated with P3MT remained in a passive state for five hours.

Under nitrogen purge, oxygen reduction, which is supposed to maintain the activity of the P3MT coating by balancing the corrosion current [8], is excluded. From Fig. 5.2, however, the distinction between the self-discharge curves under air and nitrogen purges is not obvious. The coated electrodes remained passive under nitrogen purge for the same time period (five hours) as under air purge.

## 5.3 Galvanic corrosion measurement in 1 N sulfuric acid solution

If the coatings sustain passivation galvanically, and not by acting as diffusion barriers, a sample of uncoated metal in galvanic contact with the polymer should be protected. The purpose of the galvanic corrosion measurement was to test the ability of the P3MT coating to bias the exposed metal sample (430SS) into its passive region.

When a bare 430SS RDE (working electrodes) was coupled to a bare 430SS or Ph430SS

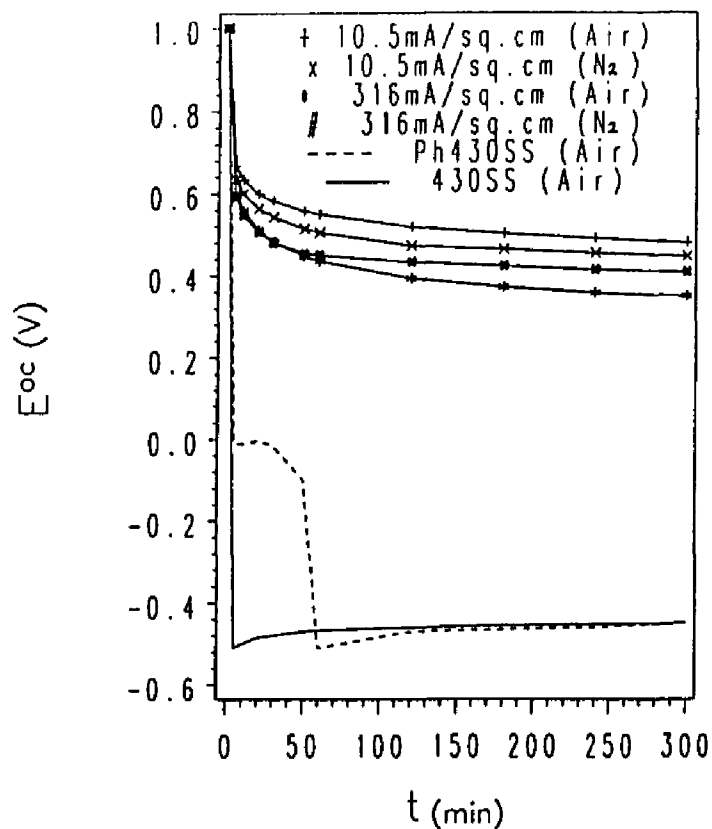


Figure 5.2: Self-discharge curves for 430SS, Ph430SS and P3MT-coated Ph430SS in 1 N sulfuric acid solution.

(reference working electrode), it showed signs of corrosion, including dulling of the surface and loss of material after 33 minutes. Values of material loss are listed in Table 5.3. When coupled to coated Ph430SS in air- or nitrogen-saturated 1 N sulfuric acid solution, the 430SS working electrode remained at a potential near +0.5 V. Over the same time period, the 430SS remained bright in appearance and suffered no measurable loss of material.

The test was not affected by the type of purge gas (air or nitrogen). In this study, nitrogen gas (high purity: O<sub>2</sub> 10ppm) was supplied by Northeast Airgas, Inc. Usually, the passive current density of iron is about 7  $\mu\text{A}/\text{cm}^2$  in 1 N sulfuric acid solution [12]. According to the calculation in Appendix B, the soluble O<sub>2</sub> under nitrogen purge is not able

Table 5.1: Loss of materials in galvanic corrosion tests (time period: 33 min) in 1 N sulfuric acid solution

reference working electrode	purging gas	loss of material from working electrode (430SS in gam)
430SS	air	0.0020
Ph430SS	air	0.0034
Ph430SS	N <sub>2</sub>	0.0025
P3MT-coated Ph430SS	air	0.0000
p3MT-coated Ph430SS	N <sub>2</sub>	0.0000

to even compensate  $1 \mu\text{A}/\text{cm}^2$  passive current density in 1 N sulfuric acid solution at room temperature. Therefore, oxygen reduction under nitrogen purge is not a major contribution to the stability of the coating which is coupled with an exposed 430SS. This result, along with the result obtained from the self-discharge experiments, compels a reconsideration of the mechanism of passivation by conductive polymers. This will be discussed in the next section.

The galvanic corrosion measurement provided evidence that the coating responds dynamically to depassivation. In one test, a 430SS RDE, coupled with a coated Ph430SS, was immersed in 1 N air-saturated sulfuric acid for eight hours without any visible sign of corrosion. The open-circuit potential of the 430SS RDE is shown in Fig. 5.3. About 95 minutes into the measurement, the open-circuit potential underwent a sharp excursion to near 0 V and then returned to a positive potential. Without coupling to the coating, uncoated steel samples that become active in this solution do not repassivate.

Since the polymer provides a galvanic current to sustain passivation of the metal, the ratio of polymer surface area to metal-surface area is a design consideration. Too low a

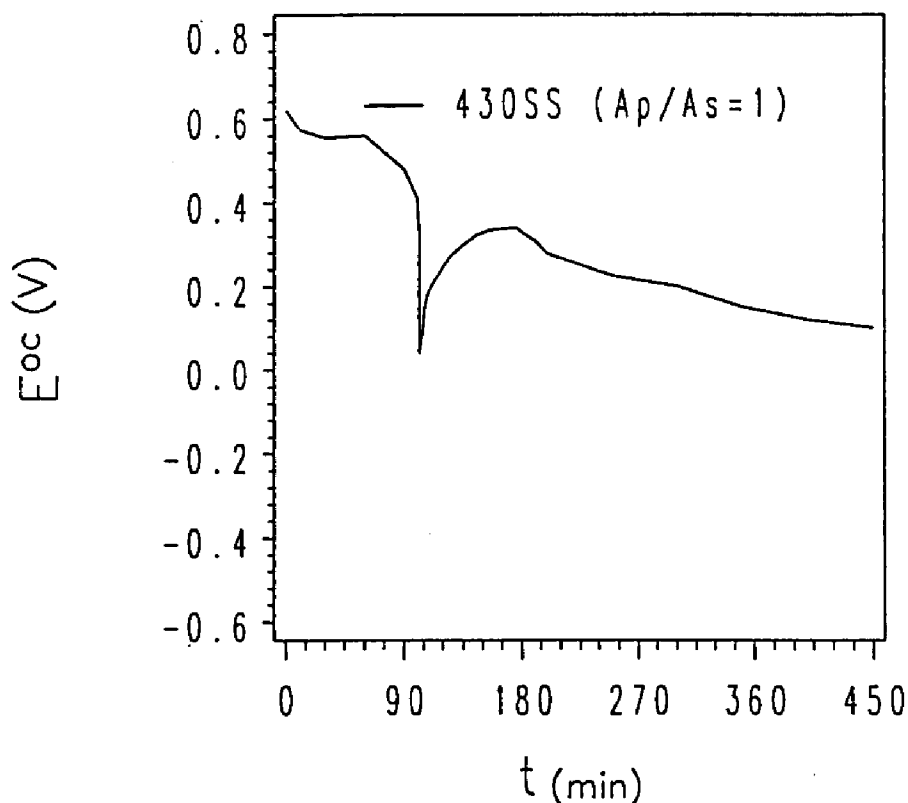


Figure 5.3: Galvanic corrosion test (1): open-circuit potential of 430SS, coupled with a P3MT-coated Ph430SS, in 1 N air-saturated sulfuric acid solution for 8 h.

ratio will result in the polymer being overwhelmed by the galvanic demand of the metal. The area ratio is written here as  $A_p/A_s$ , where  $A_p$  is the area of the polymer coating and  $A_s$  the area of the exposed steel surface.

The self-discharge curves of 430SS RDEs ( $A_s$ : 1.0 cm<sup>2</sup>) coupled to either coated Ph430SS ( $A_p$ : 1.0 cm<sup>2</sup>) or coated Pt ( $A_p$ : 0.13 cm<sup>2</sup>) are plotted in Fig. 5.4. An  $A_p/A_s$  ratio of 0.13:1 is insufficient to passivate the metal in 1 N air-saturated sulfuric acid solution. With an area ratio of 1:1 the samples remained passive up to eight hours in the same solution (see Fig. 5.3).

In a long-term galvanic corrosion test, a Ph430SS was coated with P3MT on one side, and half of the coated area was then scraped clean. The sample was left at ambient

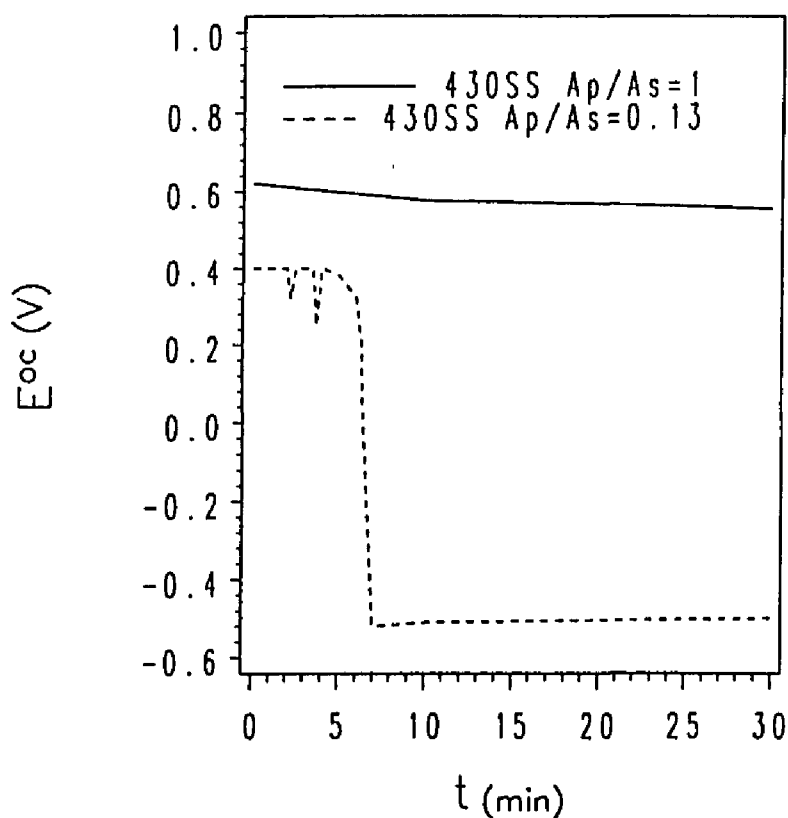


Figure 5.4: Galvanic corrosion test (2): open-circuit potential of working electrodes (430SS) versus time at different area ratios of  $A_p/A_s$  in 1 N air-saturated sulfuric acid solution.

temperature in a stationary 1 N sulfuric acid solution for thirty days with no measurable corrosion. The metal is protected even after part of the coating is removed.

## 5.4 Investigation of the passivation mechanism

It was assumed that reduction of dissolved oxygen on the polymer balanced the corrosion current. The observation that the polymer remains charged under nitrogen purge forced a reconsideration of this steady-current mechanism. To investigate the mechanism of passivation, a bare 430SS working electrode was repeatedly disconnected from and reconnected to a coated Ph430SS reference electrode. Fig. 5.5 depicts the corresponding curve of  $E_{oc}$

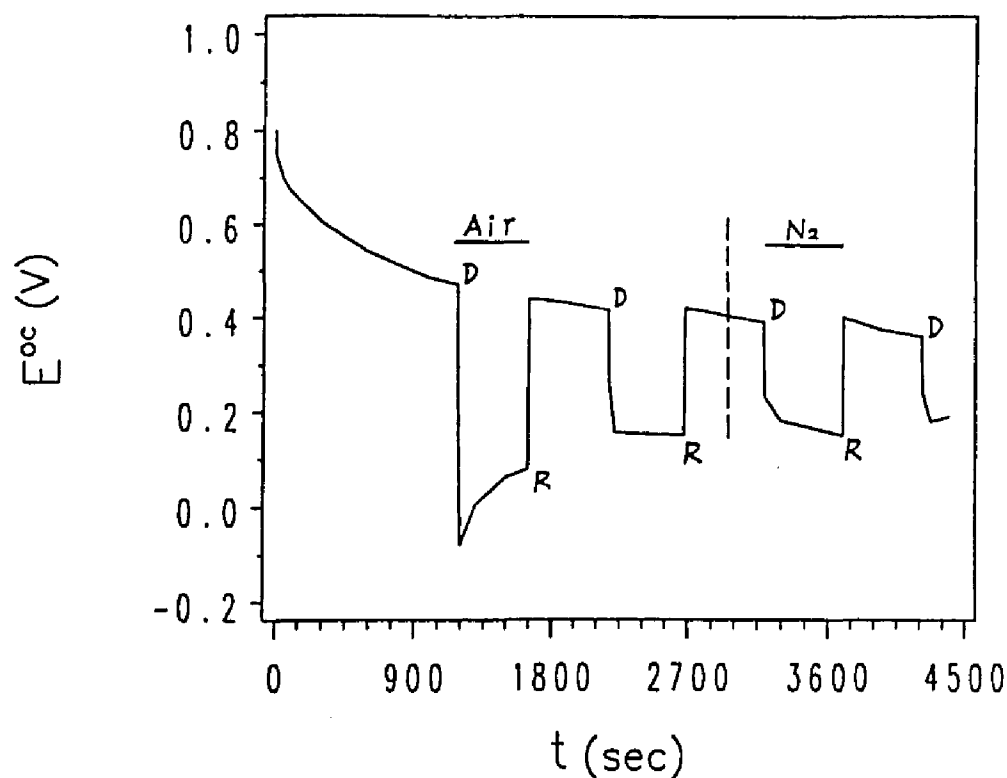


Figure 5.5: Galvanic corrosion test (3): open-circuit potential of 430SS RDE versus time, while disconnecting from and reconnecting to the P3MT-coated Ph430SS RDE in 1 N sulfuric acid solution with air or  $N_2$  purge. D: Disconnected from the P3MT coating. R: Reconnected to the P3MT coating.

vs. time. The coating does change the  $E_{oc}$  of the exposed working electrode. However, when the 430SS RDE was first disconnected from the P3MT coating after about 1100 s, the open-circuit potential of the RDE first moved to about -0.1 V and then slowly repassivated into the positive potential region without contact with the polymer. For the remainder of the cycles, the steel reverted to a  $E_{oc}$  around +0.2 V independent of the purge gas when not in contact with the polymer.

An alternative to the steady-current hypothesis is to suppose that the polymer first supplies a current to the working electrode (430SS) during the short time required to estab-



lish the passive film. This is a mechanism originally proposed by Deberry [9]. The polymer stabilizes the passive film by providing a transient current to 'heal' small holes before they expand. Under this hypothesis, the rate of oxygen reduction within the P3MT coating becomes less important since only a small charge needs to be passed from the coating to the passive film. To maintain it, the transient current can be supplied by reduction of the coating. The coating is then re-oxidized slowly by reduction of some oxidant in the environment.

A mechanism that requires steady reduction of  $O_2$  can not explain the stability of P3MT coatings and their efficiency for passivating the exposed metal (430SS) under nitrogen purge in 1 N sulfuric acid solution. Sunde et al. attributed the stability of P3MT films in aqueous solutions to the oxidizing power of the anions [68]. It is possible that some reduction reaction, other than oxygen reduction, takes place in dilute sulfuric acid solution to compensate discharge of the polymer. The evidence presented here is not conclusive.

## 5.5 Reversibility of polymer reduction/oxidation

Reversibility of P3MT-coated Ph430SS at negative potentials in sulfuric and nitric acid solutions has not been reported before. In this study, reversibility of the coatings at potentials positive of -0.3 V was demonstrated. It should be pointed out that the passive potential region of 430SS is between -0.1 V and 0.6 V (see Fig. 1.2). The active corrosion potential is about -0.5 V. A desirable property of a protective coating is to remain reversible if the substrate temporarily becomes active. The reversibility of the coatings was tested by holding them at a negative potential and then opening the circuit to see if they return to an oxidized state. For the sake of consistency, each sample was first scanned at 10 mV/s to 0.8 V and held for 2 min, then scanned (10 mV/s) to a negative potential and held for a set period before the circuit was opened.

The effect of electrolyte concentration and purge gas on the open-circuit response in sulfuric acid solutions is shown in Fig. 5.6. The composite electrode was held at a negative

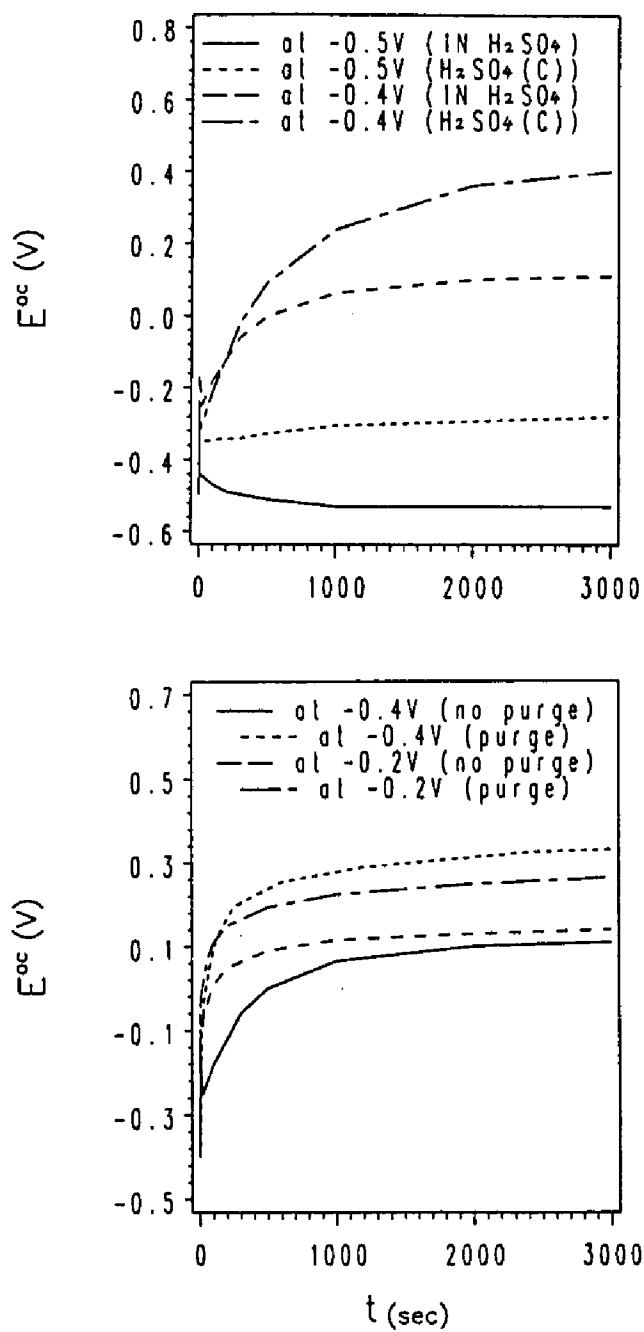


Figure 5.6: Open-circuit response of P3MT-coated Ph430SS in sulfuric acid solutions. *Top*: effect of concentration, *Bottom*: effect of purge gas in 1 N sulfuric acid solution.

potential for 3 min before the circuit was opened. The coating remained reversible at -0.4 V, but lost reversibility at -0.5 V. At -0.5 V, the substrate became active in both concentrated and 1 N sulfuric acid solutions. The type of purge gas (air, nitrogen or oxygen) provided no visible difference in affecting the open-circuit response as in the case of self-discharge measurements.

The effect of both holding potential and holding time on the reversibility of the coated Ph430SS in 1 N air-saturated sulfuric acid solution is shown in Fig. 5.7. The P3MT coating appeared to be discharged after being held at -0.5 V for 1 min and -0.4 V for 5 min. Evidently, the holding time did not affect reversibility at -0.3 V. After 450 min discharge at -0.3 V, the P3MT coating remained reversible and recharged when the circuit was opened.

The stability of P3MT coatings at potentials positive of -0.3 V was further demonstrated by cyclic voltammetry (CV) in 1 N air-saturated sulfuric acid solution. A stabilized P3MT-coated Ph430SS (after 50 potential cycles) was first held at -0.3 V for one hour. Then the circuit was opened, and cyclic voltammogram was recorded. The same method was used to plot the voltammograms after holding the RDE at -0.5 V for 10 min and 40 min respectively. As a reference, a voltammogram of a Ph430SS sample in the same solution (held at -0.5 V for 5 min) was also plotted. All the voltammograms are compared in Fig. 5.8. For Ph430SS, there are two anodic current peaks corresponding to uniform corrosion of Ph430SS, the bigger one appeared in the negative potential range (left anodic peak). After being held at -0.3 V for one hour, the voltammogram of the P3MT-coated Ph430SS only shows a little peak at the position of the left anodic peak of Ph430SS. By contrast, the left anodic peak of the P3MT-coated Ph430SS begins to show up after being held at -0.5 V for 10 min, indicating corrosion of the substrate. After being held at -0.5 V for 40 min, the P3MT coating was discharged, showing a big anodic peak due to metal dissolution. The CV results confirm the stability of the P3MT coating at -0.3 V.

Plots of  $E_{oc}$  vs. time for a clean 430SS RDE (working electrode), galvanically coupled with a P3MT-coated Ph430SS, are illustrated in Fig. 5.9. It is evident that with an area

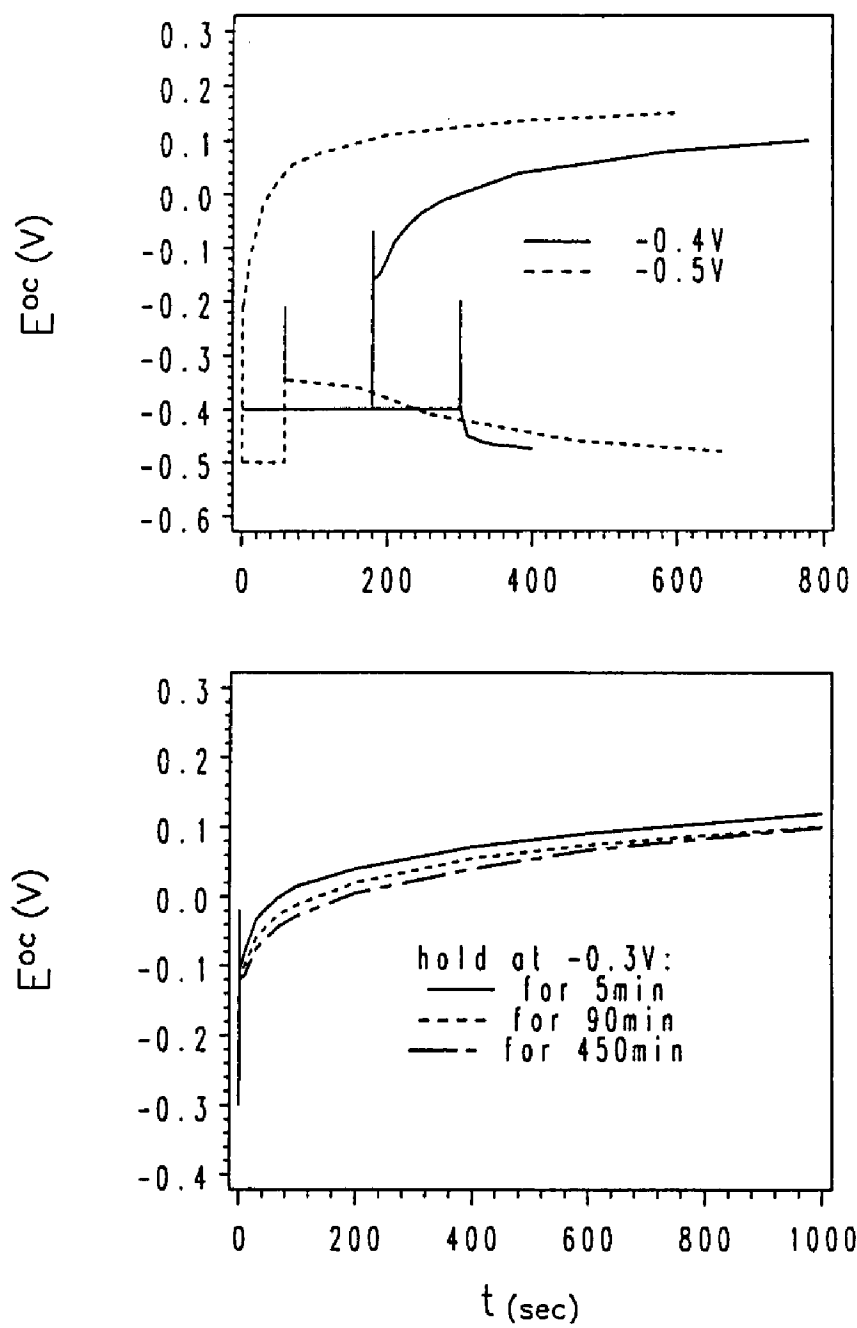


Figure 5.7: Open-circuit response of P3MT-coated Ph430SS in 1 N air-saturated sulfuric acid solution. *Top*: at  $-0.4\text{ V}$  and  $-0.5\text{ V}$ , *Bottom*: at  $-0.3\text{ V}$ .

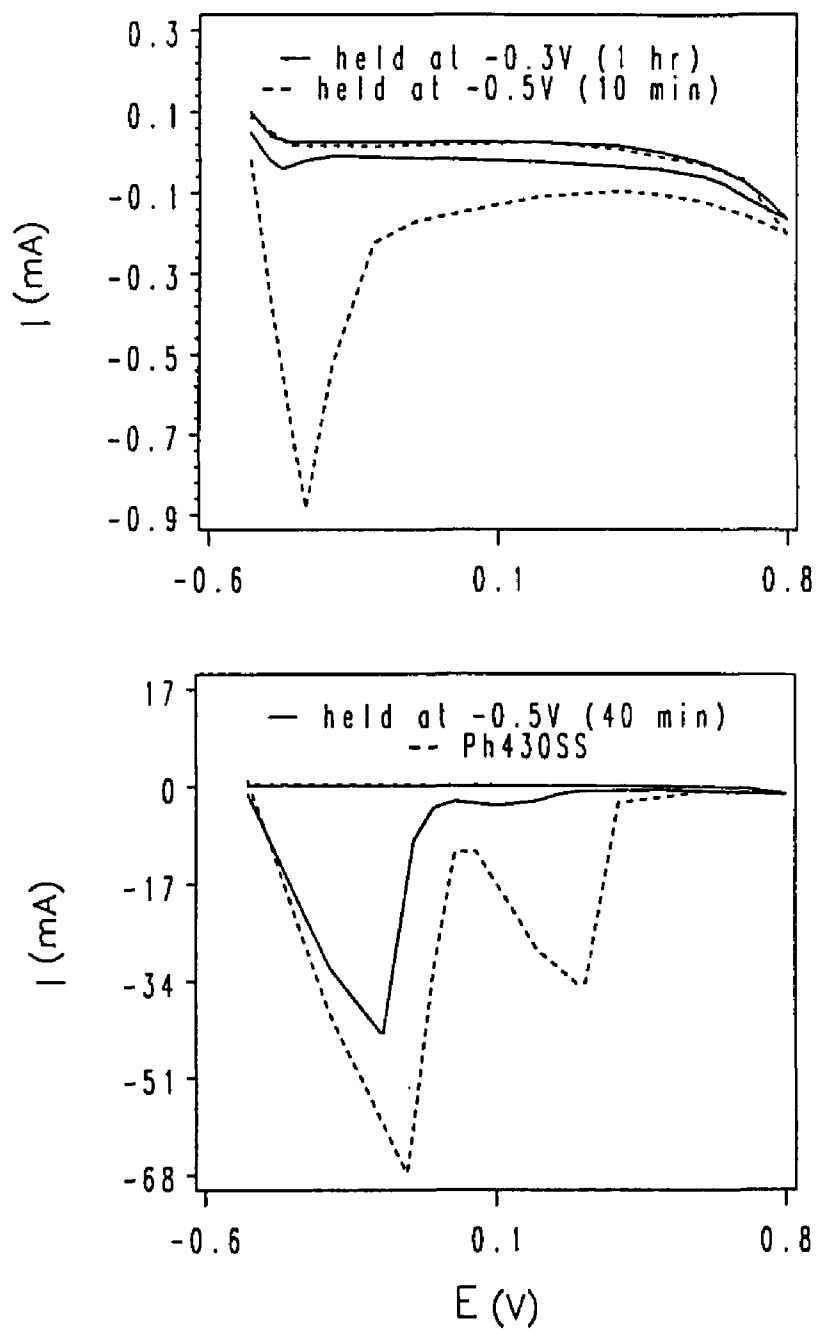


Figure 5.8: Cyclic voltammograms of P3MT-coated Ph430SS and Ph430SS in 1 N air-saturated sulfuric acid solution.

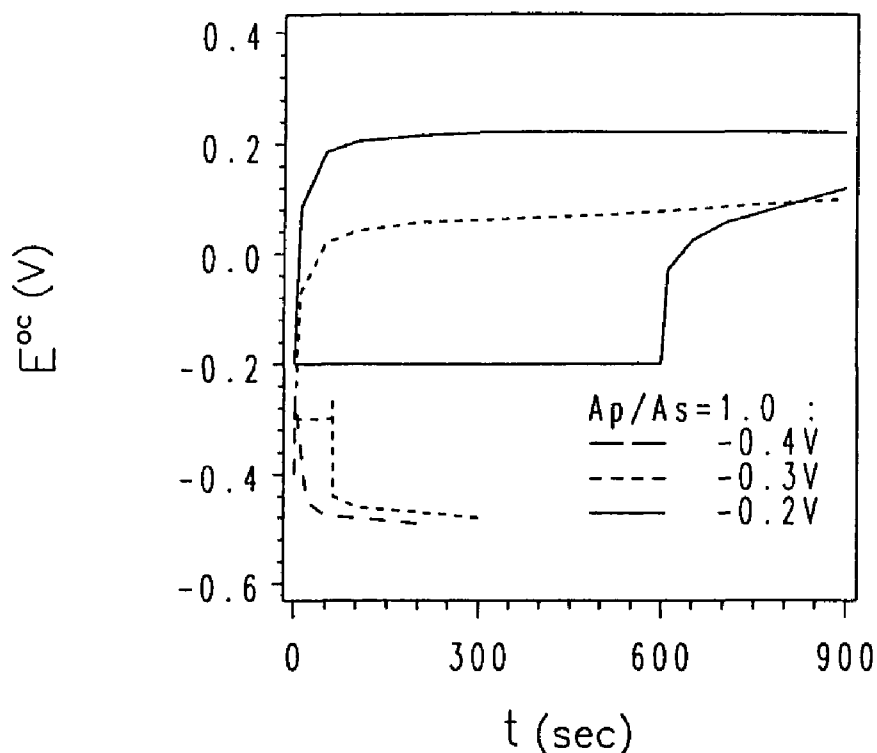


Figure 5.9:  $E_{oc}$  versus time curves of a 430SS RDE coupled with a P3MT-coated Ph430SS in 1 N air-saturated sulfuric acid solution after being held at negative potentials.

ratio of  $A_p/A_s=1.0$ , the couple was able to recharge back to a positive potential range after being held at  $-0.2$  V for 600 s. However, when the couple was held at  $-0.3$  V, a short holding period (60 s) caused a discharge of the coating and a failure of the galvanic protection of the coupled 430SS RDE. Comparing Fig. 5.9 with Fig. 5.7, it can be seen that reversibility of the coating depends on the  $A_p/A_s$  ratio. Reversibility of P3MT-coated Ph430SS was also observed in 1 N nitric acid solution (see Fig. 5.10).

Feldman et al. found that even for highly reduced poly(pyrrole) films, the current decay was very slow and could last for 20 min because the discharge rate was limited by counterion transport in 0.1 M  $\text{Et}_4\text{NClO}_4/\text{CH}_3\text{CN}$  system [86]. According to Zhang et al., anions with a radius less than 0.4 nm are capable of penetrating into P3MT films.  $\text{NO}_3^-$

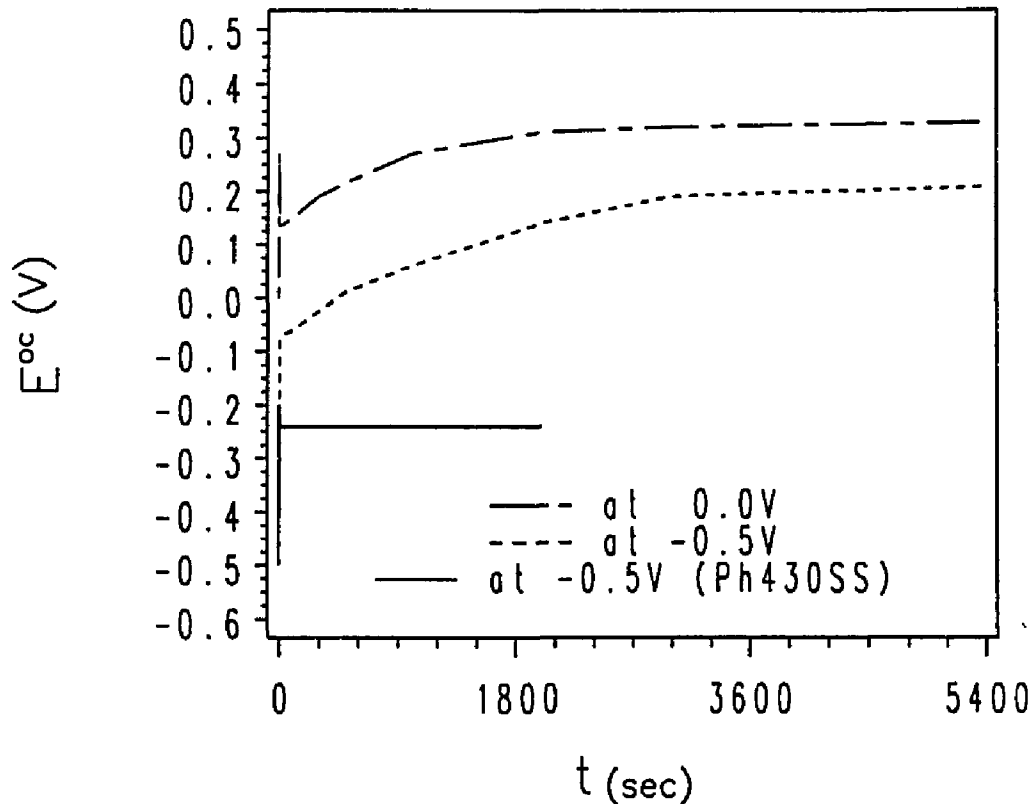


Figure 5.10: Open-circuit response of P3MT-coated Ph430SS in 1 N nitric acid solution.

ions (0.3 nm in radius) and  $\text{SO}_4^{2-}$  ions (0.4 nm in radius) are in this range [73]. Based on the work done by Tourillon [67], it is possible that  $\text{SO}_4^{2-}$  or  $\text{NO}_3^-$  ions penetrated into and doped the P3MT coating to an oxidized state and kept the coating from fully discharging. The reversibility of P3MT coatings observed in this experiment may reflect the power of anion doping.

To summarize, there are three important factors which contribute to stable passivation of 430SS by P3MT coatings in dilute sulfuric (or nitric) acid solutions. The first is the low current passed between P3MT coating and the steel after formation of a passive film. This current balances the transpassive corrosion current. Second, a reduction reaction in addition to oxygen reduction takes place in the acid solutions and keeps the coating oxidized even under  $\text{N}_2$  purge. Third is the reversibility of the coatings to reduction, possibly due to the

transport of anions during charge and discharge.

## 5.6 The effect of chloride and hydroxide

Uhlig et al. describe the action of chloride ions in breaking down passive films [12]. They point out that chloride ions can penetrate the passive oxide film through pores or defects. The breakdown of passivity by chloride ions takes place locally rather than generally. Small anodes of active metal are surrounded by large cathodic areas of passive metal. The resulting cells are called 'passive-active' cells. Since high current densities at the anode cause high rates of local metal dissolution, the 'passive-active' cells result in formation of pits. From the following experiments, it will be seen that chloride ions penetrate through the P3MT coating and pit the substrate (Ph430SS) in aqueous solutions. The coatings are unable to prevent this localized corrosion. The effect of hydroxide on P3MT coatings has not been reported before.

The self-discharge curves of P3MT-coated Ph430SS in dilute acid solutions are shown in Fig. 5.11. As expected, the electrodes were held within the passive potential region of 430SS in both 1 N sulfuric and nitric acid solutions. However, the coated Ph430SS quickly reverted to the active corrosion potential in aqueous solutions containing 1 N chloride. The other anions did not maintain the activity of the coatings.

Fig. 5.12 provides a comparison of self-discharge curves of P3MT-coated Pt in dilute acid solutions. Even with an inert substrate, the coating still lost its activity in 1 N hydrochloric acid.

In the only published study of the effect of  $\text{Cl}^-$  on P3MT, Deberry investigated a polyaniline-coated 430SS sample in 0.2 M NaCl + 0.2 M  $\text{H}_2\text{SO}_4$  aqueous solution. Oscillations in the open-circuit potential of the sample continued for over thirty hours around 0.1 V without loss of the PA coatings' activity [9]. The solution Deberry used was less aggressive than what we used here. For comparison, the material loss (after 1.5 h) of the coated Ph430SS and Tafel plot results obtained here are summarized in Table 5.6. Based



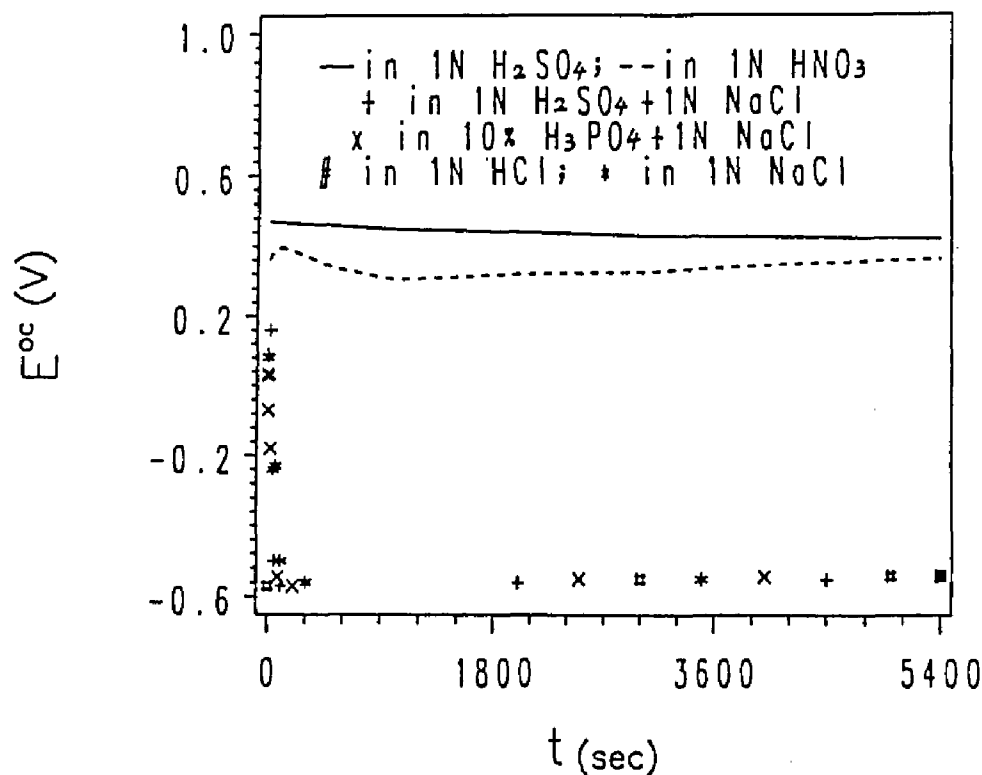


Figure 5.11: Self-discharge curves of P3MT-coated Ph430SS in dilute acid solutions.

on Table 5.6, it is evident that the anions,  $SO_4^{2-}$ ,  $NO_3^-$  and  $PO_4^{3-}$ , reduced the corrosion rate caused by chloride. The corrosion rate in 1 N NaCl aqueous solution was very low compared to that in chloride-containing acid solutions which implies that the corrosion rate due to attack of chloride depends on pH.

The effect of chloride concentration on corrosion of coated Ph430SS was examined in sodium chloride solutions. The self-discharge curves are plotted in Fig. 5.13. An increase of  $Cl^-$  concentration produced a more negative open-circuit potential. In 1 N sodium chloride, 430SS samples immediately moved into the active corrosion region. Table 5.6 gives a comparison of both material loss and Tafel plot results for the coated Ph430SS following discharge in sodium chloride solutions for one hour and a half. Consistent with the result obtained by Deberry [9], corrosion damage in a very dilute sodium chloride solution (less

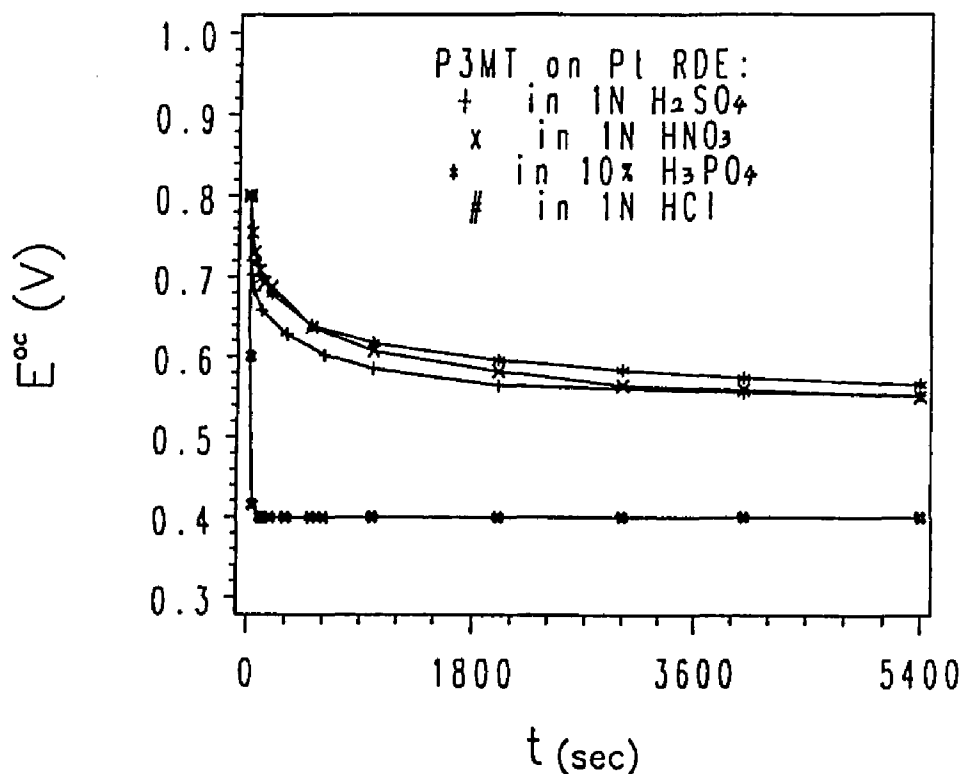


Figure 5.12: Self-discharge curves of P3MT-coated Pt in dilute acid solutions. The electrodes were first held at 0.8 V for 2 min, then opened the circuit.

than 0.25 N) is negligible.

An attempt was made to protect the coated Ph430SS from corrosion in 1 N sodium chloride solution (near the composition of sea water) by pretreatment of the coating to render it impermeable to  $\text{Cl}^-$ . The electrodes were pretreated by immersion in 70% nitric acid or 1 N sulfuric acid solution for one hour with a rotation rate of 10.5 rad/s. The pretreated electrodes were immersed in 1 N sodium chloride solution to record self-discharge curves (see Fig. 5.14). The pretreatment of the coated Ph430SS shifted the open-circuit potential by about +0.2 V. This stability improvement may be attributed to anions absorbed into the P3MT coatings. As mentioned previously, these anions occupy the micro-pores inside the coating and partially block penetration of the  $\text{Cl}^-$  ions.

Table 5.2: Material loss and Tafel plot results of P3MT-coated Ph430SS after discharge in aqueous solutions for 1.5 h. P3MT deposition condition: 300 mA/cm<sup>2</sup> and 2.62 rad/s for 5 s.

Aqueous solution	Mat. loss (g)	$E(I = 0)$ (mV)	$I_{corr}$ ( $\mu\text{A}/\text{cm}^2$ )
1 N H <sub>2</sub> SO <sub>4</sub>	0	80.99	0.23
1 N HNO <sub>3</sub>	0	153.4	0.47
1 N HCl	0.0047	-541.7	4474
1 N H <sub>2</sub> SO <sub>4</sub> + 1 N NaCl	0.0031	-546.1	3129
10% H <sub>3</sub> PO <sub>4</sub> + 1 N NaCl	0.0018	-537.4	3232
1 N NaCl	0.0004	-422.8	9.89

The behavior of coated Ph430SS in 2 N potassium hydroxide solution is shown in Fig. 5.15. No matter what the initial potential was,  $E_{oc}$  always moved to the steady open-circuit potential of the substrate. This indicates that the coating lost its activity in the KOH solution.

Cyclic voltammograms of the coated Ph430SSS were plotted in dilute acid and base solutions (see Fig. 5.16). In 1 N sulfuric or nitric solution, the first reduction peak of the electrode occurred at positive potentials. The peak was more positive in 1 N sulfuric acid solution. The second reduction peak for both solutions appeared negative of -0.4 V and was coupled with the corresponding small anodic corrosion peak of Ph430SS. Small oxidation current peaks at 0.8 V indicate recharge of the coatings.

Cyclic voltammograms in 1 N hydrochloric acid solution and 2 N potassium hydroxide solution behaved very differently from that in dilute sulfuric and nitric solutions. A large anodic current appeared for both CV curves at a positive potential. No reduction peak was observed in either solution, which implies deactivation of the coating. The anodic

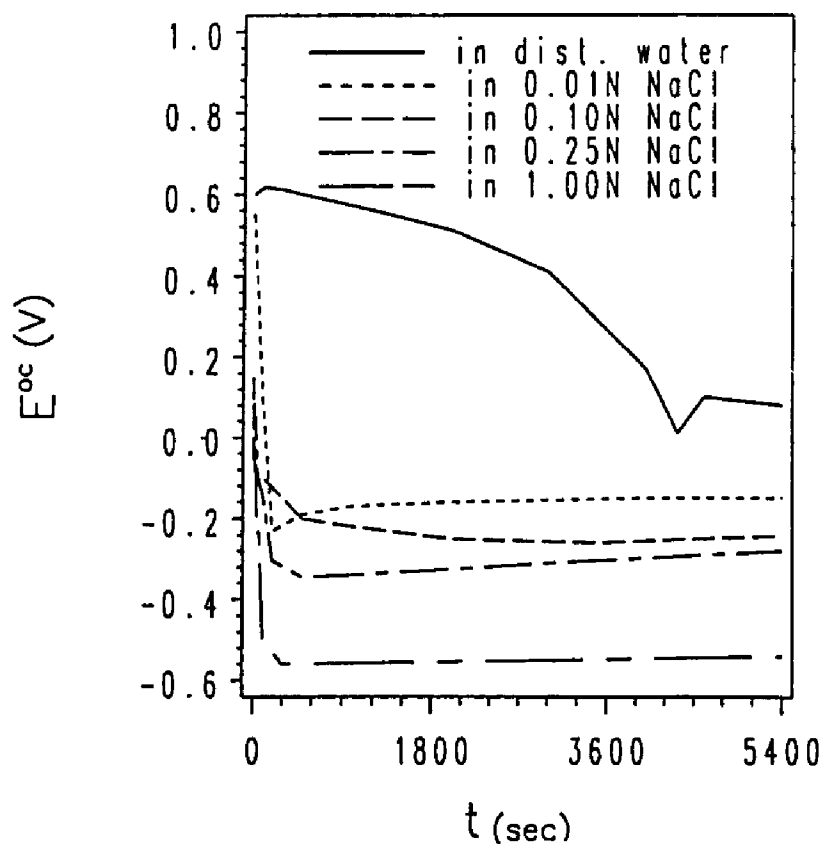


Figure 5.13: Self-discharge curves of P3MT-coated Ph430SS in sodium chloride solutions.

peak around -0.4 V in sulfuric or nitric solution did not appear in dilute HCl and KOH solutions. The cyclic voltammograms again demonstrate the stability of P3MT coatings in dilute sulfuric and nitric acid solutions.

## 5.7 Durability of coatings in concentrated acid and base solutions

To evaluate the degree of P3MT coating degradation in concentrated acid and base solutions, a coated Ph430SS was first treated in such a solution for two hours at a rotation rate of 10.5 rad/s. Then 50% of the pretreated P3MT coating was removed from the substrate to create a galvanic sample which had an area ratio of  $A_p/A_s$  equal to 1.0. The galvanic

Table 5.3: Material loss and Tafel plot results of P3MT-coated Ph430SS after discharge in NaCl solutions for 1.5 h.

Conc. (N)	Mat. loss (g)	$E(I = 0)$ (mV)	$I_{corr}$ ( $\mu\text{A}/\text{cm}^2$ )
0.00	0.0000	30.72	0.72
0.01	0.0000	-99.25	0.35
0.10	0.0001	-232.8	0.19
0.25	0.0001	-295.7	0.90
1.00	0.0004	-422.8	9.89

sample was then immersed in 1 N air-saturated sulfuric acid solution at a rotation rate of 105 rad/s. The self-discharge curve of the galvanic sample was recorded (see Fig. 5.17).

It is obvious that the coating remains active after immersion in 70% nitric acid or concentrated sulfuric acid solution. Concentrated potassium hydroxide solution damaged the P3MT coating to a certain extent. In the sulfuric acid solution, the  $E_{oc}$  vs. time curve of KOH(c)-pretreated galvanic sample first moved to near 0 V and then recharged back to near 0.2 V and remained stable for the rest of the time period. It can be concluded that P3MT coatings resist degradation in concentrated acid and base solutions.

Durability of the coating in 1 N hydrochloric acid solution was also examined. Even though the coating lost the ability to protect the substrate metal (Ph430SS) in 1 N hydrochloric acid solution, the P3MT coating was still reversible after immersion in the hydrochloric acid for two hours. The HCl-pretreated coating was able to galvanically protect the exposed metal surface in 1 N sulfuric acid solution. Reversibility of P3MT coatings in sulfuric acid solutions may play an important role in this case.

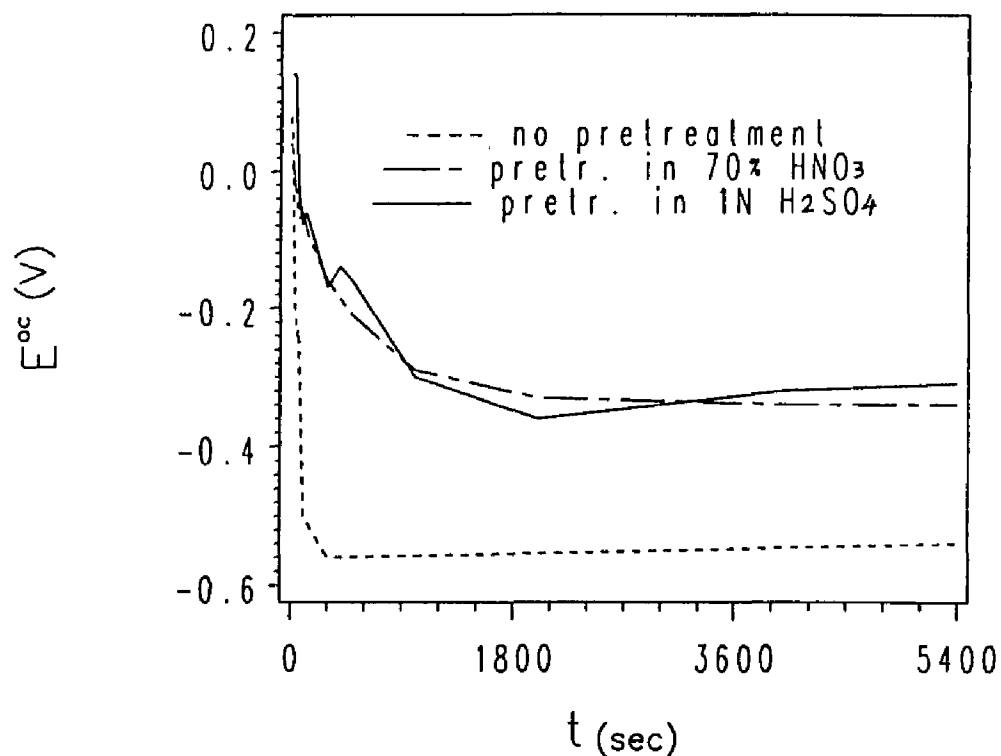


Figure 5.14: Self-discharge curves of the pretreated P3MT-coated Ph430SS in 1 N sodium chloride solution.

## 5.8 Summary

The P3MT coatings were very stable in dilute sulfuric acid and nitric acid solutions. A reduction reaction other than oxygen reduction must take place to keep the coating active under the nitrogen purge. The coatings galvanically protected the exposed 430SS from corrosion at an  $A_p/A_s$  ratio of 1.0.

Reversibility of P3MT coatings at potentials positive of -0.3 V contributed to the stabilization of the substrate metal in dilute sulfuric acid and nitric acid solutions.

The coatings failed to protect Ph430SS from corrosion in aqueous solutions containing 1 N chloride. The coatings lost their activity in KOH solutions as well. However, The

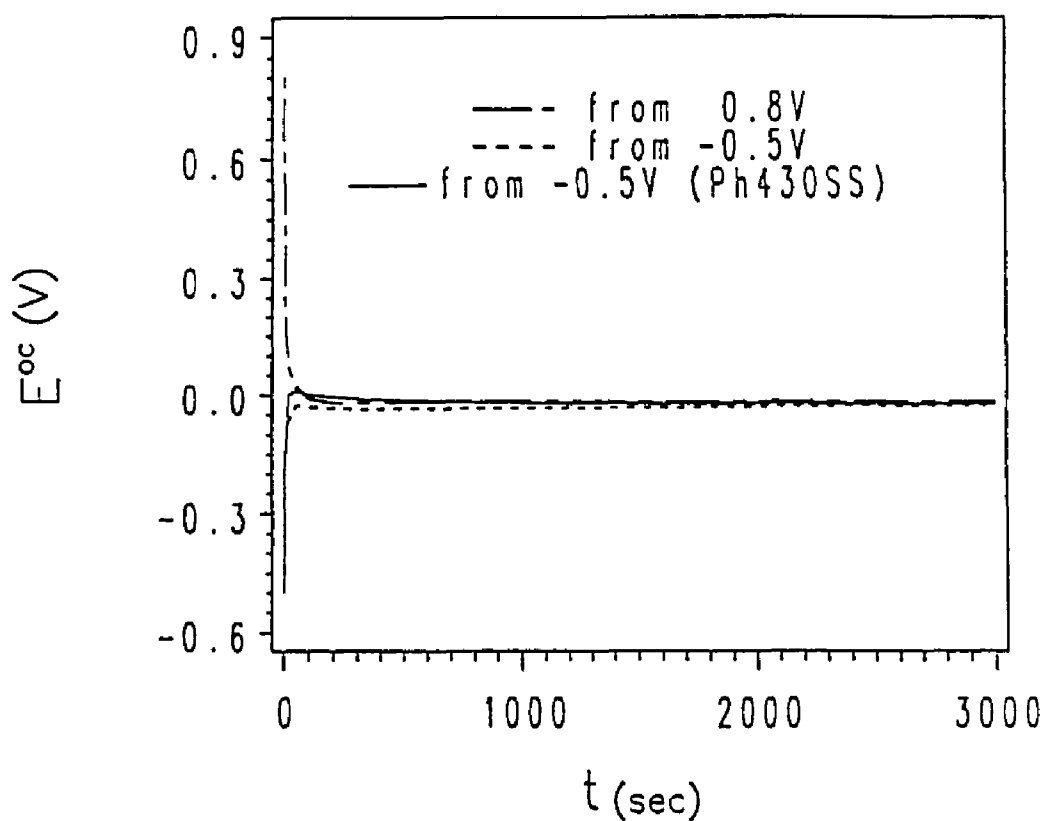


Figure 5.15: Self-discharge curves of a P3MT-coated Ph430SS in 2 N potassium hydroxide solution.

coatings were not irreversibly damaged by chloride or hydroxide ions. The coatings can sustain treatment in concentrated acid and base solutions for two hours without being degraded.

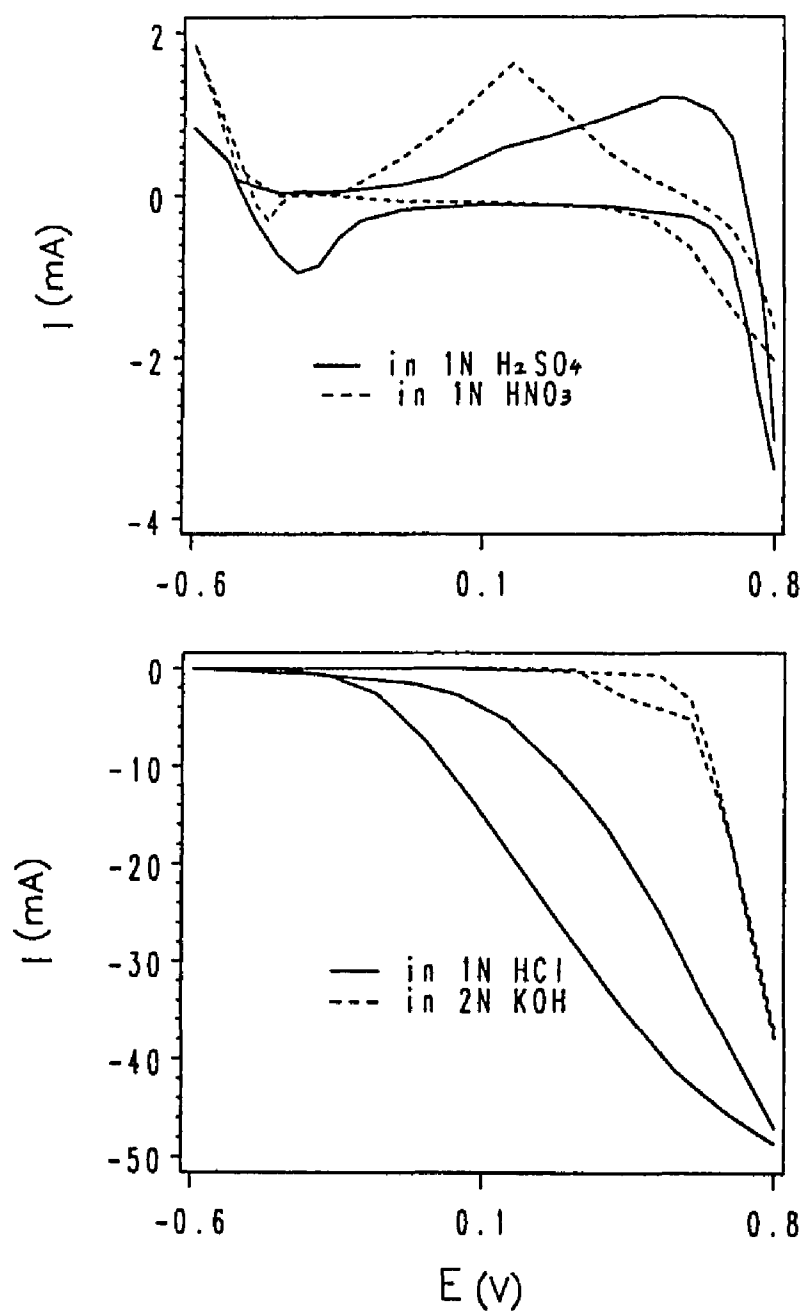


Figure 5.16: Cyclic voltammograms of P3MT-coated Ph430SS in dilute acid and base solutions. Initial potential: 0.8 V, Vertex potential: -0.6 V, Final potential: 0.8 V. Scan rate: 20 mV/s.



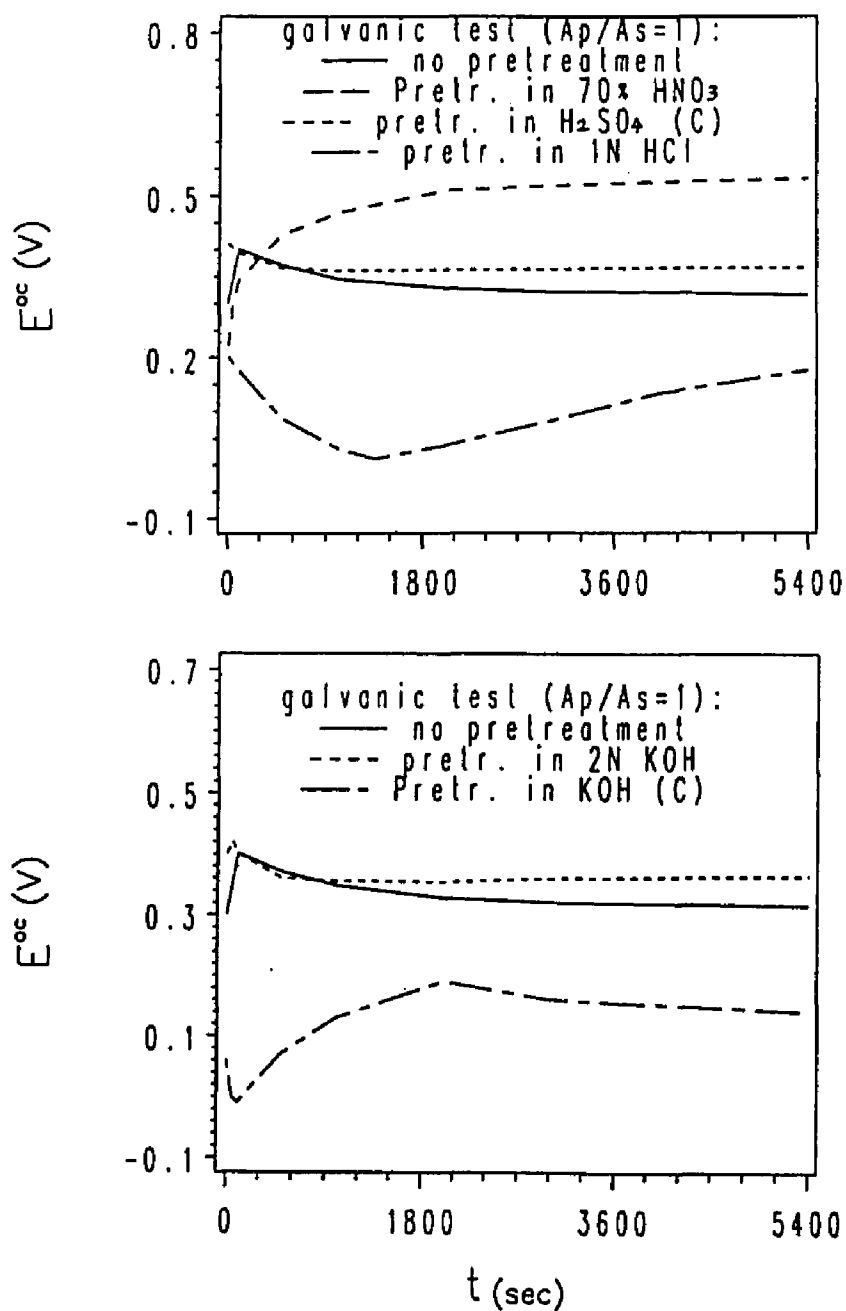


Figure 5.17: Self-discharge curves of pretreated galvanic samples ( $A_p/A_s=1.0$ ) in 1 N air-saturated sulfuric acid solution. *Top*: pretreated in severe acid solutions, *Bottom*: pretreated in severe base solutions.

## Chapter 6

# P3MT Coatings on Titanium and Carbon Steel

### 6.1 Preparation of coatings

The procedures to form adhesive P3MT precoatings (thin polymer films) on titanium (TiGr2) and carbon steel (C1010) have been given in Chapter 3. After deposition of a thin film, a coating was deposited at  $200 \text{ mA/cm}^2$  and  $52.4 \text{ rad/s}$  for 7.5 s. The thin film is formed in the presence of chloride to promote adhesion. Fig. 6.1 shows the pits developed on titanium by attack of chloride ions during formation of the thin polymer film. Since a P3MT coating can not be directly formed on top of  $\text{TiO}_2$  [15], polymer nuclei first form inside these pits and act as roots to make the thin film adhesive. SEM micrographs of both the thin film and the full coating are shown in Fig. 6.2. A similar effect is produced on C1010 surfaces (see Fig. 6.3).

### 6.2 Passivation of titanium by P3MT coatings

The surface composition of TiGr2 was obtained from an energy-dispersive X-ray spectroscopy (EDXS). Unfortunately, Al, Si, S and certain amount of Fe accidentally contaminated the sample surface. The result did not conform whether or not a  $\text{TiO}_2$  oxide film exists on the metal surface. Following Deng et al. [8], a titanium sample was treated by being slowly scanned ( $1 \text{ mV/s}$ ) to 3.0 V in 1 N sulfuric acid solution to form a thick

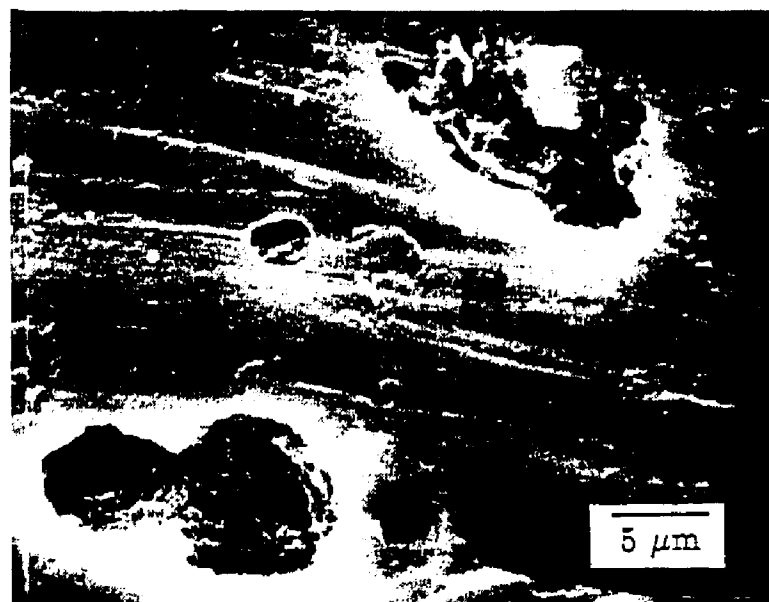
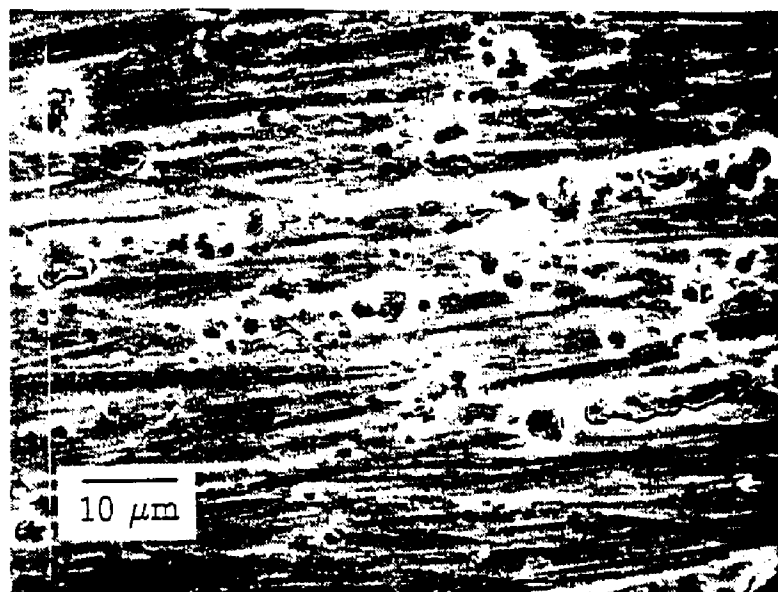


Figure 6.1: SEM micrographs showing pits on a TiGr2 surface. Anodic deposition condition:  $10 \text{ mA/cm}^2$  and  $0.52 \text{ rad/s}$  for  $20 \text{ s}$  in  $0.5 \text{ M}$  3MT/ $0.1 \text{ M}$  TBATFB/ $0.1 \text{ (g/ml)}$   $\text{ZnCl}_2$  propylene carbonate solution.

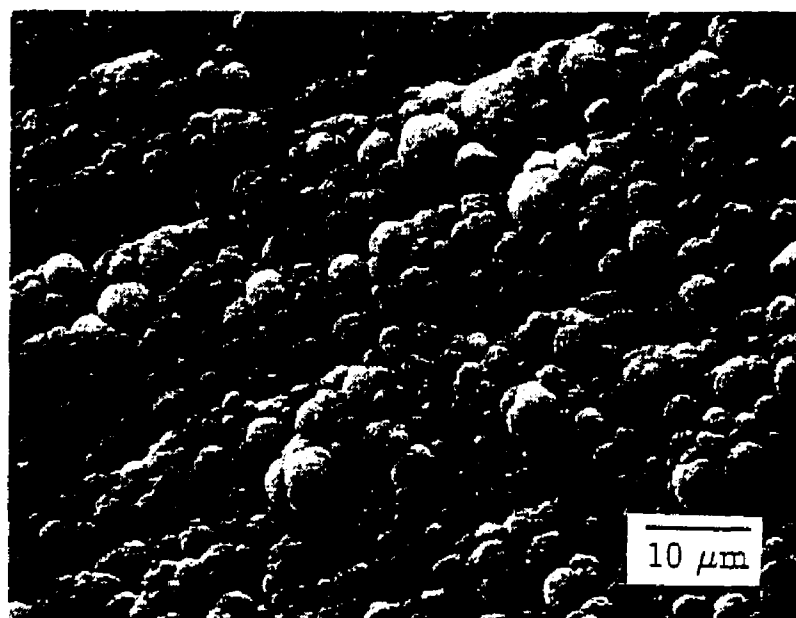
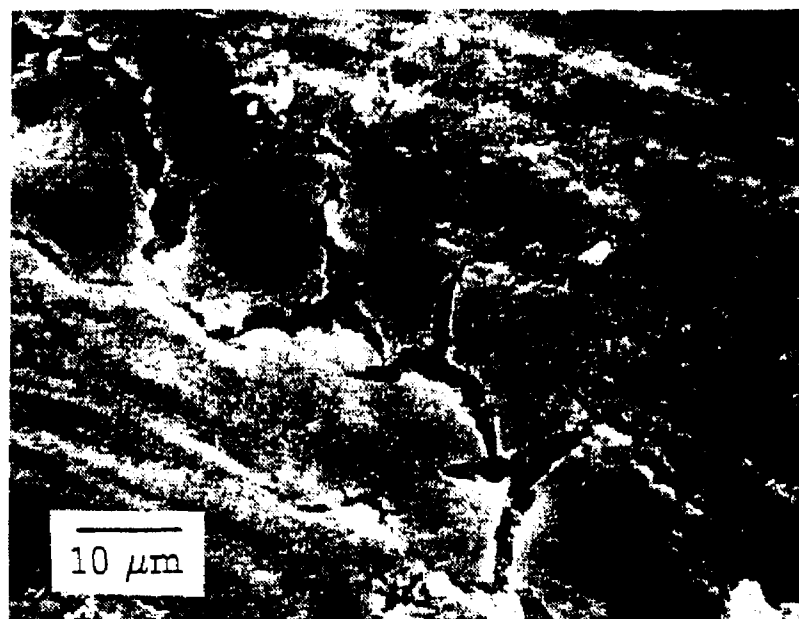


Figure 6.2: SEM micrographs. *Top*: a P3MT thin film. The same deposition condition as in Fig. 6.1 except for 40 s. *Bottom*: a P3MT full coating. 200 mA/cm<sup>2</sup> and 1.57 rad/s for 7.5 s in 1.0 M 3MT solution.

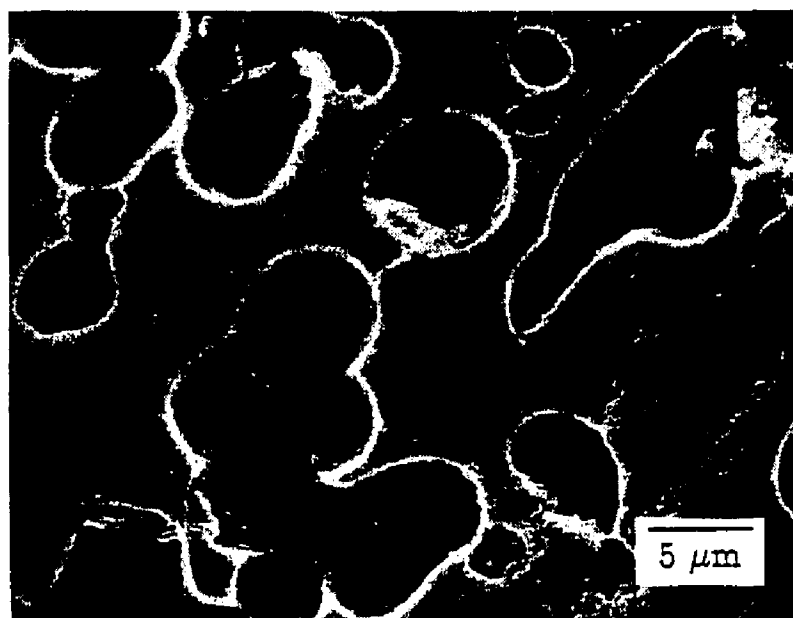
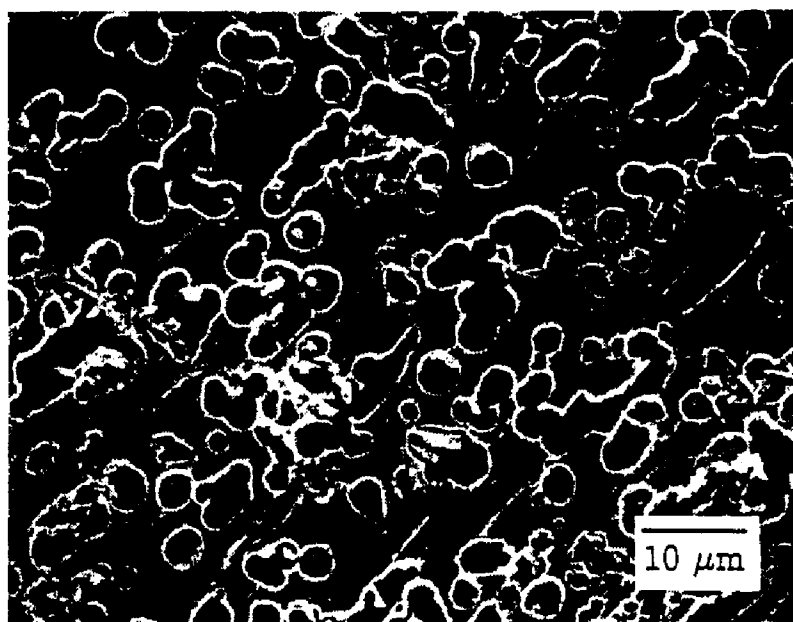


Figure 6.3: SEM micrographs showing pits on a C1010 surface. Anodic deposition condition: 500 mA/cm<sup>2</sup> and 0.52 rad/s for 20 s in 0.1 M 3MT/0.1 M TBATFB/0.1 (g/ml) ZnCl<sub>2</sub> propylene carbonate solution.

TiO<sub>2</sub> oxide film (0.1 - 0.2  $\mu$ M). Both untreated and treated titanium samples were used as working electrodes in galvanic corrosion tests.

The performance of P3MT coatings in passivating titanium was evaluated in 4 N sulfuric acid and hydrochloric acid solutions at several temperatures. The techniques used for this purpose were measurement of self-discharge and galvanic corrosion tests. For experiments at elevated temperature, hot water from a controlled-temperature bath was circulated through the jacket of an electrolysis cell (see Fig. 3.2). An Ag/AgCl reference electrode and a platinum counter electrode were used in the measurements. To record self-discharge curves, electrodes were rotated at a rate of 52.4 rad/s and held at 0.8 V vs. Ag/AgCl for 2 minutes before the circuit was opened.

Self-discharge curves of titanium, the P3MT-precoated titanium with a thin film and fully coated titanium at room temperature are shown in Fig. 6.4. Compared with the bare titanium, the fully coated titanium had a more positive open-circuit potential,  $E_{oc}$ . The  $E_{oc}$  differences were 0.275 and 0.065 V in the sulfuric acid and hydrochloric acid solutions respectively. It is clear that the P3MT thin film alone is not able to poise the substrate.

To evaluate the performance of the coatings at higher temperatures, the measurements were repeated at 50°C and 70°C. Uncoated titanium was also tested for comparison. Fig. 6.5 shows the self-discharge curves at 50°C. The  $E_{oc}$  of the bare titanium moved negative of 0 V after a short time in both acid solutions. With the coating, the substrate was held positive of 0.2 V throughout the test period in the same solutions. The coating was effective in the acid solutions at temperature up to 50°C. However, when the temperature was increased to 70°C, the coating broke up after thirty minutes in both 4 N sulfuric and hydrochloric acid solutions, following a sharp excursion of  $E_{oc}$  into the active region (see Fig. 6.6).

A galvanic corrosion measurement was done with a titanium sample with a preformed thick oxide layer as working electrode and a polymer-coated titanium electrode as reference working electrode. The galvanic current vs. time curve at 45°C is showed in Fig. 6.7. The current is 6 to 7  $\mu$ A. This current represents a flow of electrons from the working electrode to

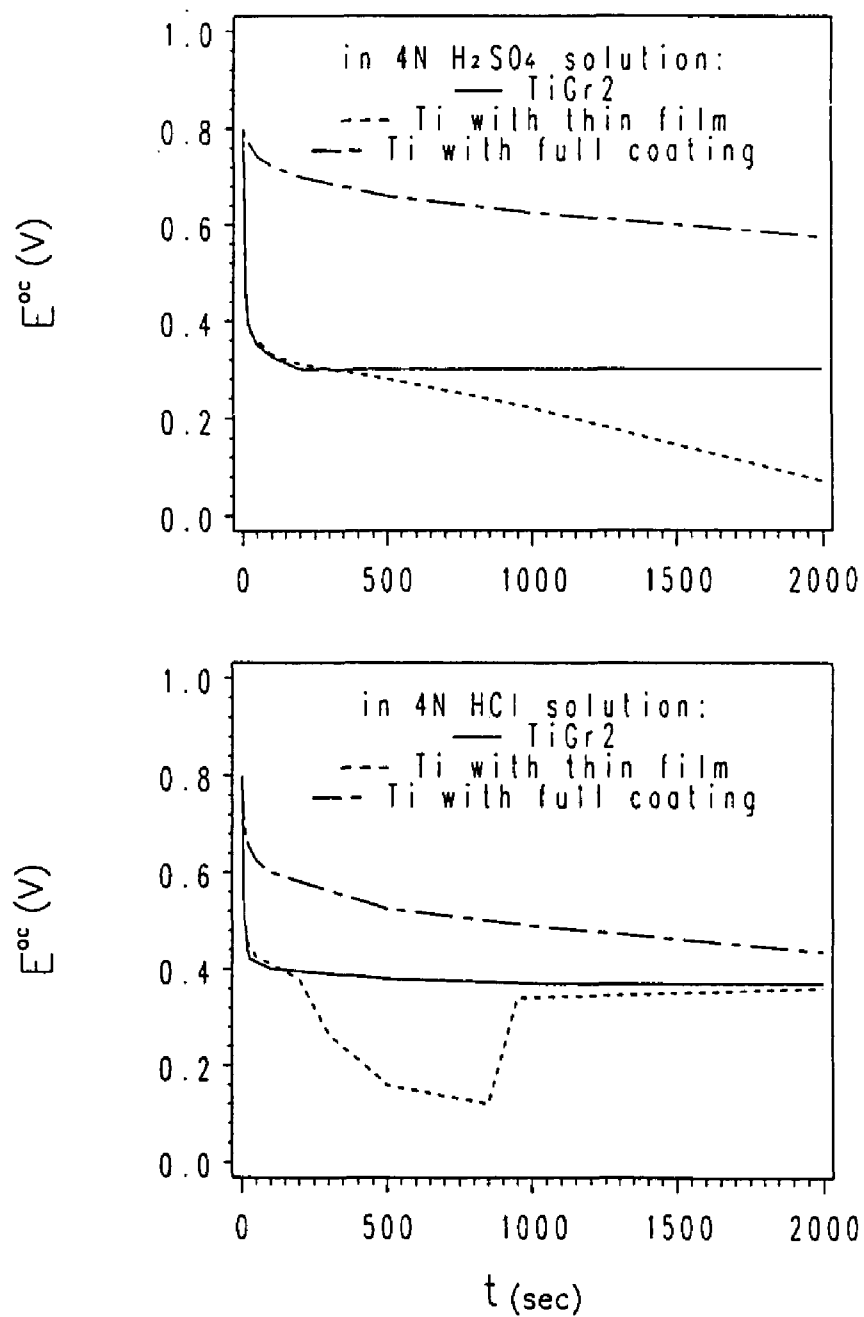


Figure 6.4: Self-discharge curves of TiGr2, P3MT-precoated TiGr2 and P3MT-coated TiGr2 at room temperature. *Top:* in 4 N sulfuric acid solution. *Bottom:* in 4 N hydrochloric acid solution.

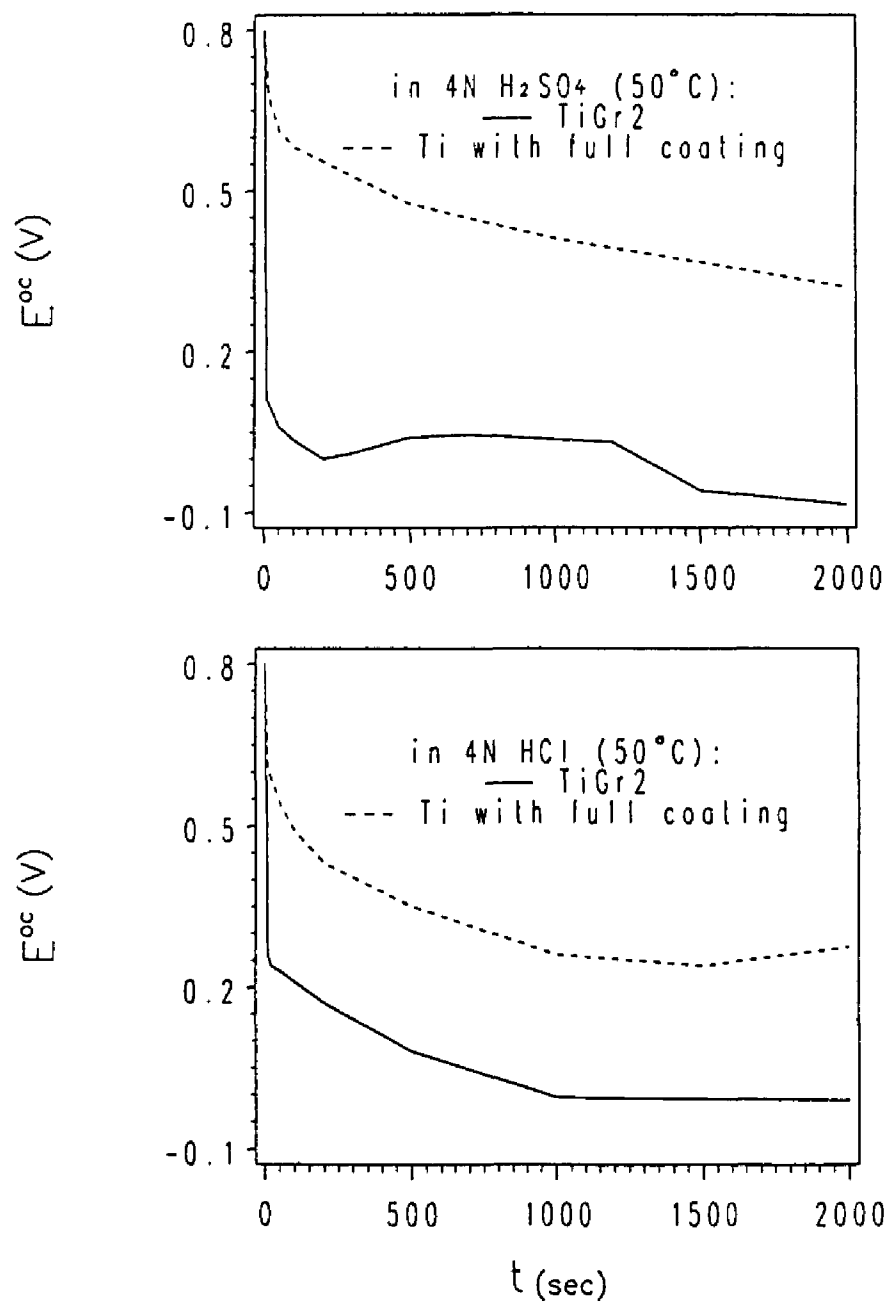


Figure 6.5: Self-discharge curves of TiGr2 and P3MT-coated TiGr2 at 50°C. *Top:* in 4 N sulfuric acid solution. *Bottom:* in 4 N hydrochloric acid solution.



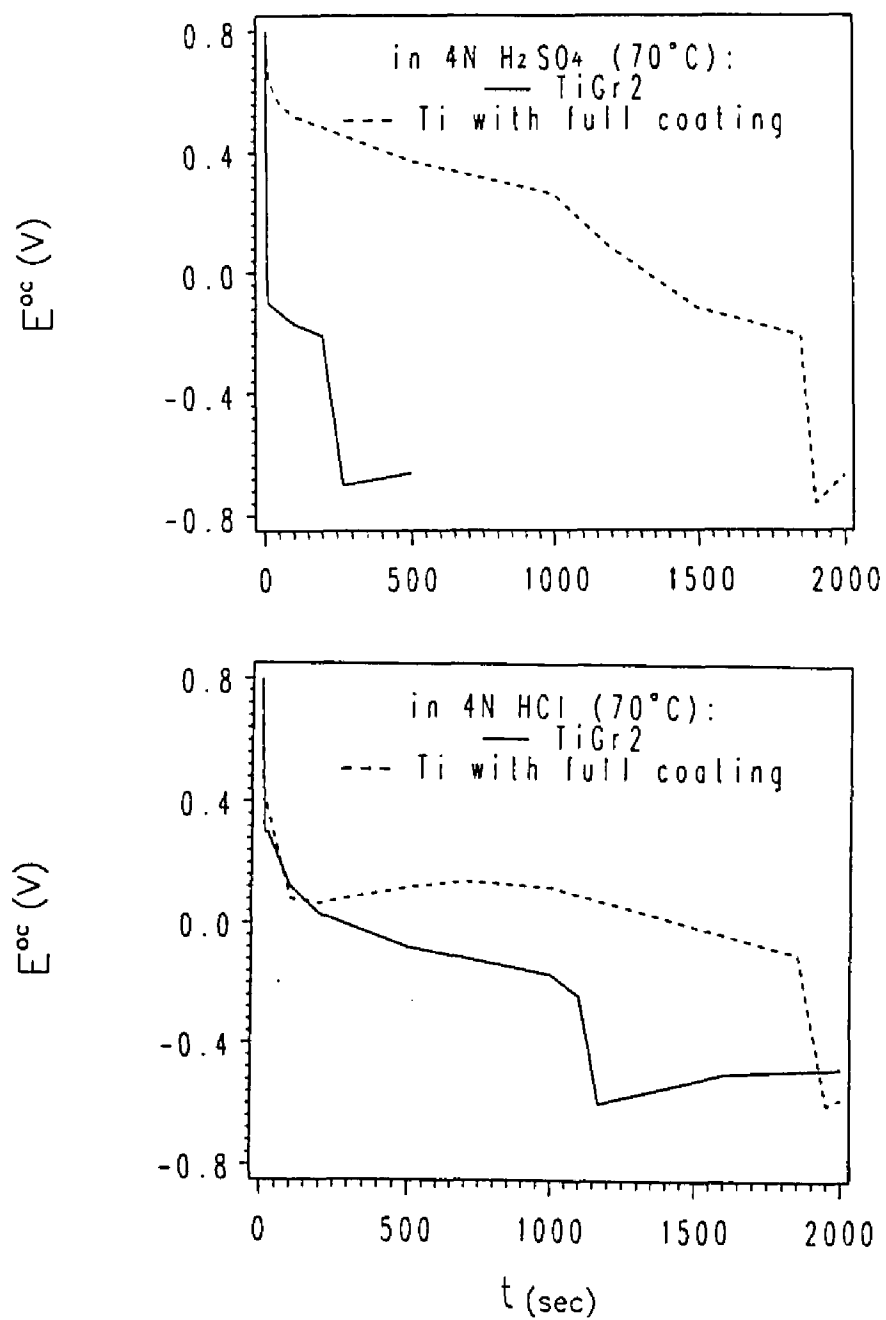


Figure 6.6: Self-discharge curves of TiGr2 and P3MT-coated TiGr2 at 70°C. *Top:* in 4 N sulfuric acid solution. *Bottom:* in 4 N hydrochloric acid solution.

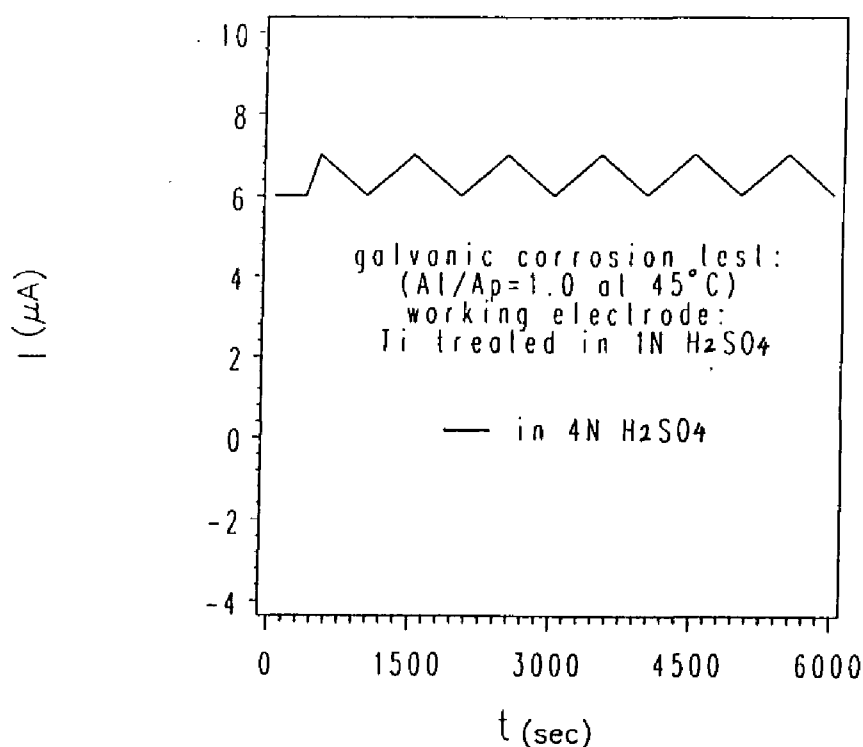


Figure 6.7: Galvanic current versus time curve of galvanic couples in 4 N sulfuric acid solution at 45°C. Working electrode: treated TiGr2; Reference working electrode: P3MT-coated TiGr2.

the coated electrode. According to Deng et al. [8], a small electron current from the working electrode to the P3MT coating implies stabilization of the exposed TiO<sub>2</sub> oxide layer by the polymer. This experiment supports their conclusion. The TiO<sub>2</sub> layer was stable for the full test at 45°C.

Another galvanic corrosion test shows that before the P3MT coating broke up at 70°C in 4 N sulfuric acid solution, it did passivate the coupled bare titanium. From Fig. 6.8, the titanium was first passivated by the coupled coating for about 350 s indicated by a very small current (a few μA), the test was then interrupted by opening the circuit for 2 s. A great current was observed in the wake of opening the circuit, corresponding to the corrosion of titanium and the discharge of the coupled coating.

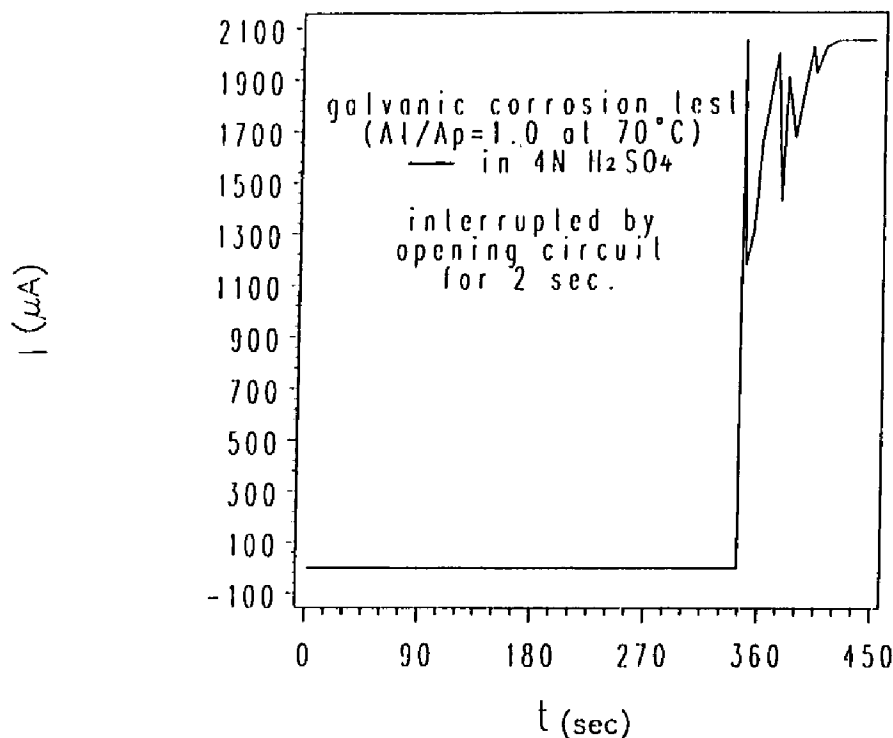


Figure 6.8: Galvanic current versus time curves of TiGr2 coupled with the P3MT-coated TiGr2 in 4 N sulfuric acid solution at 70°C. The test was interrupted by temporarily opening the circuit for 2 s.

### 6.3 Electrochemical Impedance of coated titanium electrodes

Electrochemical Impedance Spectroscopy (EIS) is a powerful tool for studies on electrode covered by organic coatings. Kendig et al. illustrated several equivalent circuits for coated electrode systems (Fig. 6.9) [90]. The Warburg interface (W) is a circuit element representing mass transfer resistance. For a coated electrode, it is dominated by resistance in the coating.  $C_{dl}$ , the double layer capacitance, arises through direct contact between substrate and electrolyte that has penetrated the coating. A double (or dipole) layer forms at the metal/electrolyte interface. The additional circuit elements are the coating capacitance ( $C_c$ ), the electrolyte resistance ( $R_\Omega$ ), the pore resistance ( $R_p$ ) and electron-transfer

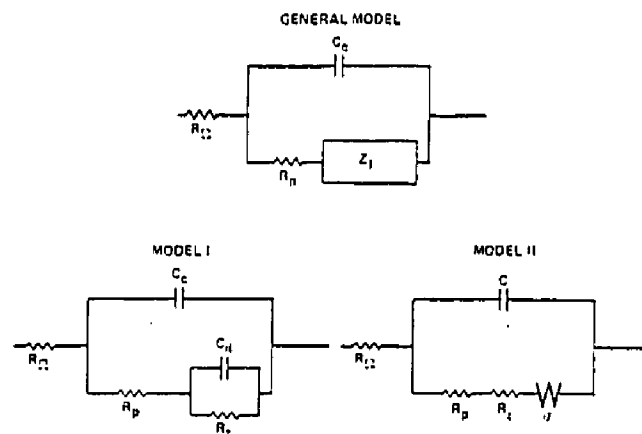


Figure 6.9: Possible equivalent circuits for organic coatings (after [90]).

resistance ( $R_t$ ). EIS is sensitive to all these effects [87,90].

EG&G PARC provides a basic introduction for evaluation of different organic coatings by EIS [88]. Many electrochemical impedance studies of resistive organic coatings have appeared [89,90,91,92]. Most of the studies concentrate on the stability and delamination of coatings in corrosive media. Hulster et al. applied impedance measurements to a conductive polymer coating, polypyrrole (PP), on aluminium in aqueous electrolytes [14]. It was found that PP deposited in the pores of anodically pretreated aluminium had a high resistivity ( $10^6 \Omega$ ) due to overoxidation at high local current densities.

In this study, the stability of P3MT coatings on titanium in both an acid solution and ambient air was investigated by EIS. A coated sample was first immersed in 1 N sulfuric acid solution at a rotation rate of 52.4 rad/s. EIS measurements were then conducted periodically, with the electrode left at open-circuit between measurements. The impedance data were obtained at frequencies from  $10^{-3}$  to  $10^5$  Hz, and the results were displayed as Bode plots (see Fig. 6.10).

The Bode plot (A) (after 1 h) is dominated by capacitance character since the phase angle stays close to  $-60^\circ$  over almost the entire frequency range. The total resistance of

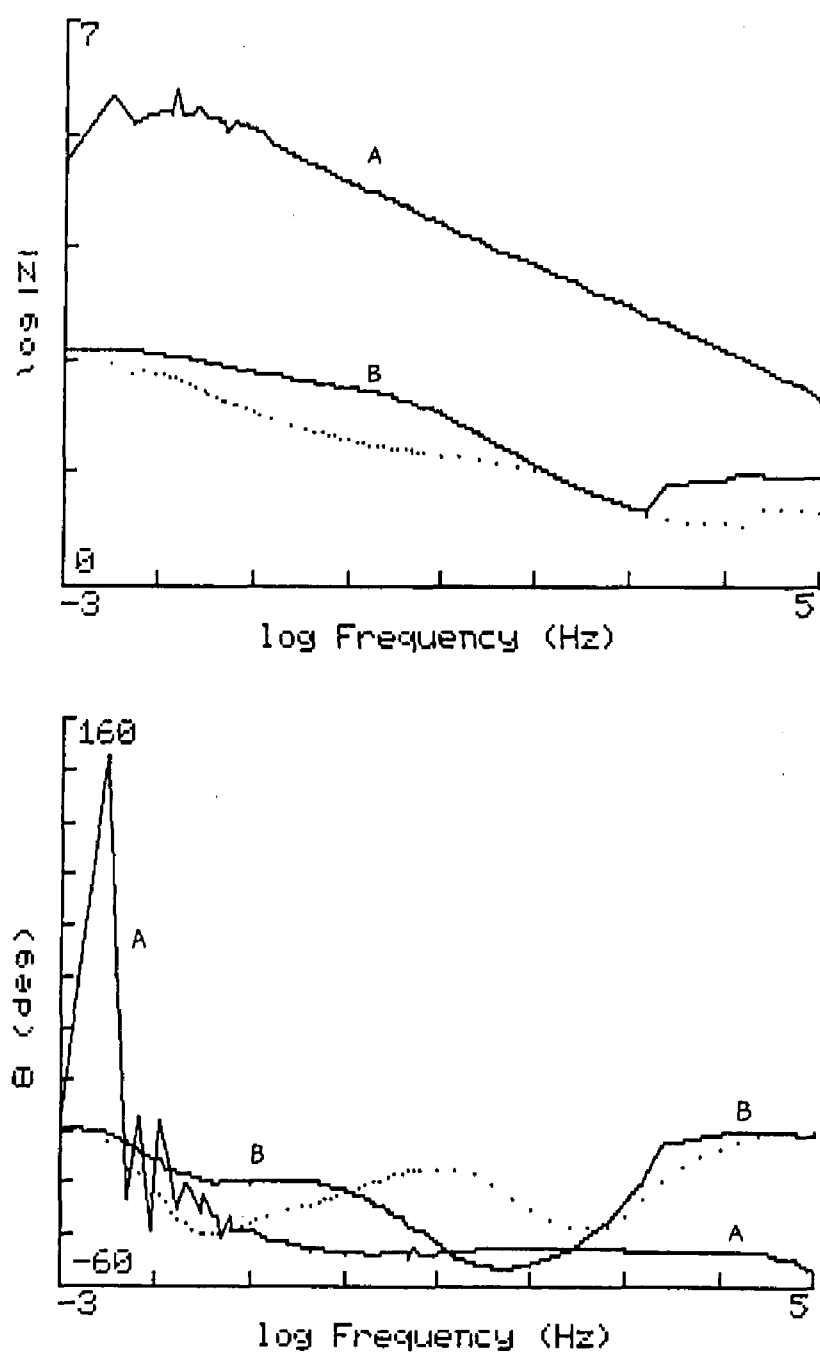


Figure 6.10: Bode plots for a P3MT-coated TiGr2 in 1 N sulfuric acid solution. P3MT deposition condition: 200 mA and 1.57 rad/s and 7.5 s. (A). after 1 hour, (..). after 1 day, (B). after 2 days.

the coating is around  $10^6 \Omega$  after one hour of immersion (read from the intercept of  $\log |Z|$  vs.  $\log f$  curve). This value is about the same as that of the PP coatings on aluminium measured by Hulser et al. at higher local current densities [14]. After immersion in the acid solution for one day, the total resistance of the P3MT coating dropped to about  $10^3 \Omega$  due to the increase of capacitance and decrease of porous resistance to ionic species [90,92]. The corresponding  $\theta$  vs.  $\log f$  (..) curve shows two peaks indicating a double layer capacitance,  $C_{dl}$ , as discussed by Kendig et al. [87]. Since it arises by interaction between substrate and electrolyte,  $C_{dl}$  is a signal of delamination of an organic coating.

The consecutive Bode plot (B), obtained after immersion for one more day, shows no further decrease of the total resistance. In the  $\log |Z|$  vs.  $\log f$  curves of the P3MT coating, the plot (B) overlaps the plot (..) right in the middle slop range, which implies that there was no further capacity increase. From the  $\theta$  vs.  $\log |Z|$  curve (B), the peak for  $C_{dl}$  disappears, resulting in a more regular curve. The stabilization of the coating after two days may be attributed to the formation of a thin layer of corrosion product on the delaminated surface area.

The stability of coatings on titanium in ambient air was also examined. Fig. 6.11 depicts Bode plots of the coating before and after exposure to ambient air for forty days. The first Bode plot shows that the coating was resistance-dominated (the total resistance is about  $10^4 \Omega$ ). After exposure to ambient condition for 40 days, the P3MT coating became capacitance-dominated with a total resistance over  $10^3 \Omega$ . The decrease of the coating resistance was much slower in air than in the acid solution. The increase of capacity may be due to the uptake of water [87] from ambient air.

The Bode plot of the precoated titanium resembles that of bare titanium. The very thin P3MT film did not seriously affect the surface properties of the substrate.

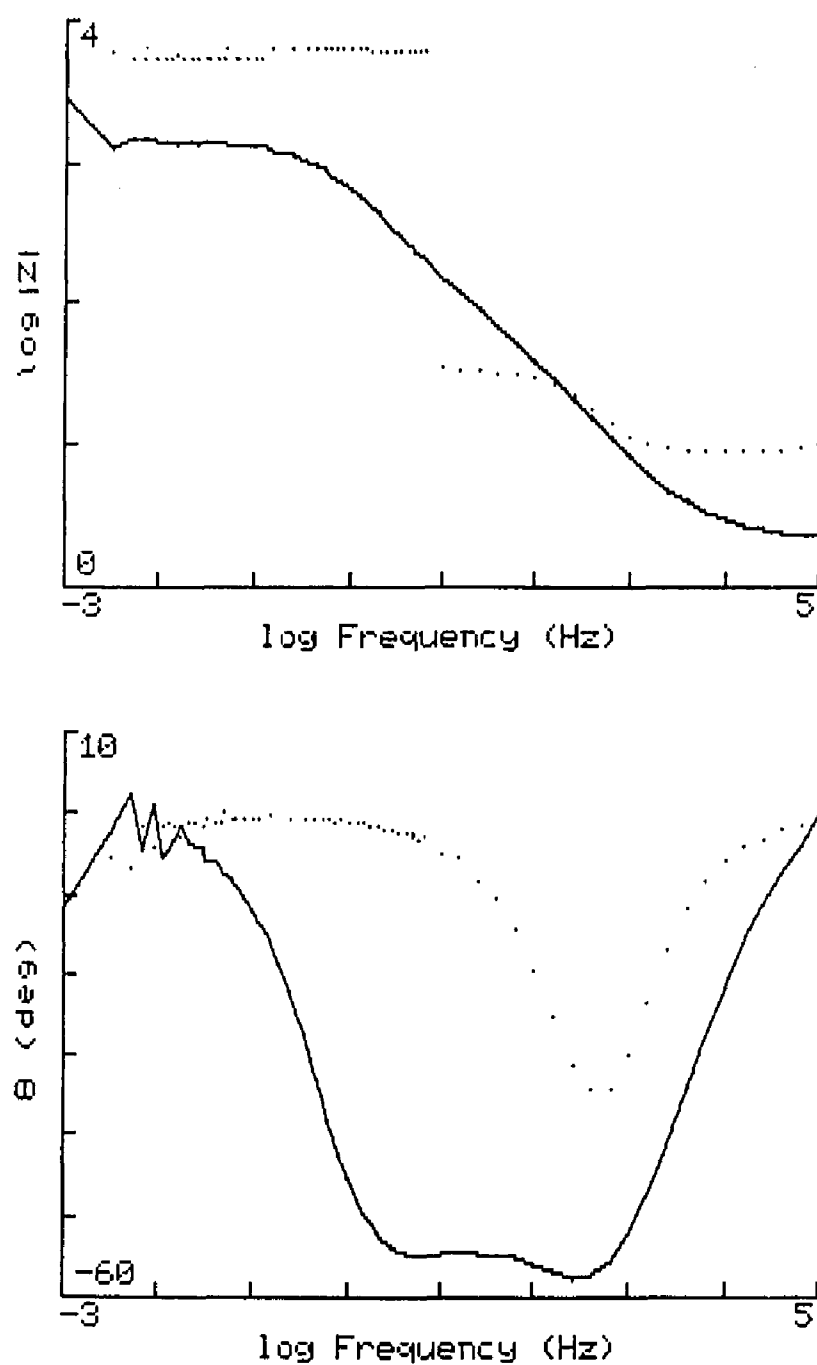


Figure 6.11: Bode plots for a P3MT-coated TiGr2 in 1 N sulfuric acid solution. P3MT deposition condition: 200 mA, 52.4 rad/s and 7.5 s. (..) initial test, (-) after exposed in ambient air for 40 days.

## 6.4 Approaches for protection of carbon steel by P3MT coatings

A Tafel plot of C1010 in 1 N air-saturated sulfuric acid solution is shown in Fig. 6.12. Because of the importance of carbon steel in industrial application, it is worthwhile if

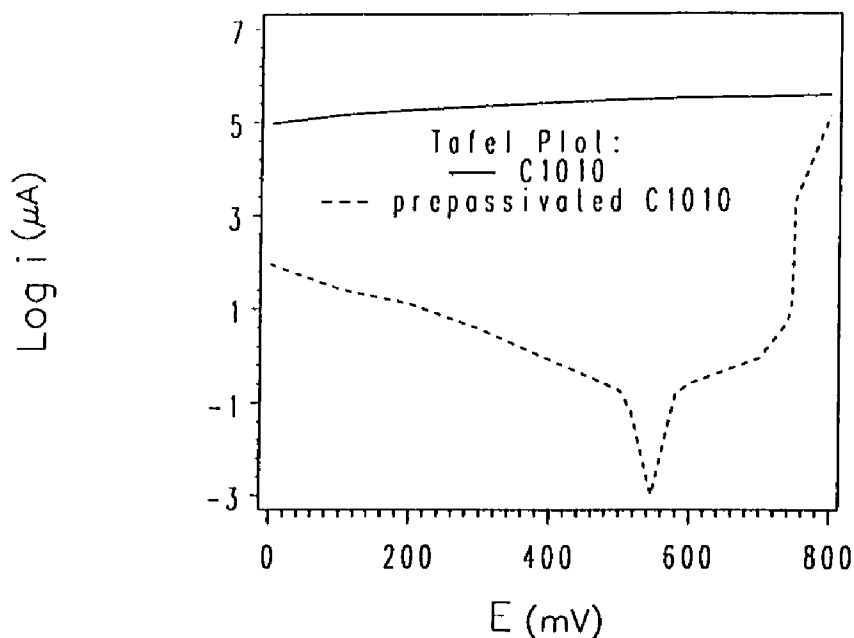


Figure 6.12: Tafel plots of C1010 and the prepassivated C1010 in 1 N air-saturated sulfuric acid solution. The prepassivation of C1010 was conducted by holding C1010 at 0.6 V in 70% nitric acid solution (10.5 rad/s) for 1.5 h.

C1010 could be protected by a conductive polymer in certain circumstance. In this study, two approaches were made for addressing this problem. Though the approaches were not successful, they may give some clues for further study.

The first approach was to prepassivate the metal by forming an oxide film on the surface of C1010. Prepassivation was intended to reduce the galvanic load on the polymer. The oxide film was formed in concentrated nitric solution (70%) by holding the sample at 0.6 V for 1.5 h. A Tafel plot of the prepassivated C1010 is also shown in Fig. 6.12. A



passive region between 200 mV and 700 mV can be easily identified. This range matches with the  $E_{oc}$  region of a P3MT coating, indicating the possibility of passivation by the coating. Nevertheless, the polymer coatings did not stabilize the prepassivated C1010.

A second approach was to form a composite polymer/phosphate-conversion coating. Sugama et al. found that water-soluble PAA macromolecules significantly improved the stiffness and ductility of zinc phosphate conversion coating on carbon steel surface [93,94]. In addition, the surface sites of PAA on the complex zinc phosphate coating acted efficiently to promote interfacial adhesive bonding to polymeric topcoats. My task was to first make a polyacrylic acid (PAA)-modified zinc phosphate conversion precoat on C1010 and then form a P3MT coating on top of it. In this laboratory, the best solution to form the zinc phosphate precoat has the following composition: 3% phosphoric acid, 3%  $Zn(PO_4)_2$  and 2% PAA (MW 90,000) in distilled water. Coating temperature range: 55 – 60°C. Coating time period: 15 min. A uniform coating with fine crystals was formed under these conditions. Unfortunately, the precoat has very high electrical resistance, and it is impossible to electrochemically deposit a complete coating onto it. This approach may yet be possible for polymers that can be processed in solution and applied mechanically to the surface.

## 6.5 Summary

An adhesive P3MT thin film was first formed on titanium or carbon steel surface. Then a thick P3MT coating was deposited onto the thin film. This treatment produces an adherent full coating.

At temperatures below 50°C, the P3MT coatings were stable and protected titanium from corrosion in the tested acid solutions. Successful protection by a coating deposited directly onto titanium represents an advance towards a practical protective coating.

# Chapter 7

## Conclusions and Recommendations

This study has demonstrated the application of poly(3-methylthiophene) (P3MT) coatings for passivating substrates, including 430 stainless steel (430SS) and titanium (TiGr2) in certain corrosive media. An attempt to protect C1010 carbon steel was unsuccessful.

430SS was anodically phosphated to form a uniform porous surface (Ph430SS) to which the deposited P3MT coating firmly adhered. An adhesive P3MT thin film was first deposited on the surface of TiGr2 or C1010 from a dilute 3MT propylene carbonate solution containing chloride ions. A full P3MT thick coating was then formed on top of the thin film.

Electropolymerization (or deposition) conditions substantially affected the properties of the coatings. For P3MT films deposited on platinum, increase of the deposition current density increased the exchange current density and redox capacity of the resulting coating in 1 N sulfuric acid solution. Increase of convective transport during formation decreased the exchange current and redox capacity of the coating. Deposition conditions had complex effects on coating morphology. These effects are probably determined by the interfacial concentration of free radicals during coating formation, as well as other factors. Deposition parameters, especially deposition current density, affected the self-discharge behavior of the coatings as well.

The P3MT coatings, which were stable within the test periods of this study, stabilized

430SS in its passive state in 1 N sulfuric acid solution. The coatings galvanically protected exposed 430SS surface from corrosion in 1 N sulfuric acid solution at an  $A_p/A_s$  ratio of 1:1. The type of purge gases, such as air and nitrogen, did not affect the tests. A reduction reaction other than oxygen reduction takes place to keep the coatings active.

It was found that reduction of P3MT-coated Ph430SS is reversible if the potential is not driven negative of -0.3 V in sulfuric and nitric acid solutions. Reversibility contributes to the stability of the coatings.

The coatings failed to protect Ph430SS from corrosion in aqueous acid and salt solutions with 1 N chloride. A likely corrosion mechanism is the penetration of  $\text{Cl}^-$  ions through the polymer coating and pitting on the substrate surface. The coatings lost their activity in KOH solutions as well. However, the coatings were not irreversibly damaged by immersion in these solutions. The coatings can also sustain the treatment in concentrated acid and base solutions.

Titanium (TiGr2) can be galvanically passivated in 4 N sulfuric and hydrochloric acid solutions at a temperature below 50°C. At 70°C, P3MT coatings broken up after a short time and failed to protect the substrate. A galvanic current of about  $6\mu\text{A}/\text{cm}^2$  between the  $\text{TiO}_2$  oxide film and coupled P3MT coating was recorded at 45°C.

Electrochemical Impedance Spectroscopy (EIS) was used to evaluate the short-term stability of P3MT coatings on titanium. The result indicates that the total resistance of the coating was sharply reduced after immersion in 1 N sulfuric acid solution for one day and then stabilized after one more day. The P3MT coating lost some resistance after forty days in ambient air.

The following issues are recommended for future study.

- Besides oxygen reduction in dilute sulfuric or nitric acid solutions, another reduction reaction plays an important role to stabilize the P3MT coatings. Further study is required to identify this reaction.
- The vulnerability of P3MT to attack by  $\text{Cl}^-$  is a severe limitation. Attention should

be given to modification of the polymer to make it more resistant.

- Reversibility at negative potentials needs to be further explored since it is a critical factor for the stability of the coatings.

- Kinetic studies on electropolymerization of 3MT could be another interesting task.

- It was shown that a Keggin-type heteropolyacid, such as  $\text{H}_3\text{Mo}_{12}\text{O}_{40}\text{P}$ , immobilized in P3MT coatings during the electropolymerization, catalyzes oxygen reduction. However, the acid gradually dissolved in aqueous solutions. Further investigation of heteropolyacids as catalysts in P3MT coatings would be worthwhile.

- From the economic point of view (see Appendix C), conductive coatings electropolymerized in aqueous solutions are more practical. Polypyrrole would be a good choice for future study of metal corrosion protection.

# Bibliography

- [1] N. C. Bilingham and P. D. Calvert, *Advanced in Polymer Science*, Springer-Verlag Berlin Heidelberg, New York, 1 (1989).
- [2] B. Balcius, *Electrical Conductive Polymers*, (1987).
- [3] R. H. Baughman, J. L. Bredas, R. R. Chance, R. L. Elsenbaumer and L. W. Shacklette, *Chem. Rev.*, 82, 209 (1982).
- [4] R. J. Waltman and J. Bargon, *Can. J. Chem.*, 64, 76 (1986).
- [5] T. S. Kuan and R. Cameron, *Issue*, 26, 49 (1988).
- [6] G. E. Wnek, *MRS Bulletin.*, 12(8), 36 (1987).
- [7] *C&EN.*, 20 (June 22, 1987).
- [8] Z. Deng, W. H. Smyrl and H. S. White, *J. Electrochem. Soc.*, 136(8), 2152 (1989).
- [9] D. W. Deberry, *J. Electrochem. Soc.*, 132, 1022 (1985).
- [10] S. Ren and D. Barkey, *J. Electrochem. Soc.*, 139(4), 1021 (1992).
- [11] G. Wranglen, *An Introduction to Corrosion and Protection of Metals*, Chapman and Hall, New York (1985).
- [12] H. H. Uhlig and R. W. Revie, *Corrosion and Corrosion Control, Third Edition*, John Wiley & Sons (1985).
- [13] M. Schirmeisen and F. Beck, *J. Appl. Electrochem.*, 19, 401 (1989).
- [14] P. Hulser and F. Beck, *J. Appl. Electrochem.*, 20, 596 (1990).

- [15] Z. Deng and W. H. Smyrl, *J. Electrochem. Soc.*, 138(7), 1911 (1991).
- [16] A. McGee, J. F. Cassidy, P. Quigley and J. G. Vos, *J. Appl. Electrochem.*, 22, 678 (1992).
- [17] D. D. Macdonald and M. C. H. Mckubre, *Impedance Spectroscopy: Emphasizing solid materials and system*, edited by J. R. Macdonald, John Wiley & Sons, pp260-399 (1987).
- [18] F. Mansfeld, *Corrosion*, 36(5), 301 (1981).
- [19] F. Mansfeld, M. W. Kendig and S. Tsai, *Corrosion*, 38(11), 571 (1982).
- [20] *Application Note (AC-1): Basics of Electrochemical Impedance Spectroscopy (EIS)*, EG&G PARC (1989).
- [21] H. Shirakawa, E. J. Louis, A. G. MacDiarmid and A. J. Heeger, *J. Chem. Soc. Chem. Commun.*, 578 (1977).
- [22] H. S. Nalwa, *Polymer*, 32(4), 745 (1991).
- [23] R. L. Elsenbaumer, K. Y. Jen, G. G. Miller and L. W. Shacklette, *Synth. Met.*, 18, 277 (1987).
- [24] M. Andersson, P. O. Ekeblad, T. Hjertberg and O. Wennerstrom, *Polymer Commun.*, 32(18), 546 (1991).
- [25] P. Chicart, R. J. P. Corriu and J. J. E. Moreau, *Chem. Mater.*, 3, 8 (1991).
- [26] K. Tanaka, K. Yoshizawa, T. Takeuchi and T. Yamabe, *Synth. Met.*, 38, 107 (1990).
- [27] W. Torres and M. A. Fox, *Chem. Mater.*, 4, 146 (1992).
- [28] Y. Wei, C. Chan, J. Tian, G. Jang and K. F. Hsueh, *Chem. Mater.*, 3, 888 (1991).
- [29] E. M. Peters and J. D. Van Dyke, *J. Polymer Sci.: Part A: Polymer Chem.*, 29, 1379 (1991).

- [30] J. Roncali, A. Mastar and F. Garnier, *Synth. Met.*, 18, 857 (1987).
- [31] S. Kuwabata, S. Ito and H. Yoneyama, *J. Electrochem. Soc.: Electrochem. Sci. Tech.*, 135(7), 1691 (1988).
- [32] M. Satoh, K. Kaneto and K. Yoshino, *Synth. Met.*, 14, 289 (1986).
- [33] M. Takakubo, *Synth. Met.*, 16, 167 (1986).
- [34] S. Dong and W. Zhang, *Synth. Met.*, 30, 359 (1989).
- [35] G. Tourillon and F. Garnier, *J. Electroanal. Chem.*, 135, 173 (1982).
- [36] J. R. Reynolds, S. Hsu and H. J. Arnott, *J. Polymer Sci.: Part B: Polymer Phys.*, 27, 2081 (1989).
- [37] J. Roncali, M. Lemaire, R. Garreau and F. Garnier, *Synth. Met.*, 18, 139 (1987).
- [38] T. F. Otero and E. de Larreta-Azelain, *Polymer*, 29(8), 1522 (1988).
- [39] M. Ito, H. Shioda and K. Tanaka, *J. Polymer Sci.: Part C: Polymer. Lett.*, 24, 147 (1986).
- [40] G. Zotti, S. Cattarin and N. Comisso, *J. Electroanal. Chem.*, 235, 259 (1987).
- [41] S. Hotta, T. Hosaka and W. Shimotsuma, *Synth. Met.*, 6, 317 (1983).
- [42] L. Laguren-Davidson, C. V. Pham, H. Zimmer and H. B. Mark, Jr., *J. Electrochem. Soc.: Electrochem. Sci. Tech.*, 135(6), 1406 (1988).
- [43] K. Kaneto, Y. Kohno, K. Yoshino and Y. Inuishi, *J. Chem. Soc., Chem. Commun.*, 382 (1983).
- [44] T. F. Otero, J. Rodriguez and E. de Larreta-Azelain, *Polymer*, 31, 220 (1990).
- [45] T. F. Otero and E. de Larreta-Azelain, *Polymer Commun.*, 29, 21 (1988).

- [46] G. Caple, B. L. Wheeler, R. Swift, T. L. Porter and S. Jeffers, *J. Phys. Chem.*, 94(15), 5639 (1990).
- [47] R. Yang, D. F. Evans, L. Christensen and W. A. Hendrickson, *J. Phys. Chem.*, 94(15), 6117 (1990).
- [48] G. Gustafsson and O. Inganas, *Polymer*, 32(9), 1574 (1991).
- [49] H. Neugebauer, G. Nauer, A. Neckel, G. Tourillon, F. Garnier and P. Lang, *J. Phys. Chem.*, 88(4), 652 (1984).
- [50] G. Tourillon and F. Garnier, *J. Electroanal. Chem.*, 161, 51 (1984).
- [51] R. J. Waltman, J. Bargon and A. F. Diaz, *J. Phys. Chem.*, 87(8), 1459 (1983).
- [52] S. Panero, P. Prospero, D. Zane and B. Scrosati, *J. Appl. Electrochem.*, 22(3), 189 (1992).
- [53] T. Nagatomo and O. Omoto, *J. Electrochem. Soc.: Electrochem. Sci. Tech.*, 135(9), 2144 (1988).
- [54] A. Yassar, J. Roncali and F. Garnier, *Macromolecules*, 22, 804 (1989).
- [55] M. Satoh, H. Yamasaki, S. Aoki and K. Yoshino, *Polymer Commun.*, 28(5), 144 (1987).
- [56] G. Tourillon and F. Garnier, *J. Phys. Chem.*, 87, 2289 (1983).
- [57] G. Tourillon, A. M. Flank and P. Lagarde, *J. Phys. Chem.*, 92, 4397 (1988).
- [58] J. L. Bredas, B. Themans, J. G. Fripiat, J. M. Andre and R. R. Chance, *Phys. Rev. B: Condens. Matter*, 29, 6761 (1984).
- [59] P. J. S. Foot, F. Mohammed, P. D. Calvert and N. C. Billingham, *J. Phys. D: Appl. Phys.*, 20, 1354 (1987).
- [60] G. Tourillon and F. Garnier, *J. Polymer Sci.: Polymer Phys. Edit.*, 22, 33 (1984).



- [61] M. Ito, A. Tsuruno, S. Osawa and K. Tanaka, *Polymer*, 29(7), 1161 (1988).
- [62] G. Tourillon and F. Garnier, *J. Electrochem. Soc.: Electrochem. Sci. Tech.*, 130(10), 2042 (1983).
- [63] F. Garnier and G. Tourillon, *J. Electroanal. Chem.*, 148, 299 (1983).
- [64] K. Kaneto, H. Agawa and K. Yoshino, *J. Appl. Phys.*, 61(3) 1197 (1987).
- [65] S. N. Hoier and D. S. Ginley, *J. Electrochem. Soc.: Electrochem. Sci. Tech.*, 135(1), 91 (1988).
- [66] J. Wang and R. Li, *Anal. Chem.*, 61(24), 2809 (1989).
- [67] G. Tourillon and F. Garnier, *J. Electroanal. Chem.*, 161, 407 (1984).
- [68] S. Sunde, G. Hagen and R. Qdegard, *J. Electrochem. Soc.*, 138(9), 2561 (1991).
- [69] A. Czerwinski, H. Zimmer, A. Amer, C. Van Pham, S. Pons and H. B. Mark, Jr., *J. Chem. Soc., Chem. Commun.*, 1158 (1985).
- [70] P. Burgmayer and R. W. Murray, *J. Am. Chem. Soc.*, 104, 6140 (1982).
- [71] P. Burgmayer and R. W. Murray, *J. Phys. Chem.*, 88, 2515 (1984).
- [72] H. Shinohara, M. Aizawa and H. Shirakawa, *J. Chem. Soc., Chem. Commun.*, 87 (1986).
- [73] W. Zhang and S. Dong, *J. Electroanal. Chem.*, 284, 517 (1990).
- [74] A. O. Patil, Y. Ikenoue, N. Basescu, N. Colaneri, J. Chen and F. Wudl, *Synth. Met.*, 20, 151 (1987).
- [75] Y. Ikenoue, J. Chiang, A. O. Patil, F. Wudl and A. J. Heeger, *J. Am. Chem. Soc.*, 110, 2983 (1988).
- [76] G. Tourillon and F. Garnier, *J. Phys. Chem.*, 88(22), 5281 (1984).

- [77] J. W. Thackeray and M. S. Wrighton, *J. Phys. Chem.*, 90(25), 6674 (1986).
- [78] A. Leone, W. Marino and B. R. Scharifker, *J. Electrochem. Soc.*, 139(2), 438 (1992).
- [79] B. Keita and L. Nadjo, *J. Electroanal. Chem.*, 227, 265 (1987).
- [80] B. Keita, L. Nadjo and J. P. Haeussler, *J. Electroanal. Chem.*, 230, 85 (1987).
- [81] G. Bidan, E. M. Genies and M. Lapkowski, *J. Electroanal. Chem.*, 251, 297 (1988).
- [82] K. M. Cheung, D. Bloor and G. C. Stevens, *Polymer*, 29(9), 1709 (1988).
- [83] G. Bidan, E. M. Genier and M. Lapkowski, *Synth. Met.*, 31, 327 (1989).
- [84] A. Schirmeisen and F. Beck, *J. Appl. Electrochem.*, 19, 401 (1989).
- [85] S. Swathirajan and Y. M. Mikhail, *J. Electrochem. Soc.*, 139(8), 2105 (1992).
- [86] B. J. Feldman, P. Burgmayer and R. W. Murray, *J. Am. Chem. Soc.*, 107, 872 (1985).
- [87] M. Kendig and J. Scully, *Corrosion*, 46(1), 22 (1990).
- [88] *Application Note (AC-2): Evaluation of Organic Coatings by Electrochemical Impedance Measurements*, EG&G PARC.
- [89] G. W. Walter, *J. Electroanal. Chem.*, 118, 259 (1981).
- [90] M. Kendig, F. Mansfeld and S. Tsai, *Corrosion Science*, 23(4), 317 (1983).
- [91] J. Hubrecht, J. Vereecken and M. Piens, *J. Electrochem. Soc.: Sci. Tech.*, 131(9), 2010 (1984).
- [92] M. M. Musiani, C. Pagura and G. Mengoli, *Electrochimica Acta*, 30(4), 501 (1985).
- [93] T. Sugama, L. E. Kukacka, N. Carciello and J. B. Warren, *J. Appl. Polym. Sci.*, 30, 4357 (1985).

- [94] T. Sugama, L. E. Kukacka, N. Carciello and J. B. Warren, *J. Appl. Polym. Sci.*, 32, 3469 (1986).
- [95] A. J. Bard and L. R. Faulkner, *Electrochemical Methods*, John Wiley & Sons, Inc., p288 (1980).
- [96] R. C. Weast, *CRC Handbook of Chemistry and Physics* (1984-1985).
- [97] *International Critical Tables*, III (1929).
- [98] G. E. Weismantel, *Paint Handbook*, McGraw-Hill Book Company (1981).
- [99] G. D. Ulrich *A Guide to Chemical Engineering Process Design and Economics*, John Wiley & Sons, p269 (1984).

## NOMENCLATURE

430SS: 430 stainless steel

$A_c$ : measured cathodic peak area,  $\text{cm}^2$

$A_w$ : total graph area in X-Y recorder,  $\text{cm}^2$

$A_p$ : polymer coating area,  $\text{cm}^2$

$A_s$ : exposed steel area,  $\text{cm}^2$

$A_t$ : exposed titanium area,  $\text{cm}^2$

AVN: average vernier number for coulometry

$C_a$ : charge capacity of P3MT coating in 1 N sulfuric acid solution,  $\text{C}/\text{cm}^2$

$C_c$ : polymer coating capacitance,  $\text{C}/\text{cm}^2$

$C_{dl}$ : double layer capacitance,  $\text{C}/\text{cm}^2$

$C_p$ : redox capacity of P3MT coating,  $\text{C}/\text{cm}^2$

$C_t$ : current charge corresponding to  $A_w$ ,  $\text{C}/\text{cm}^2$

CV: cyclic voltammetry

C1010: C1010 carbon steel

$E_{oc}$ : open-circuit potential, V

EIS: Electrochemical Impedance Spectroscopy

EDXS: Energy Dispersive X-ray Spectroscopy

f: frequency in EIS, Hz

HPA: heteropolyacid

$i_0$ : exchange current density of possible oxygen reduction,  $\text{mA}/\text{cm}^2$

$i_d$ : deposition current density,  $\text{mA}/\text{cm}^2$

$i_{corr}$ : corrosion current density, mA/cm<sup>2</sup>

Pt: platinum RDE

PA: polyaniline

PC: propylene carbonate

PP: polypyrrole

PT: polythiophene

PAA: polyacrylic acid

P3MT: poly(3-methylthiophene)

Ph430SS: phosphated 430 stainless steel

$R_{\Omega}$ : electrolyte resistance, ohm

$R_p$ : pore resistance of coating, ohm

$R_t$ : electron-transfer resistance, ohm

rpm: rotation per minutes

RDE: rotating disk electrode

SCE: standard calomel reference electrode

SEM: Scanning Electron Microscopy

$t_d$ : deposition time, s

TiGr2: grade-2 titanium

TBATFB: tetrabutylammonium tetrafluoroborate

Z: total impedance in EIS, ohm

#### Greek Letters:

$\Omega$ : rotation rate of a RDE, rad/s or rpm

$\phi_{corr}$ : corrosion potential, V

$\theta$ : phase angle in EIS, degree

# Appendix A

## Composition and Properties of Metal Samples

All the metal samples were purchased from Metal Samples Corporation. The physical properties and composition of the metal samples are summarized in the following tables. The surface composition of the TiGr2 samples was analyzed by EDXS in Instrumentational Service at UNH.

Table A.1: Physical Properties of Metals

Property	430SS	TiGr2	C1010
Tensile Str.	na	78 Ksi	na
Yield PT	na	48 Ksi	na
Elongation	na	28%	na
Red. of Area	na	47%	na
Hardness	na	na	na

Table A.2: Composition of Metal Samples (%)

Element	430SS	TiGr2	C1010
Al	0.005		
C	0.036	0.010	0.080
Cr	16.60		
Cu	0.100		
Fe	Balance	0.040	Balance
Mn	0.500		0.380
Mo	0.040		
Ni	0.310		
Ti		Balance	
Si	0.530		
P	0.028		0.022
S	0.013		0.012
O		0.130	
N		0.010	
H		35E-6	

# Appendix B

## Calculation of Oxygen Concentrations

### (I) Concentration of oxygen required to support a galvanic current in the diffusion-limited regime

For a galvanic current test in 1 N sulfuric acid solution, assume the limiting galvanic current density is due to oxygen reduction at the P3MT/electrolyte interface and has a value of  $1 \mu\text{A}/\text{cm}^2$ . According to the Levich equation [95]

$$i_l = 0.62nFD_0^{2/3}\Omega^{1/2}\nu^{-1/6}C_0 \quad (\text{B..1})$$

where  $n$  is electrons transferred (equiv/mole),  $F$  Faraday's constant (96,487 C/equiv),  $D_0$  diffusivity of oxygen in a given solution ( $\text{cm}^2/\text{s}$ ),  $\Omega$  rotation rate of the RDE (rad/s),  $\nu$  kinematic viscosity of a given solution ( $\text{cm}^2/\text{s}$ ) and  $C_0$  bulk concentration of oxygen in the solution ( $\text{mole}/\text{cm}^3$ ) at the limiting current condition.

For 1 N sulfuric acid solution, taking  $i_l=1 \mu\text{A}$ ,  $n=4$ ,  $D_0=3.0*10^{-5} \text{ cm}^2/\text{s}$  [96],  $\Omega=105 \text{ rad/s}$  and  $\nu=0.011 \text{ cm}^2/\text{s}$  [96],  $C_0$  can be calculated from the Levich equation as  $1.99*10^{-10} \text{ mole}/\text{cm}^3$  or  $1.99*10^{-7} \text{ mole/L}$ .

### (II) Solubility of oxygen in water at room temperature

The solubility of oxygen in water is higher than that in sulfuric acid solutions [97].



At 23°C (room temperature) [97]:

$$10^{-7} * K = 3.215 \quad (B..2)$$

where K is the Henry's constant

$$K = \frac{p_{O_2}}{x_{O_2}} \quad (B..3)$$

where  $p_{O_2}$  is the partial pressure of oxygen (mmHg) in the gas phase,  $x_{O_2}$  is the mole fraction of oxygen in the solution.

(a) air purge: 21% oxygen is contained in air.

$$x_{O_2} = \frac{0.21 * 760 * 10^{-7}}{3.215} = 4.96 * 10^{-6} \quad (B..4)$$

So that

$$C_0 = (4.96 * 10^{-6})(55.56) = 2.76 * 10^{-4} \text{ mole/L} \quad (B..5)$$

(b) N<sub>2</sub> purge: Nitrogen gas used in this study contains 10ppm oxygen.

$$x_{O_2} = \frac{10^{-5} * 760 * 10^{-7}}{3.215} = 2.36 * 10^{-10} \quad (B..6)$$

So that

$$C_0 = (2.36 * 10^{-10})(55.56) = 1.31 * 10^{-8} \text{ mole/L} \quad (B..7)$$

By comparison with the calculated result from (I), it can be seen that under nitrogen purge, oxygen reduction is not able to balance the galvanic current density during the galvanic corrosion tests in 1 N sulfuric acid solution at room temperature.

## Appendix C

# A Rough Estimation of Unit Cost for P3MT and PP Coatings

Coating engineers are concerned about unit painting cost. Therefore a rough economic analysis of electroconductive polymer coatings, such as poly(3-methylthiophene) (P3MT) and polypyrrole (PP), has been conducted by author.

The price of a chemical reagent is taken as the price at the laboratory research scale. The expected cost of the conductive coatings are discounted by 50% relative to this scale. The unit cost of a coating is estimated as dollars/per square foot as compared with regular organic coatings. Cost of maintenance is not taken into account. However, we assume the conductive coatings would cost less than regular organic coatings to maintain because of their ability to function even after being scratched or partially removed.

### Part I: Estimation of cost for P3MT coatings

(1) Price of the chemicals purchased from Aldrich:

3MT                      \$53.90/100 grams

Propylene carbonate                      \$204.85/18 L

TBATFB (supporting electrolyte)                      \$129.90/100 grams

(2) Solution:

1.0 M 3MT with 0.1 M TBATFB in propylene carbonate.

(3) Electrode area: 1 ft<sup>2</sup>

Electrolyte volume in cell: 150 L or 5.3 ft<sup>3</sup>

Possible cell size: 2 \* 2 \* 1.5 (in foot)

(4) Total cost for raw materials:

3MT                      \$7,939 for 14.5 L or 14.73 kg

Propylene carbonate                      \$1,542 for 135.5 L

TBATFB                      \$6,481 for 4.99 kg

Total Cost:                      \$15,962

If discounted 50%, the total cost should be: \$7,981.

(5) If we apply low current density (e.g. 50 mA/cm<sup>2</sup>) and make a coating of moderate thickness (about 1.0 C/cm<sup>2</sup>), we can make approximately 40 coatings. Then the unit cost of the P3MT coating would be: \$200/ft<sup>2</sup>.

The unit labor and electricity costs are negligible compared with the cost of the coating itself. It is possible to find some less expensive supporting electrolyte to reduce the unit cost of P3MT coatings.

## **Part II: Estimation of cost for PP coatings**

Is is obvious that if a conductive coating can be synthesized in an aqueous solution, it will save the cost for organic solvent, indicating the more expensive organic supporting electrolyte. The unit cost of the conductive coating would therefore be drastically reduced. Polypyrrole is one of the suitable candidates which can be formed in aqueous media. The following is a cost estimation for PP as a conductive coating.

(1) Price of the chemical reagents:

Pyrrole                      \$104.55/0.5 L (Aldrich)

Distilled water                      \$0.5/L (approximation)

(2) Solution:

1.0 M pyrrole in distilled water.

(3) Electrode area, electrolyte volume as well as cell size are same as Part I.

(4) Total cost for raw materials in above cell:

Pyrrole	\$2,171 for 10.38 L
Distilled water	\$70 for 140 L
Total cost:	\$2,241

If discounted for 50% off price due to industrial application, the total cost should be: \$1,120.5

(5) For a coating similar to that in Part I, approximately 40 coatings could be formed. Then the unit cost of the PP coating should be: \$28/ft<sup>2</sup>. It can be seen that the unit cost of the PP coating is reduced about 85% compared with that of the P3MT coating.

### **Part III: Unit cost comparison between conductive coatings and regular organic coatings.**

A table for material costs of paint and protective coatings in 1978 is given in Table C [98]

Table C [98] shows the coating cost data for structural steel in 1978. Field labor, equipment, and related costs were added upon the material cost in this table.

If we add one dollar for all other costs in the case of a conductive coating. A comparison between the unit cost of P3MT or PP coating and three-coat vinyl (see Table C) can be illustrated as following:

The CE Index [99] can be used to account for inflation. The unit cost of three-coat vinyl is corrected to \$3.073/ft<sup>2</sup> in 1992 if we take CE index of 230 for 1978 and 600 for 1992 respectively. Therefore, in the case of the P3MT coating, the ratio of unit costs

Table C.1: 1978 Typical Material Costs for Paint and Protective Coatings

TABLE 20.3 1978 Typical Material Costs for Paint and Protective Coatings

Type	Typical dry film thickness per coat (mils)	Approximate cost per square foot at typical dry film thickness (cents)		
		Theoretical	Spray (practical)*	Roller or brush (practical)†
Alkyds				
Primer	1.5	1.7	2.5	1.9
Gloss topcoats	1.5	1.6	2.2	1.7
Silicone alkyd	2.0	3.2	4.5	3.5
Latex				
Primer	2.0	2.5	3.5	2.7
Topcoats	1.5	2.3	3.3	2.6
Epoxy ester				
Primer	1.5	1.9	2.7	2.1
Topcoats	1.5	2.3	3.3	2.6
Zinc-rich primers				
Inorganic; self-cured	3.0	6.1	8.7	†
Organic; epoxy	3.0	7.4	10.5	8.2
Epoxy				
Primer	2.0	2.9	4.1	3.2
High-build intermediate coat or topcoat	4.0	5.5	7.9	†
Finish (enamel) coat	2.0	2.6	3.7	2.9
Chlorinated rubber				
Primer	2.0	3.8	5.4	4.2
High-build intermediate coat or topcoat	4.0	6.0	9.2	†
Finish (enamel) coat	1.5	2.7	3.8	3.0
Solution vinyls				
Primer	1.5	3.9	5.6	†
High-build intermediate coat or topcoat	4.0	9.5	13.6	†
Finish (enamel) coat	1.5	3.7	5.3	†
Urethane				
Aliphatic urethane	1.5	4.1	5.9	4.6
Coal-tar epoxy				
Standard	8.0	5.8	8.2	†
C200 version	8.0	6.2	8.9	†

SOURCE: Presented at the NACE Annual Conference, Atlanta, Ga., March 1979.

NOTE: Costs are approximate, based on 1978 data.

\* 30 percent spray loss.

† 10 percent loss by brush or roller.

‡ Spray only.

Table C.2: 1978 Coating Cost data for Structural Steel on the Ground

TABLE 20.5 1978 Coatings Cost Data for Structural Steel on the Ground\*  
East Coast; all work at jobsite

System	Cleaning	Dry film thickness (mils)	Total material cost	Field labor, equipment, and related costs				Total cost
				Surface preparation	Prime coat	Intermediate coat	Topcoat	
Two-coat alkyd	SP-2; SP-3	3.5	\$ .047	\$ .35	\$ .10	\$ ...	\$ .10	\$ .597
Three-coat alkyd	SP-2; SP-3	5.0	.069	.35	.10	.10	.10	.719
Three-coat alkyd	SP-6	5.0	.069	.45	.10	.10	.10	.819
Two-coat latex	SP-2; SP-3	3.5	.068	.35	.10	...	.10	.618
Three-coat latex	SP-2; SP-3	5.0	.101	.35	.10	.10	.10	.751
Three-coat latex	SP-6	5.0	.101	.45	.10	.10	.10	.851
Two-coat epoxy	SP-6	6.0	.12	.45	.15	...	.15	.897
Three-coat epoxy	SP-6	10.0	.199	.45	.15	.15	.15	1.099
Three-coat inorganic zinc, high-build epoxy	SP-10	11.0	.245	.55	.20	.15	.15	1.295
Three-coat inorganic zinc, high-build epoxy, aliphatic urethane	SP-10	8.5	.225	.55	.20	.15	.15	1.275
Three-coat vinyl	SP-10	9.5	.328	.55	.10	.10	.10	1.178
Three-coat chlorinated rubber	SP-6	10.0	.238	.45	.10	.10	.10	.988
Two-coat coal-tar epoxy	SP-6	16.0	.164	.45	.15	...	.15	.914

SOURCE: Presented at the NACE Annual Conference, Atlanta, Ga., March 1979.

## NOTE:

1. All prices on square-foot basis. To convert to typical ton size, multiply by 250.
2. 30 percent spray loss.
3. A 10 percent area for touch-up is assumed.
4. Material based on 1978 prices.
5. Labor based on \$20 per person-hour, loaded rate.

\* For prices in the air after erection, add 25 percent for simple structures and 50 percent for intricate and complex structures. See Tables 20.1, 20.11, or 20.12 for factors on other structures and surfaces.

is:

$$\frac{201}{3.073} = 65.4 \quad (C..1)$$

Accordingly, in the case of the PP coating, the ratio of unit costs is:

$$\frac{28}{3.073} = 9.1 \quad (C..2)$$

Obviously, the cost of the conductive coatings is high for the time being, but they may become economical for protection of some delicate devices.